Effects of amyloid-beta (Aβ) on homeostatic network plasticity in human iPSC-derived neuronal networks

Dissertation

zur

Erlangung des Doktorgrades

der Naturwissenschaften

(Dr. rer. nat.)

dem

Fachbereich Pharmazie der

Philipps-Universität Marburg

vorgelegt von

Gaye Tanrıöver

aus **İstanbul**

Marburg/Lahn 2017

Erstgutachter: Jun. Prof. Dr. Katja Nieweg

Zweitgutachter: Prof. Dr. Carsten Culmsee

Eingereicht am 01.11.2017

Tag der mündlichen Prüfung am Datum 15.12.2017

Hochschulkennziffer: 1180

Sevgili anne ve babama

To my beloved parents

Meinen Eltern

Above all, don’t fear difficult moments. The best comes from them.

Rita Levi-Montalcini

Erklärung

Ich versichere, dass ich meine Dissertation

"Effects of amyloid-beta on homeostatic network plasticity in human iPSC-derived neuronal networks"

selbständig ohne unerlaubte Hilfe angefertigt und mich dabei keiner anderen als der von mir ausdrücklich bezeichneten Quellen bedient habe. Alle vollständig oder sinngemäß übernommenen sind Zitate als solche gekennzeichnet.

Die Dissertation wurde in der jetzigen oder einer ähnlichen Form noch bei keiner anderen Hochschule eingereicht und hat noch keinen sonstigen Prüfungszwecken gedient.

Marburg, den 01.11.2017

.....

Gaye Tanriöver

Abstract

Alzheimer's disease (AD) is a progressive, neurodegenerative disorder and it is the most common cause of dementia in elderly. The disease is characterized by memory loss, mood swings, and communication problems. This uniquely human disease has been investigated in various mouse models mimicking different pathological hallmarks of AD, which supplied valuable insight into disease mechanisms; however, clinical trials based on these models failed and current treatments are unsatisfactory. To overcome the limitations of animal models of AD, the emerging induced pluripotent stem cell (iPSC) technology promises great potential. It offers the possibility to investigate underlying disease mechanisms, screen for drug targets and validate therapeutic effects in disease-relevant cell types of human origin on a patient-specific background. Current iPSC studies to model AD have been addressing the questions of the pathological hallmarks such as an increase in amyloid beta (Aβ) and hyperphosphorylated tau. However, to investigate the AD-related phenomenon of neuronal hyperactivity, mature human neuronal cultures with spontaneously active networks are necessary, and their generation remains a challenge.

In this study, to achieve spontaneously firing mature neuronal networks, human iPS cells were differentiated into neurons and were supported with endogenously differentiated human astrocytes or primary cortical astrocytes (PCA) isolated from rat brains. Neuronal activity was recorded by using multi electrode array (MEA) to detect single spikes and network bursts. Calcium imaging of spontaneously firing networks was performed to monitor synchronously active neurons in cultures. To trigger hyperactivity-induced homeostatic plasticity in human networks, iPSC-derived cultures were treated with 4-Aminopyridine (4AP), a non-selective inhibitor of voltage-gated K^+ channels. It increased the network activity only in mature (burst firing) cultures. This induced hyperactivity further led to activation of homeostatic plasticity dependent mechanisms to reduce the firing rate. Single spike analysis suggested Na^+ channel removal from the axonal membrane as one of these compensatory mechanisms. Moreover, repressor element-1 silencing transcription factor (REST) was identified as a key player in this process.

To study AD-related impairments in the established model, cell-derived and synthetic Aβ oligomers were prepared and characterized by semi-native western blot. Synthetic Aβ oligomers were surprisingly stable when added to neuronal cultures and caused no cell

death and no change in spontaneous network activity. However, upon 4AP treatment, Aβ-treated networks showed impaired homeostatic plasticity and were not able to reduce the firing rate appropriately. According to the analysis of spike properties, the plasticity-associated reduction of axonal Na^+ channels was also impaired. In Aβ-treated cultures, nuclear REST expression was diminished at basal levels and after triggering homeostatic plasticity by 4AP. Thus, AD-related hyperactivity may be caused by dysfunctional homeostatic plasticity in a REST-dependent manner.

Taken together, the results of this study provided the first hint on a previously unknown impairment of homeostatic plasticity mechanisms in AD and identified REST as a target which might contribute to the hyperactivity phenomenon at early stages of AD. This knowledge of plasticity impairment might expand our understanding of disease development and REST manipulation might be a new target for potential therapeutic strategies.

Zusammenfassung

Die Alzheimer Erkrankung (AE) ist eine progressive, neurodegenerative Krankheit und die häufigste Ursache für Demenz bei älteren Menschen. Sie ist charakterisiert durch Gedächtnisverlust, Stimmungsschwankungen und Kommunikationsprobleme. Diese ausschließlich beim Menschen vorkommende Erkrankung wurde in unterschiedlichen Mausmodellen untersucht, die verschiedene pathologische Merkmale der AE adressieren. Diese lieferten wertvolle Einblicke in die Krankheitsmechanismen, jedoch scheiterten darauf basierende Klinische Studien und existierende Therapien sind unzulänglich. Um die Einschränkungen von Tiermodellen bei der Modellierung der AE zu überwinden, verspricht die aufkommende Technologie der induzierten pluripotenten Stammzellen (iPSZ) großes Potenzial. Sie ermöglicht es, zugrunde liegende Krankheitsmechanismen, Medikamentenforschung und Validierung an krankheitsrelevanten Zelltypen menschlichen Ursprungs vor einem Patienten-spezifischen Hintergrund durchzuführen. Bisherige iPSZ Alzheimer-Studien haben sich vor allem mit den Fragen der pathologischen Kennzeichen der AE, wie der Zunahme von Amyloid-beta (Aβ) und hyperphosphoryliertem Tau beschäftigt. Um das bei der AE auftretende Phänomen der neuronalen Hyperaktivität zu untersuchen, werden reife menschliche neuronale Kulturen mit spontan aktiven Netzwerken benötigt. Deren Generierung stellt eine Herausforderung dar.

Um spontan feuernde reife Netzwerke zu erhalten, wurden in dieser Studie menschliche iPS Zellen zu Neuronen differenziert. Deren Ausreifung wurde unterstützt durch endogen differenzierte menschliche Astrozyten oder durch primäre kortikale Astrozyten (PCA) der Ratte. Die neuronale Aktivität wurde unter Verwendung eines Multielektroden-Arrays (MEA) gemessen, um einzelne Aktionspotenziale (Spikes) und Netzwerk-Bursts zu detektieren. Bildgebende Kalzium-Messungen wurden an spontan aktiven Netzwerken durchgeführt, um synchron aktive Neuronen zu detektieren. Um mittels Hyperaktivität homöostatische Plastizität in menschlichen neuronalen Netzwerken auszulösen wurden aus iPS Zellen hergestellte Kulturen mit 4-Aminopyridin (4AP), einem nicht-selektiven Inhibitor spannungsabhängiger K^+-Kanäle behandelt. Dies erhöhte die Netzwerkaktivität allerdings nur in reifen Kulturen, welche ein Burst-Feuerverhalten aufwiesen. Die induzierte Hyperaktivität führte zur Aktivierung von Mechanismen homöostatischer Plastizität, um die Netzwerkaktivität zu reduzieren. Die Analyse einzelner extrazellulärer Spikes deutete auf die Reduktion axonalen Na+

Kanälen als einen dieser kompensatorischen Mechanismen hin. Eine Schlüsselrolle in diesem Prozess kam dabei dem Repressor Element 1 Silencing Transkriptionsfaktor (REST) zu.

Des Weiteren wurden, um AE-bezogene Beeinträchtigungen in diesem Modell zu untersuchen, zelluläre und synthetische Aβ-Oligomere hergestellt und mit Hilfe eines semi-nativen Western-Blots charakterisiert. Synthetische Aβ-Oligomere zeigten eine überraschende Stabilität während der Behandlung der neuronaler Kulturen und verursachten keinen Zelltod und keine Veränderung der spontanen Netzwerk-Aktivität. Allerdings was in Aβ-behandelten Netzwerken die homöostatische Plastizität beeinträchtigt und die 4AP-induzierte Hyperaktivität führte nicht zur entsprechenden Runterregulation der neuronalen Aktivität. Die Spike Analyse deutete außerdem darauf hin, dass die Plastizitäts-assoziierte Reduktion der axonalen Na^+ Kanäle in Aβ-behandelten Netzwerken vermindert war. Gleiches galt für die nukleare Expression von REST im Grundzustand und nach dem Auslösen homöostatischer Plastizität durch 4AP. Demnach könnte die mit der AE verbundene Hyperaktivität durch eine unzureichende Fähigkeit zur homöostatischen Plastizität zu Stande kommen, bewirkt durch einen REST abhängigen Prozess.

Zusammenfassend offenbaren die Ergebnisse dieser Studie erste Hinweise auf eine bisher nicht bekannte Beeinträchtigung eines homöostatischen Plastizitätsmechanismus in der AE und identifizieren REST als einen wichtigen Faktor, der bei dem Phänomen der Hyperaktivität im frühen Stadium der AE eine Rolle spielen könnte. Dieses Wissen über Plastizitätsbeeinträchtigungen könnte unser Verständnis der Krankheitsentwicklung verbessern. Weiterhin könnte die Manipulation von REST ein neues Ziel für potentielle therapeutische Strategien darstellen.

Contents

1. Introduction

1.1 Neuronal networks

The brain is the most complex organ of the human body. It consists of approximately one hundred billion nerve cells, which are the information processing units in the brain (Pakkenberg & Gundersen 1997). Neurons are surrounded and protected by glial cells. Astrocytes are the most abundant glial cells in the brain. Microglial cells are the immune defense cells and they are activated by external cues to clear waste material by endocytosis. Ependymal cells secrete cerebrospinal fluid (CFS) to rinse the toxic waste, produced as a result of the brain metabolism. Oligodendrocytes produce the myelin sheet wrapping the axons of neurons (Kandel et al. 2000). Neurons are highly compartmentalized. They are classified morphologically as multipolar, bipolar, and unipolar. They also differ in their neurotransmitter secretion which distinguishes excitatory pyramidal or inhibitory interneurons. Neurons are irreplaceable, amitotic, and the longest-lived cells in the body with a very high metabolic rate using 20 % of the calories taken by the human body to maintain neuronal signal transmission (Kandel et al. 2000).

1.1.1 Action potential propagation and synaptic transmission

Neurons fire an impulse called action potential (AP), which is generated at the axon initial segment upon depolarization of the neuron above the voltage threshold (Figure 1.1). The neuronal cell membrane acts as an insulator and the ion channels within the membrane allow the ion exchange between intra- and extra- cellular space. Neuronal membrane is 20 times more permeable to K^+ ions compared to Na^+ (Cohen 1973). Therefore, a resting neuron is polarized due to the leaky K^+ efflux causing negativity in the inside of the cell (-70 mV). The higher abundance of K^+ ions inside and Na^+ ions outside creates an electrochemical gradient. Depolarization of the resting neuronal membrane via ion diffusion through ligand gated channels triggers the opening of voltage-gated Na^+ channels and the membrane depolarization. After reaching 0 mV, voltage-gated Na^+ channels close and voltage-gated K^+ channels open, which leads to K^+ efflux and repolarization. After hyperpolarization, the Na^+-K^+ pump takes over and the membrane reaches its resting potential (Bean 2007).

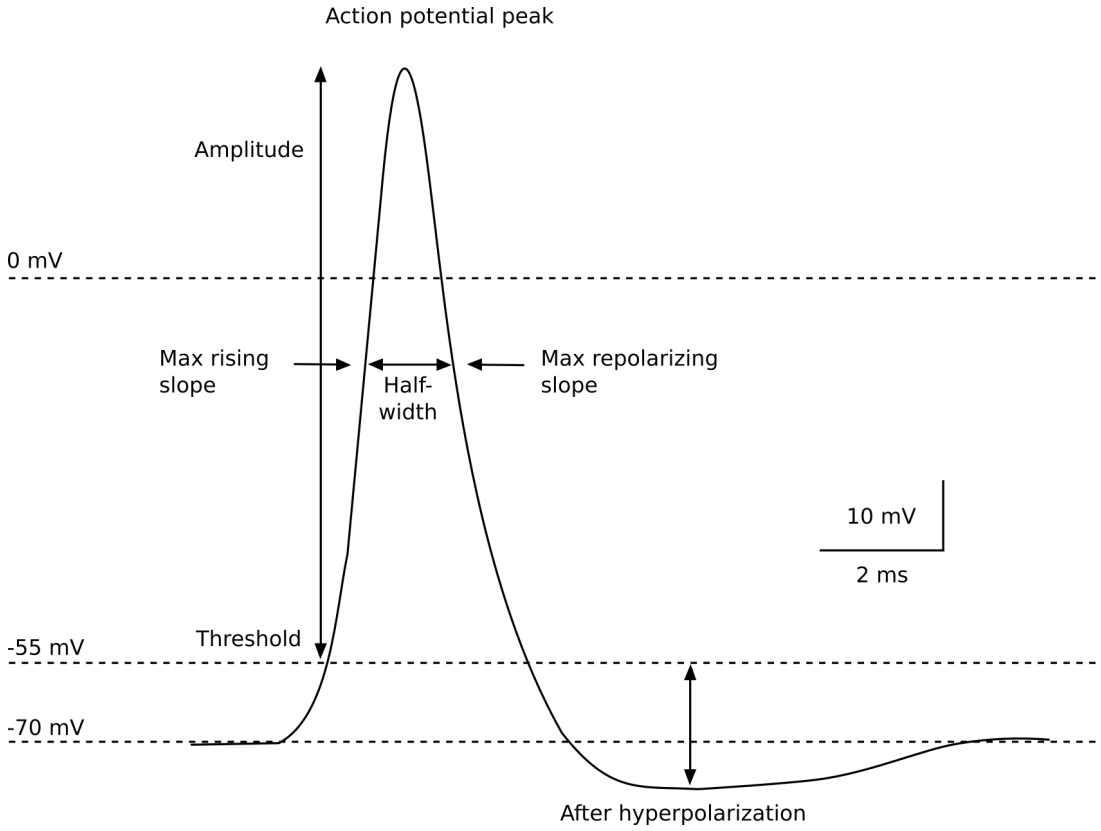

Figure 1.1: **Action potential (AP) characteristics.** Illustration of commonly measured AP parameters according to Bean et al. (2007). Resting membrane potential is at -70 mV. The threshold (the depolarization voltage level that must be achieved for an AP firing) for firing is at -55 mV. The amplitude of an AP is defined as the peak relative to the threshold. Maximum rising and depolarizing slopes are the values defining the rate of rise of membrane voltage during spike rising phase and the rate of rise of membrane voltage during spike falling phase, respectively. Spike width is most commonly measured as the width at half-maximal spike amplitude. Afterhyperpolarization is calculated as the voltage difference to AP threshold.

The neuronal signal transmission (synaptic transmission) occurs at the connecting point of two neurons called synapse (Figure 1.2). When an AP reaches the axonal terminal, it triggers signal transmission via electrical or chemical synapses, which transmit ion currents via gap junctions or neurotransmitter release to the synaptic cleft, respectively. The chemical synapse is slower, yet more precise and selective (Kandel et al. 2000). The AP acts according to all-or-none principle. The signal in the chemical synapse can be modified, amplified, or inhibited. The signal passing neuron (the presynaptic neuron) releases neurotransmitters, packed in synaptic vesicles, which are in a close vicinity to the axon terminal. When an AP reaches the axon terminal, voltage-gated Ca^{2+} channels open, Ca^{2+} enters the cells, synaptic vesicles fuse with the neuronal membrane, neurotransmitters diffuse to the synaptic cleft and bind to postsynaptic receptors such as α-amino-3-hydroxy-5-methyl-4-isoxazole propionic acid (AMPA) and N-Methyl-

D-aspartic acid (NMDA) for glutamate. Activated receptors change the postsynaptic membrane potential in either an inhibitory (inhibitory post synaptic potential, IPSP) or an excitatory (excitatory post synaptic potential, EPSP) manner.

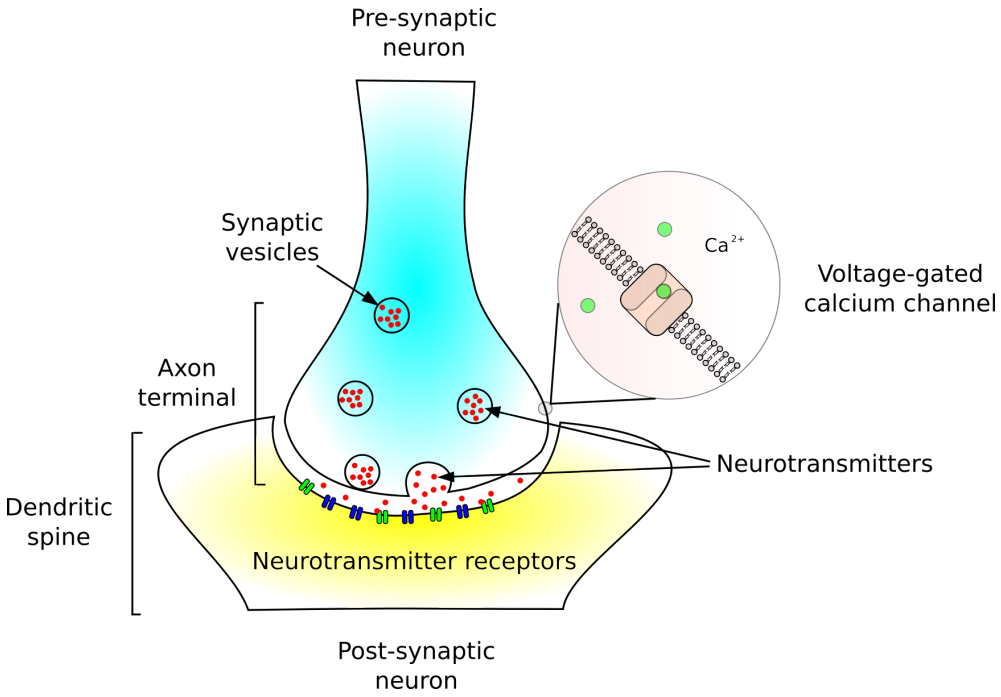

Figure 1.2: **Scheme of a chemical synapse.** According to Purves et al. (2001). Upon arrival of the AP, presynaptic membrane depolarizes, voltage-gated Ca^{2+} channels open, and presynaptic Ca^{2+} levels increase. This cascade leads to the release of neurotransmitters from the membrane-docked neurotransmitter-containing synaptic vesicles to the synaptic cleft. Others are stored in the reserve pool, just above the docked vesicles. Released neurotransmitters bind to ionotropic or metabotropic postsynaptic receptors and thereby lead to a change of the postsynaptic membrane potential.

Neurotransmitter-triggered postsynaptic changes are not restricted to the occurrence of IPSP and EPSP. Long-term changes can also occur at the synapse. The structure and therefore the function of a synapse can be altered with a mechanism called synaptic potentiation. This activity dependent change of the synapse is the main suggested mechanism of learning and memory (Brown et al. 1988). Long-term potentiation (LTP) and long-term depression (LTD) are the most prominent processes. LTP occurs as a result of presynaptic high-frequency stimulus which involves glutamate binding to NMDA receptors, following Ca^{2+} influx and activation of the calcium-calmodulin-dependent kinase II (CaMKII). The active kinase phosphorylates AMPA receptors leading to a higher permeability of Na^{+} ions and increased depolarization. An elevated Ca^{2+} concentration in the cell can alter signaling cascades and leads to structural changes in

the postsynaptic membrane. On the other hand, LTD occurs in a similar manner; however, with a low-frequency electrical stimulation. It reduces the number of AMPA receptors at the synapse. The occurrence of LTP and LTD in a single synapse might lead to synapse loss and cell death via over-excitation or inhibition, respectively. To be able to keep neuronal transmission and prevent synapse loss, neurons control their excitability with another plasticity mechanism, namely homeostatic plasticity.

1.1.2 Homeostatic plasticity

Neuronal networks have the ability to keep their activity at a basal state to maintain stable function when they face activity alterations during learning and development (Figure 1.3). During development, neuronal networks are hyperactivated to maintain strong synaptic connections, which are fine-tuned to basal states at later stages of development. Burst firing networks of the hyper-synchronized state of the brain are considered to be epileptic if they occur in adult brains; however, it is a sign of maturity of dissociated cultures *in vitro* (Chiappalone et al. 2006). The regulation of activity by homeostatic plasticity mechanisms occurs in a time scale of days. Those mechanisms are considered as homeostatic when the regulation maintains an average neuronal firing rate around some set-point value (Turrigiano 2012). There are many suggested homeostatic plasticity mechanisms, such as synaptic scaling (Turrigiano & Nelson 2004), homeostatic regulation of intrinsic firing (Marder & Prinz 2003), adjustment of the excitation-inhibition balance (Maffei et al. 2004), activity-dependent spine loss (Kirov et al. 1999) and tuning of intrinsic excitability (Marder & Goaillard 2006).

Synaptic scaling

Activity-dependent increase in synaptic strength of individual synapses by Hebbian mechanism (Abbott & Nelson 2000) can be scaled down by homeostatic mechanisms (Turrigiano 2008) to protect cells from over-excitation. Synaptic scaling is the ability of neurons to detect their firing rate changes through calcium-dependent mechanisms and as a result, alter receptor trafficking. Synaptic scaling is identified as bidirectional compensatory mechanism upon pharmacological manipulations of the network activity (Turrigiano 1999). As a result of altered network activity, miniature excitatory postsynaptic currents (mEPSCs), that represent the response of a postsynaptic neuron to neurotransmitter release, show increased or decreased amplitudes. This altered response is the result of a postsynaptic scaling mechanism, which changes the synaptic

strength up or down to compensate the activity (Desai et al. 1999).

Mechanistically, selectively blocking voltage-gated Na^+ channels with tetrodotoxin (TTX) or postsynaptic AMPA receptors leads to an upscaling of the synaptic strength via decreased Ca^{2+} signaling and reduced activation of calcium/ calmodulin-dependent protein kinase type IV (CaMKIV) (Ibata et al. 2008). As a result, AMPA-type glutamate receptors accumulate in the postsynaptic membrane. The abundance of AMPA receptors facilitates scaling up the miniature amplitude in the postsynaptic cell. The suppressed neuronal activity also causes enlarged active zones and increases the number of docked vesicles, which thereby facilitates the transmitter release and increased synaptic strength (Pozo & Goda 2010).

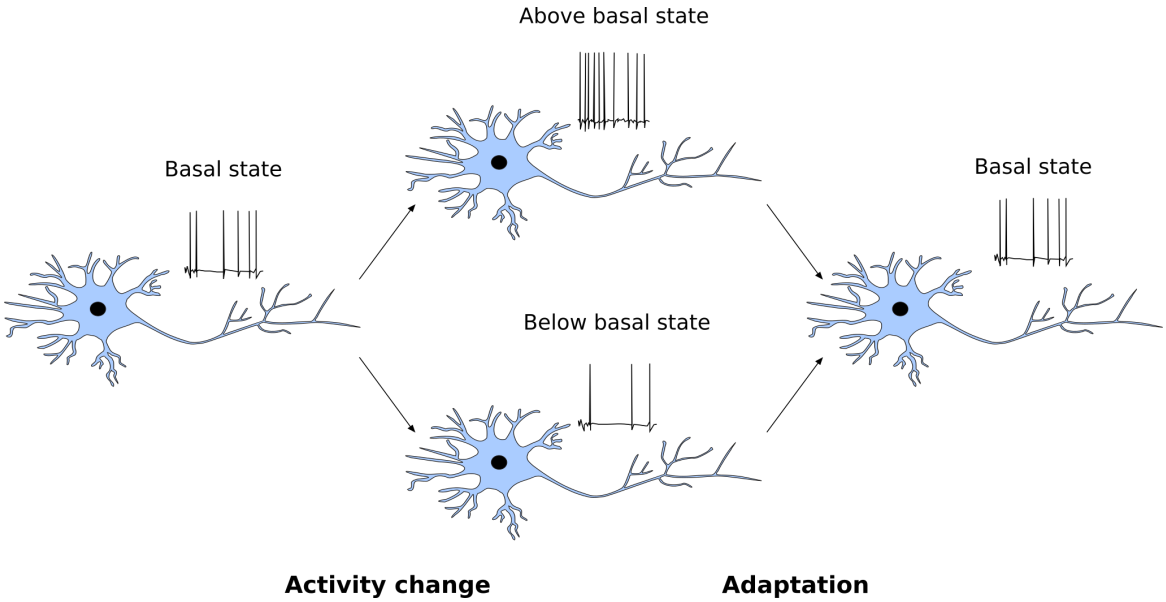

Figure 1.3: **Homeostatic plasticity.** Illustration of homeostasis of neuronal firing rate according to Turrigiano (2012). Activity perturbations induced by different mechanisms such as learning and memory formation might result in hyper- or hypo-active neurons. Neurons can adapt their firing rates by changing their synaptic properties (homeostatic synaptic scaling) or their ion channels composition which controls neuronal excitability (homeostatic intrinsic plasticity) via homeostatic mechanisms to restore the basal firing rates.

Elevated firing rate, on the other hand, leads to an enhanced calcium influx, activated CaMKIV signaling pathway, AMPA receptor removal and a scaling down of the synapse (Goold & Nicoll 2010). One of the identified calcium-dependent mechanisms is the immediate early gene Homer1a mediated signaling which includes the regulation of mGluRs and reduction of the tyrosine phosphorylation of GluA2 (Hu et al. 2010). Degradation of AMPA receptors upon ubiquitination is another proposed mechanism for

synaptic scaling which is regulated by elevated Eph4A activity (Fu et al. 2011). The enhanced firing rate also affects the presynapse causing a reduced number of docked vesicles and thereby neurotransmitter release (Moulder et al. 2004). Moreover, vesicular glutamate transporter v-Glut1 expression levels are also altered by homeostatic adaptations in the presynapse which causes further changes in the vesicular glutamate content (De Gois et al. 2005).

Intrinsic plasticity

Intrinsic plasticity is a form of homeostatic adaptation which mainly involves changes in the number, type, and distribution of the voltage-gated ion channels on the neuronal cell membrane. Extended blockage of neuronal network activity results in an upregulation of intrinsic excitability in cortical and hippocampal neurons (Desai et al. 1999). Conversely, increasing network activity above basal levels leads to a decrease of the excitability. Manipulations of neuronal excitability change the membrane conductance allowing the neuron to maintain stable output properties (Surmeier & Foehring 2004). This form of plasticity in hippocampal neurons involves calcineurin-dependent dispersion and changes in the gating of K^+ channels, reducing the cell's excitability (Misonou et al. 2004). Although the phenomenon of homeostatic intrinsic plasticity has now been widely investigated, very little is known about the underlying molecular mechanisms. Furthermore, the importance of homeostatic plasticity mechanisms during abnormal activity patterns in neurological diseases, particularly in epilepsy and their exact role in hyperexcitable disease states are to be elucidated.

One of the attempts to investigate the molecular role players in intrinsic plasticity has brought to light the REST/NRSF (Repressor Element-1 Silencing Transcription Factor/ Neuron-Restrictive Silencer Factor) protein in a 4AP model of increased activity (Pozzi et al. 2013). In addition to its role in reducing Na^+ channels as a result of intronsic plasticity, REST has been further shown to decrease the presynaptic vesicle pool (Pecoraro-Bisogni et al. 2017). The involvement of REST in various neurodegenerative diseases such as Huntington's disease (Zuccato et al. 2003), Alzheimer's disease (Lu et al. 2014), and finally as a candidate biomarker for plasma-based diagnoses of AD (Ashton et al. 2017) has been reported with some controversial results. Collectively, these studies outline that alterations in REST-dependent homeostatic plasticity may play a role in especially early stages of neurodegenerative diseases.

1.2 Alzheimer's disease (AD)

Alzheimer's disease (AD) is the most common form of dementia and it is characterized by progressive memory loss followed by personality changes, visuospatial deficits, loss of language skills and sometimes depression. One in ten people aged 65 and one in three over 85 years are affected by dementia. In 2015, there were 47.5 million people suffering from dementia and 70% of them were AD patients according to the Alzheimer's Association. By 2050, the projections point out that there will be 135.5 million people with dementia and approximately 95 million of them will be suffering from AD (Qiu & Fratiglioni 2017). AD is classified as early onset familial AD (FAD) where a single mutation in one of the PSEN2 (Levy-Lahad et al. 1995), PSEN1 (Sherrington et al. 1995) or APP (Goate et al. 1991) genes causes AD in an autosomal dominant manner and late onset sporadic AD (SAD) where several risk factors, both genetic and environmental, are thought to result in AD.

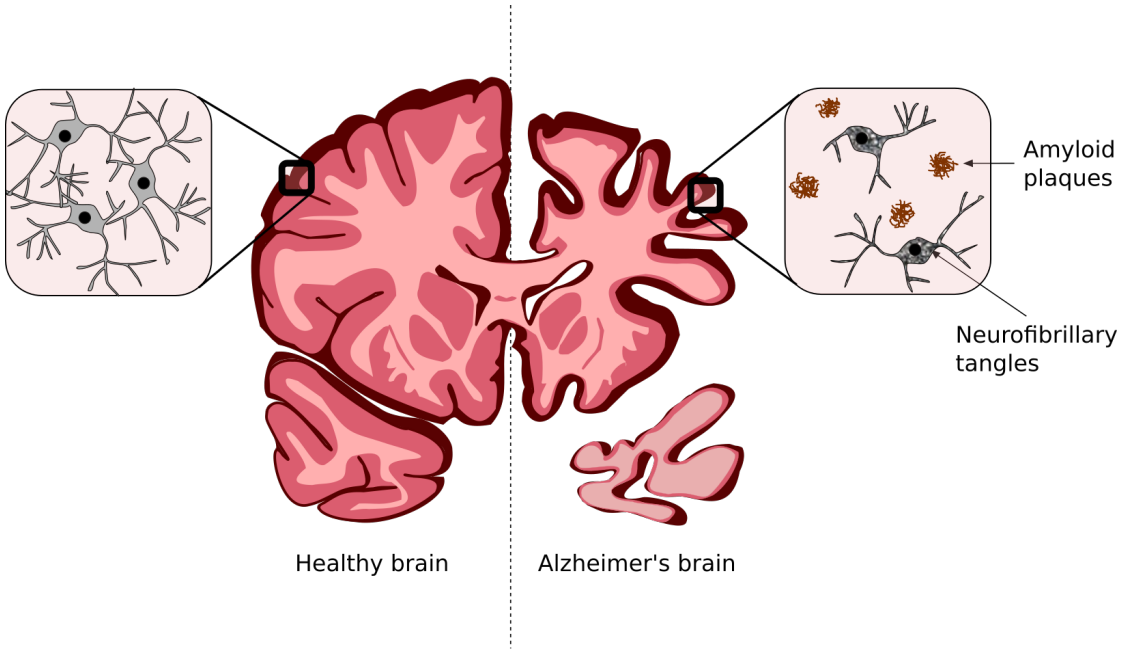

Figure 1.4: **Alzheimer's disease brain.** Illustration of healthy vs AD brain according to Holtzman et al. (2011). AD brain shows massive atrophy, cortical thinning, and larger ventricles compared to healthy brain. Extracellular insoluble amyloid plaques and intracellular accumulation of neurofibrillary tangles are the main pathologies of AD.

1.2.1 Symptoms and diagnosis

Alzheimer's disease has been first described by the German psychiatrist Alois Alzheimer (Alzheimer 1907). During the course of the disease, the patient first shows indications of

short term memory impairment such as forgetting simple words and misplacing things which were followed by losing the ability to process logical thoughts, showing erratic mood changes, paranoia and hallucinations. In later stages of the disease, deepest memories of the patient are erased and finally, heart rate and breathing control centers cease to function. Persistent and progressive memory loss and other cognitive deficits along with massive brain atrophy and pathological hallmarks of AD (Figure 1.4) results in impaired social and functional activities of daily life of a patient. Since AD is a condition which has a considerable impact on society, early diagnosis is crucial to inform and support patients and caregivers and to decide on suitable treatment strategies.

To date, there is no single test to diagnose Alzheimer's disease. However, there are several methods and tools to determine whether the patient might have Alzheimer's dementia or any other dementia-causing disorders. Traditionally, the post mortem investigation of AD-related hallmarks (plaques and tangles, see Figure 1.4) following a progressive cognitive deterioration of the patient was the main diagnosis of AD. Today, the diagnosis is mainly based on clinical assessments about overall health, the ability to carry out daily activities, and changes in behavior and personality since the disease is foremost characterized by early anterograde amnesia and as the disease progresses this is followed by a retrograde amnesia (Salmon & Bondi 2009). To evaluate cognitive status of the patient, Mini-Mental State Examination (MMSE) is commonly used (Tombaugh & McIntyre 1992). For the biochemical examination, the presence of Aβ and tau in the cerebrospinal fluid (CSF) is scanned (Blennow et al. 2010) since the senile plaques consist of the 42 amino acid long amyloid-beta peptide Aβ_{42} (Glenner & Wong 1984) and the hyperphosphorylated tau protein accumulates as tangles (Grundke-Iqbal et al. 1986). The tangle pathology mainly follows the transentorhinal, hippocampal, and extensive neocortical involvement reflecting the disease progression (Braak & Braak 1991). Furthermore, brain imaging analyses such as computed tomography (CT), magnetic resonance imaging (MRI), and positron emission tomography (PET) are also used routinely. The Pittsburg compound B (PiB) is a radioactive analog of the fluorescent amyloid dye Thioflavin which crosses the blood brain barrier (BBB) and allows in vivo imaging of Aβ with PET (Klunk et al. 2004). The studies using PiB confirmed the early Aβ deposition in the brain decades before the existence of any clinical symptoms of AD (Zhang et al. 2013).

1.2.2 Molecular neuropathology

Two major pathologies of AD are the extracellular senile plaques and intracellular neurofibrillary tangles (NFT) as first indicated by Alois Alzheimer (Alzheimer 1907). The extracellular senile plaques consist of a byproduct of the amyloid precursor protein (APP) which is extensively processed to release an active peptide ligand in AD (Allsop et al. 1988). APP is a type-1 transmembrane protein found in all mammals and it shares structural similarities with other family members called APLPs (APP like proteins, APLP1 and APLP2) (Müller & Zheng 2012). Even though they also share similar functions, they do not completely overlap since the single knockout (KO) mice of any of the members are viable but triple KO mice die early. On the other hand, Down syndrome patients (trisomy 21, APP is overexpressed) get AD early in life (Salehi et al). APP also functions as a signal protein which might have a role in axon formation and neurogenesis in adults (Müller & Zheng 2012). It has been indicated that neuronal stem cells subjected to APP antibodies showed decreased differentiation suggesting its function as an adhesion molecule of the developing brain (Sosa et al. 2017).

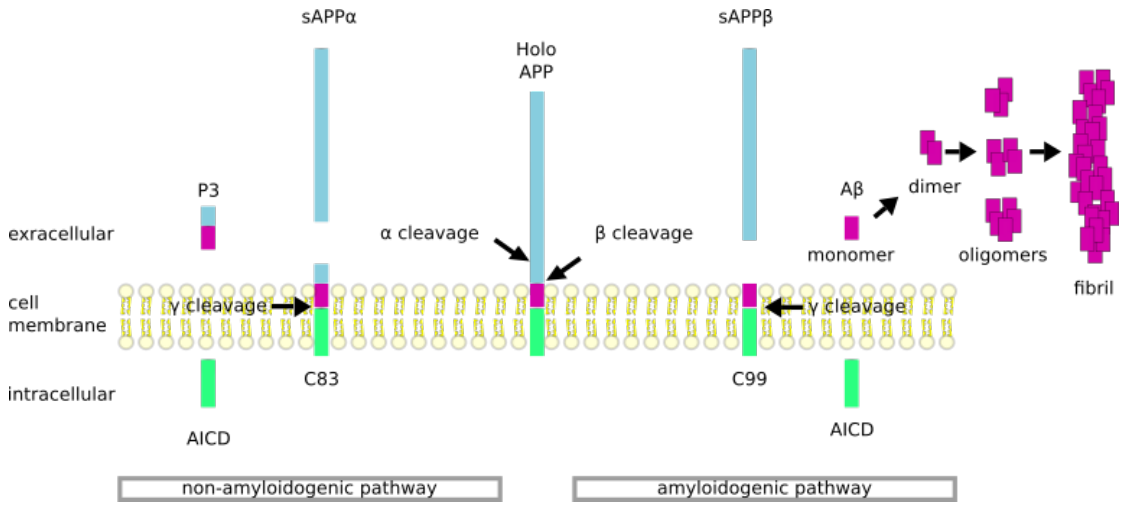

Figure 1.5: **Proteolytic cleavage of APP.** ccording to Zhang et al. (2011). Membrane-tethered APP (Holo APP) is cleaved by α- and γ-secretases via the non-amyloidogenic pathway. α-secretase cleavage releases neuroprotective sAPPα fragment. γ-secretase cleaves the C83-fragment resulting in the extracellular release of P3 and intracellular release of AICD. On the other hand, β-secretase cleavage via the amyloidogenic pathway allows the release of sAPPβ in the extracellular space and further γ-secretase cleavage leads to intracellular release of AICD and the release of Aβ in the extracellular space. Hydrophobic Aβ peptide further forms dimers and oligomers, and accumulate in non-soluble fibril forms. AICD: amyloid intracellular domain.

APP is processed by two main pathways (Figure 1.5): the non-amyloidogenic pathway

which primarily involves α-secretase (ADAM10) and the amyloidogenic pathway which involves β-secretase (Beta-Amyloid precursor protein Cutting Enzyme, BACE). In the non-amyloidogenic pathway, α-secretase cuts APP within the Aβ sequence and gives rise to the 83 residue-long C-terminal fragment (CTFα, C83) and the N-terminal fragment (NTFα) which is further cleaved by γ-secretase (a four-protein complex consisting of Presenilin1 or 2, nicastrin, PEN-2, and APH-1) into sAPPα and P3 fragment (Zhang et al. 2011). On the other hand, when APP is cleaved by the membrane bound β-secretase into the 99 residue CTF (C99) and NTF which is consecutively cut by γ-secretase into a heterogeneous group of Aβ peptides with various lengths between 38-43 amino acids and slightly different characteristics (Selkoe 2001). Furthermore, N terminally truncated or modified isoforms of the Aβ peptide were found (Portelius et al. 2010) which have different toxicity inducing abilities (Deshpande et al. 2006).

One of the main N-terminally truncated forms of Aβ is the pyroglutamylated ([Pyr3]Aβ_{3-42}) form which was found in frontal and entorhinal cortices of post mortem adult brains with AD (Mandler et al. 2014). A previous study pointed out that [Pyr3]Aβ_{3-42} is more frequently found in plaques of sporadic AD cases (Güntert et al. 2006). Furthermore, only [Pyr3]Aβ_{3-42} or [Pyr3]Aβ_{3-42}-containing Aβ_{1-42} oligomers showed prion-like activity with higher cytotoxicity compared to Aβ_{1-42} only oligomers in neuronal cultures and this effect was eliminated in the cultures of tau-knockout neurons (Nussbaum et al. 2012). This brings us to the neurofibrillary tangle pathology of AD.

The second hallmark of AD is the neurofibrillary tangle pathology which is found as bundles of abnormal fibers composed of the microtubule-associated protein tau intracellularly in neurons of the affected brain regions of AD patients (Buée et al. 2000). Microtubules are the neuronal cytoskeletal proteins and tau regulates the stability of the neuronal cytoskeleton which is vital to vesicle transport (Grundke-Iqbal et al. 1986). Total tau and phosphorylated tau levels are increased in both the brains and the CSF of patients with Alzheimer's disease (De Strooper & Karran 2016). In neurodegeneration, tau is hyperphosphorylated and loses the ability to stabilize the neuronal cytoskeleton. Hence, structural modification of neurons and impaired cellular transport mechanisms are followed by cell death (Gendron & Petrucelli 2009). However, the mechanism of increased and aggregated tau which is whether it is due to increased production or impaired clearance and the relation of tau with Aβ (directly downstream or in parallel) are not known.

1.2.3 The amyloid cascade hypothesis

The amyloid cascade hypothesis was first proposed in 1991 by John Hardy and Gerald Higgins. It suggests that the Aβ production as a result of APP dysmetabolism is the initiating factor, followed by aggregation of overproduced Aβ which contributes to neurofibrillary tangle formation, synaptic disruption, and ultimately dementia (Hardy & Allsop 1991) (Figure1.6). The 25-year old hypothesis has been leading the field of Alzheimer's disease research (Hardy & Selkoe 2002). This hypothesis mainly stems from familial genetic mutations which cause an increased Aβ production and additional harmful effects of Aβ on brain cells.

In recent years, growing evidence on Aβ deposition and AD challenged the leading hypothesis and hence some modifications of the hypothesis have been proposed. The main criticisms are the poorly correlated plaque load and dementia. Severity of dementia rather correlates with the number and location of neurofibrillary tangles than with the extent of senile plaque depositions (Bierer et al. 1995), and AD-like neurological symptoms occur prior to plaque deposition (Hsia et al. 1999). Furthermore, evidence on the pathological role of soluble oligomeric Aβ species such as synapse loss and memory impairment (Terry et al. 1991) supported the idea that plaques might be inert end products and possibly protect the brain from the toxic soluble Aβ species.

There is another challenging relationship between the plaques and the neurofibrillary tangles. It has been shown that even though the plaque load does not alter, transgenic mice with APP and tau mutations suffer from a more severe tau pathology than only tau expressing mice (Ashe & Zahs 2010). This contributed to the view that neurofibrillary tangles are downstream to Aβ pathology but not downstream to plaque formation.

Overall, although Aβ may not be the main culprit in AD pathology, Aβ deposition can be the signifying point of the irreversible pathological changes. Thus, it is critical to understand the mechanisms of Aβ-related alterations to find the optimal time point for interventions before the take over of the irreversible pathological cascade which may help to prevent further progression of the AD.

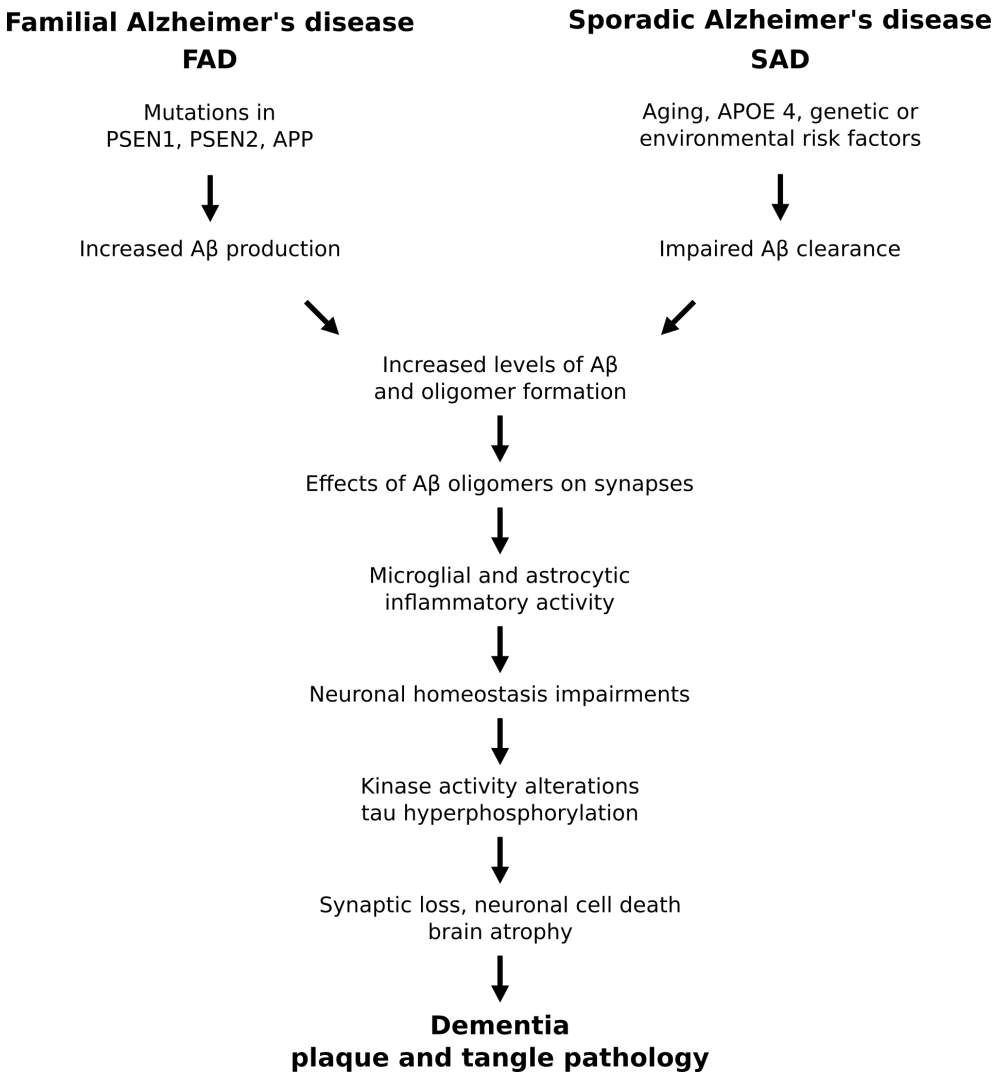

Figure 1.6: **Amyloid cascade hypothesis.** According to Selkoe & Hardy (2016). Altered Aβ metabolism in FAD or SAD leads to increased levels of soluble Aβ which is thought to be the initial step for the pathological downstream effects such as early synaptic alterations, inflammation, oxidative stress, and tau phosphorylation. Early on in this cascade, Aβ was shown to impair synaptic function. Later processes lead to neuronal dysfunction, cell death and dementia with the plaque and tangle pathologies.

1.2.4 Synaptotoxicity

The main issue related to AD is amnesia which impairs learning and memory. Since learning and memory are considered to be correlates of synaptic strength and plasticity, AD's main hallmark Aβ might primarily have an effect on synapses. This observation stems from studies in which APP overexpressing mice show fewer synapses and decreased spine density (Hsieh et al. 2006). Plaque bearing mice show excitatory synapse loss near the plaques (Koffie et al. 2009), on the other hand, APP KO mice have more synapses than wild type mice (Priller et al. 2006).

Hippocampal LTP is the main model to investigate synaptic changes (Martin et al. 2000).

Further research on Aβ-related synaptic alterations has been carried out predominantly in brain slices or primary neuronal cultures. FAD mutation carrying mice show LTP deficits in an age-related manner before plaque and tangle pathology (Oddo et al. 2003). It was reported that application of Aβ dimers isolated directly from Alzheimer brains to hippocampal slice preparations induces synapse elimination, impair synaptic plasticity and memory (Shankar et al. 2008). Naturally secreted Aβ oligomers lead to hippocampal LTP inhibition in vivo (Walsh et al. 2002). Emerging cellular models of AD with PSEN overexpressing hESC-derived neurons showed that the mEPSP frequency is decreased (Honda et al. 2016). Overall, reported findings support the hypothesis that AD is primarily a synaptic disease.

It has been extensively reviewed that Aβ inhibits LTP (Klein 2013), however, the exact mechanism is not yet clear. There have been various studies showing the pathways which Aβ acts through or interferes one of its proteins. Protein phosphatase 1 (Knobloch et al. 2007), c-Jun N-terminal kinase, cyclin-dependent kinase 5 (cdk5), and p38 mitogen-activated protein kinase as well as metabotropic glutamate receptor type 5 (Wang et al. 2004) were implicated in Aβ-induced LTP impairment. Moreover, Aβ inhibits several kinases such as Erk/MAPK, CaMKII, and the phosphatidylinositol 3-kinase activated protein Akt/protein kinase B (Townsend et al. 2007) and activates glycogen synthase kinase-3β (GSK-3β) (Takashima et al. 1996). The receptor for advanced glycation end products (RAGE) (Arancio et al. 2004) has been implicated in the Aβ-induced LTP inhibition.

There are also in vitro studies which suggest that LTD has a lower threshold (Hsieh et al. 2006) in APP overexpressing primary mouse hippocampal neurons and the mechanism involved in this process is glutamate uptake (Li et al. 2009) in primary mouse hippocampal neurons treated with Aβ. Interestingly, it has been shown that LTD can lead to synapse elimination (Nägerl et al. 2004) and the synaptic loss is correlated with the severity of AD-related symptoms (Scheff & Price 2003). The evidence presented in this section suggests that Aβ indeed leads to synaptic impairment. However, it is important to keep in mind that different Aβ preparations have different effects and acts through various mechanisms (Ladiwala et al. 2012).

Overall, the existing literature on AD is extensive and focuses particularly on Aβ induced synaptic failure. However, another significant aspect of AD is hyperactivity which was neglected for many years.

1.2.5 Hyperactivity

The main functional deficits in AD are the massive neuronal activity loss and synaptic failure. However, recent studies with animal models as well as early stage AD patients demonstrate that hyperactivity in various brain regions is not a coincidence. It was reported that neurological functions of AD patients fluctuate rapidly, which cannot be explained by neuronal loss. Instead, it is more likely that abnormal neuronal network activity is the reason behind rapid neurological changes (Palop et al. 2006). FAD patients showed hyperactivity and complex partial seizures before silencing of the networks (Noebels 2011). Further studies with animal models of AD showed that spontaneous nonconvulsive seizure activity in cortical and hippocampal networks might be associated with impaired GABAergic synaptic inhibition (Palop et al. 2007). In addition to decreased neuronal activity in animal models of AD, there are hyperactive neurons exclusively near the plaques which might be due to the decreased synaptic inhibition (Busche et al. 2008).

It has been reported that patients with sporadic and familial forms of AD share the seizure incidence (Palop & Mucke 2009). As suggested, the main reason behind the seizures might be the pathological accumulation of oligomeric Aβ-induced dysfunction of inhibitory interneurons and their contribution to the network destabilization (Palop & Mucke 2010). Further research had shown that inhibitory parvalbumin (PV) interneurons in hAPP mice had decreased levels of voltage-gated sodium channel subunit Nav1.1 (Verret et al. 2012) leading to impaired inhibition and epileptic seizures. In vivo two photon calcium imaging study showed that the early hippocampal hyperactivity was detected in young mice before the formation of plaques, suggesting that soluble Aβ species underlie this impairment. (Busche et al. 2012)

Seizures and epilepsy are not rare phenomena (Friedman et al. 2012) and the epilepsy drug levetiracetam showed an effective reduction in abnormal spike activity detected by electroencephalography (EEG). It reversed hippocampal remodeling, behavioral abnormalities, synaptic dysfunction, and deficits in learning and memory in hAPP mice (Sanchez et al. 2012). In early stages of AD, patients showed seizures and epileptiform activity (Vossel et al. 2013). This might be linked to the dendritic neurodegeneration caused by early hyperexcitability (Šišková et al. 2014) which has been recapitulated by different AD mouse models showing increased hippocampal excitability in 3xTgAD (Davis et al. 2014) and PS2APP mice (Fontana et al. 2017).

One of the main methods used to investigate network activity is the multi electrode array

(MEA). To date, a few attempts to monitor AD-related changes by MEAs have been made, however, they were mainly on synaptic effects of AD. It has been found that along with LTP impairment in transgenic animals, region specific synaptic changes occur at a young age before the occurrence of the typical amyloid or tau pathology (Chong et al. 2011). The decrease of neuronal activity by synthetic Aβ has been observed and reversed by using memantine (Charkhkar et al. 2015). A study using AD-CSF on rat cortical networks showed significantly enhanced burst durations (Görtz et al. 2013) which might be the first hint of epileptic discharges related to AD. Findings on AD-related hyperactivity bring us to the question whether enhanced neuronal activity during the presymptomatic stages of AD provide protection against the earliest disease processes or whether it is a pathogenic contributor to AD (Stargardt et al. 2015).

Collectively, these studies outline a critical role for hyperactivity rather than hypoactivity during early phases of AD. Growing evidence of Aβ-related seizures from AD mouse models and AD patients puts hyperexcitability and possible further excitotoxicity in the focus of AD-related research (Scharfman 2012). Therefore, hyperexcitability and epileptiform discharges in AD are long-neglected important phenomena to be investigated for future diagnosis and therapy.

1.2.6 Current treatment

Currently, there is no drug to slow down or stop the disease progression, synaptic, loss and neuronal atrophy; therefore, there is no cure for AD. Approved treatments are mainly symptomatic with variable effectiveness from patient to patient and 60 % of the treated patients face side effects like nausea, vomiting, loss of appetite, headache, confusion, and dizziness (Kumar et al. 2015).

Basal forebrain cholinergic neurons projecting to the hippocampus and the cerebral cortex are affected in the brains of patients with AD. Impairment in their cholinergic transmission were correlated with a decline in learning and memory, and a deficit in excitatory amino acid (EAA) neurotransmission (Francis et al. 1999). Therefore, a cholinergic substitution therapy, which inhibits acetylcholinesterase to allow the extended presence of acetylcholine at the synaptic cleft, was developed. Recently used cholinesterase inhibitors such as donepezil, galantamine, and rivastigmine can alleviate cognitive symptoms of mild to moderate AD (Kumar et al. 2015).

Excitatory amino acid neurotransmission, mainly the release and uptake of the neurotransmitter glutamate are thought to be impaired in AD. Memantine, an

uncompetitive N-methyl D-aspartate (NMDA) receptor antagonist is used for treatment of moderate to severe AD. The drug blocks the current flow through NMDA receptors and reduces glutamate-induced neurotoxicity (Johnson & Kotermanski 2006). A recent study is implying another mechanism of memantine action in AD models, which might reduce both insoluble Aβ and Aβ oligomer levels (Ito et al. 2017).

Investigating new treatment strategies is a continuing concern within the Alzheimer's field, therefore, establishing human models using emerging stem cell based assays might provide new insights into mechanisms of AD.

1.3 Induced pluripotent stem cells (iPSCs)

In 2007, human fibroblasts were reprogrammed to generate the first human induced pluripotent stem cells (iPSCs) (Takahashi et al. 2007) by the same method that was successfully used a year before to create mouse iPSCs via retroviral transduction of four transcription factor genes (Oct3/4, Sox2, Klf4, and c-Myc) (Figure 1.7) into mouse fibroblasts to obtain embryonic stem cell (ESC)-like cells (Takahashi & Yamanaka 2006). iPS cells have shown ES cell properties such as the capability of differentiation into cells of all germ layers; however, they had different global gene expression patterns. Since then, the interest in iPSC research and the number of laboratories working on iPSCs are increasing as iPSC research does not face the ethical problems linked to human embryonic stem cell research.

1.3.1 Induced pluripotency

During development, a fertilized egg cell (zygote) divides and reaches the 16-cell stage (morula) which is a ball like structure with identical totipotent cells and has the ability to develop into an organism (Moore et al. 2011). From this stage on, the morula develops into a blastocyst which has a distinguishable outer cell layer and inner cell mass, the source of embryonic stem cells which are pluripotent. Pluripotency is described as the ability of a cell to develop into the three primary germ cell layers such as ectoderm, mesoderm, and endoderm. Waddington's epigenetic landscape metaphor (Moris et al. 2016) explains why a neuron and a smooth muscle cell have enormous structural and molecular differences as a result of their differential transcriptomes which are regulated by epigenetic modifications. Waddington's hypothesis explains that a cell, which is represented as a pebble rolling down the landscape through the hills and valleys, changes the activity of genes during differentiation (Noble 2015). It suggests that

differentiated cells are only separated by "hills" (epigenetic barriers) and they have the ability to become another type of cell if the cell gains sufficient energy (epigenetic modifications) to overcome the barrier and even go back to the starting point (pluripotency). As the model suggests, it is possible to convert terminally differentiated cells to the stem cell stage (induced pluripotency) via a process called reprogramming.

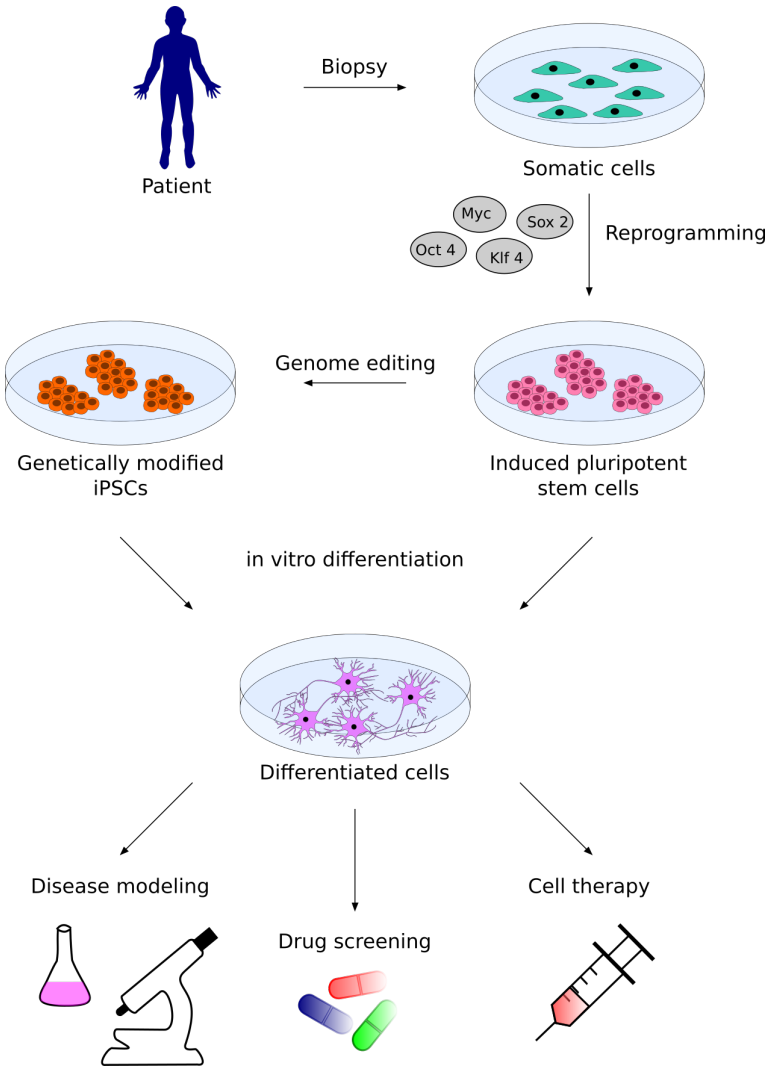

Figure 1.7: **Applications of induced pluripotent stem cells (iPSCs).** Illustration of iPSC generation, differentiation, and applications according to Sterneckert et al. (2014). Human cells can be removed by biopsy, cultured in a dish, and converted into iPSCs by introducing reprogramming factors (Myc, Sox2, Klf4, and Oct4). iPSCs can be differentiated into cells of interest with or without genetic modifications which allow researchers to investigate disease mechanisms, drug screening, and cell therapy.

1.3.2 Neuronal differentiation

The human nervous system develops from the ectodermal layer which forms the neural plate consists of neuroepithelial neural progenitor cells (NPCs). These cells are progenitors of the neurons and glia and they proliferate and migrate. Invagination of the neural plate results in the formation of the neural tube with radial glial cells and early born neurons. Radial glial cells further give rise to post mitotic neurons during brain development from the neural tube (Stiles & Jernigan 2010).

Neuronal differentiation from iPSCs follows human brain development. iPSCs represent the inner cell mass of the blastocyst which have the ability to produce any cell type of the human body. iPSCs are responsive to directed differentiation which leads to the formation of regional or subtype specific neural progenitor cells (Mertens et al. 2016). NPCs with a more posterior characteristic differentiate into spinal cord motor neurons or midbrain neurons which can be initialized with SHH, RA, and FGF2 or FGF8 treatments during the neural rosette stage, an in vitro correlate of the neural tube (Danjo et al. 2011). On the other hand, forebrain neurons develop via the inhibition of the WNT and SMAD signaling (Shi et al. 2012) using Dickkopf-related protein 1 (DKK1), Noggin and small molecules, such as SB431542 (Chambers et al. 2009). Dorsal forebrain structure gives rise to excitatory cortical neuron with CTIP2 (COUP-TF-interacting protein 2) -expressing deeper layer neurons (Chen et al. 2008) and SATB2 (special AT-rich sequence-binding protein 2)-expressing upper layer neurons (Alcamo et al. 2008), whereas medial and caudal ganglionic eminences give rise to cortical interneurons however their maturation takes a remarkably long time in vitro (Maroof et al. 2013).

Differentiated post mitotic neurons also need glial support to finally gain function with axonal and dendritic morphology and form synapses. A further astrocyte differentiation from astrocytic progenitors through initial iPSCs with FGFs and RA (for posterior patterning) and following ciliary neurotrophic factor (CNTF) treatment give rise to functional astrocytes in a time frame of 6 months (Mertens et al. 2016). The maturity of neurons can be tested via electrophysiological characterization. Although in vitro culture systems cannot recapitulate human brain development, the generation of 3D cerebral organoids from human iPSCs is a promising strategy to overcome this limitation.

The shortage of human neurons for experimental purposes was the main limitation for the investigation of human specific mechanisms of neurological diseases. Recent advances in neuronal differentiation of human iPSCs allow researchers to study neurodevelopmental and neurodegenerative diseases at the cellular level.

1.3.3 Application of iPSCs in AD modeling

Alzheimer's disease has been described more than 100 years ago and a considerable amount of literature has been published on AD using FAD mouse models. These studies contributed to our knowledge in the area of Aβ-induced synaptic and memory deficits however the models do not fully recapitulate distinct neurofibrillary tangle pathology.

The progress in iPSC field promotes the research of neurodegenerative diseases which was challenging because of the lack of human material. Researchers are investigating disease related mechanisms in patient-specific human iPSC-derived neurons in AD field. The first described study with patient specific iPSC-derived neurons carrying familial PSEN mutations showed elevated Aβ_{42} levels which were reversed by γ-secretase modulation (Yagi et al. 2011). Another study suggested that along with the elevated Aβ_{40} levels, phospho-tau(Thr 231) and active glycogen synthase kinase-3β (aGSK-3β) were increased in both FAD and SAD models (Israel et al. 2012). Further mechanistic study investigated the changes in endoplasmic reticulum (ER) and oxidative stress and the results were variable depending on the response of the cells generated from different patients (Kondo et al. 2013). Another study monitoring NSAIDs as γ-secretase modulators showed that their effects on Aβ_{42} reduction failed in human neurons derived from FAD iPSCs (Mertens et al. 2013).

To rule out the differences between the generated iPSCs as a result of the background patients' cells, the researchers investigated PSEN1 functions with a controlled isogenic genetic background which was established by using genome-editing technology with TAL effector nucleases (TALENs) (Woodruff et al. 2013). Furthermore, neurons carrying FAD mutation in APP showed alterations in subcellular location of APP and tau expression which was rescued by anti Aβ antibodies (Muratore et al. 2014). To note, this study compared the electrophysiological differences in spontaneous activity using a microelectrode array (MEA) platform and found no difference in spike shapes from control and FAD lines. The presence of APP in endosomes has been confirmed (Mahairaki et al. 2014) and the tau proteostasis was not only mediated through extracellular Aβ signaling since APP mutations led to increase total and phosphorylated tau but not PSEN1 mutations (Moore et al. 2015).

Gene expression studies with different FAD mutations from affected and unaffected individuals revealed differential expression of 14 genes from different gene families (Sproul et al. 2014) and genes of subunits of the proteasome complex (Hossini et al.

2015)

Human iPSC-derived neurons from healthy individuals has been used for drug secreening and Aβ toxicity. γ-secretase inhibitors, β-secretase inhibitors, and an NSAID showed differential Aβ secretion levels (Yahata et al. 2011). Aβ-mediated synaptotoxicity study using iPSC-neurons showed postsynaptic AMPA receptor density decrease and AMPA mini amplitude decrease with no effect on cell death (Nieweg et al. 2015).

Recent developments of culturing conditions allow the use of 3D iPSC-derived organoids or matrix-embedded 3D cultures for research. Hence, 3D cultures have a more stable local micro environment which 2D cultures lack upon media changes. Therefore, it may allow Aβ to form aggregates to mimic AD-like morphological changes. To this end, the first study with human neural stem cell derived 3D cultures with FAD background showed that Aβ plaques and hyperphosphorylated tau form and that inhibition of Aβ processing reduced those pathologies (Choi et al. 2014). Furthermore, a comparative study recapitulated the previously known aberrant activated p21-activated kinase (PAK) translocation upon Aβ sensing in 3D but not in 2D cultures (Zhang et al. 2014). More recent studies with 3D organoids with FAD backgrounds showed conflicting results where β- and γ-secretases lead to less potency reducing Aβ levels in one study (Lee et al. 2016) and reducing amyloid and tau pathology in another (Raja et al. 2016).

Overall, these studies highlight the need for human material to model neurodegenerative diseases. However, to recapitulate all disease-related pathologies remains challenging and the differentiation of cultures needs to be further optimized. All in all, such studies remain narrow in focus dealing only with molecular changes of AD and to date, no study attempted to investigate an early electrophysiological phenomenon such as hyperactive neuronal networks in human iPSC-derived neurons.

1.4 Aims of the study

Hippocampal hyperactivation and increased epileptic activity are common phenotypes in the early symptomatic phase of AD patients (Vossel et al. 2017). This study aimed at testing a hypothesis on how AD-related hyperactivity could result from increased amyloid beta (Aβ) levels. The hypothesis is based on the findings of two key-publications, showing that the transcriptional repressor REST (a) plays a major role in mediating homeostatic plasticity in hyperactive neuronal networks (Pozzi et al. 2013) and (b) is reduced in aged AD brains and Aβ treated human neurons (Lu et al. 2014). Together, these studies indicated that increased Aβ may cause epileptic activity by

impairing counteracting homeostatic plasticity responses in a REST-dependent manner. This study aimed at testing the hypothesis in functionally mature human neuronal networks derived from induced pluripotent stem cells (iPSCs).

The first part of this study focused on the development, maturation, and characterization of human neuronal networks. To this end, human iPSCs were targeted to small molecule directed differentiation. Post-mitotic neurons were purified and characterized to distinguish the neuronal subtypes in the cultures. Neuronal maturation was monitored and network parameters were extracted. Networks were used for toxicity assays.

Second, to develop a homeostatic plasticity model and to observe the homeostatic capacity of human neuronal networks, network activity was blocked or increased pharmacologically, the response of the networks was monitored and extracellular spike properties were analyzed for plasticity-induced changes related to neuronal excitability. The role of REST in neuronal homeostatic plasticity of human neurons was investigated.

Furthermore, to establish an AD model, synthetic amyloid beta (Aβ) oligomers were prepared, characterized and their effects on cell viability, synapse function, neuronal excitability, and network activity were investigated.

Finally, the homeostatic plasticity model was used to investigate the effect of Aβ oligomers on hyperactivity induced homeostatic plasticity and on REST regulation as a part of this process.

2. Materials and Methods

2.1 Cell Culture

2.1.1 Human iPSC culture

Thawing hiPS cells

Human induced Pluripotent Stem (iPS) cell lines (DF6 and 8/25 were previously described in Nieweg et al. (2015), SZ02 was reprogrammed by Shadaan Zulfiqar from human neonatal foreskin fibroblasts, NuFF1, GlobalStem) were kept in CryoStor (Sigma C2874) freezing medium containing cryotubes (Thermo Scientific 377267) in a liquid nitrogen tank. iPS cells were cultured under feeder-free conditions. Cells were thawed in a 37 °C water bath by shaking the vial gently. E8 medium (Table 2.1) was prepared by adding the components freshly and used only for maximum 2 days. The cell suspension was diluted in the pre-warmed E8 medium at a ratio of 1 part sample in 10 parts medium and centrifuged at 118 g for 3 min. The supernatant was removed with a pipette, leaving a small amount of medium to ensure the cell pellet is not disturbed. The cell pellet was resuspended in 2 ml fresh pre-warmed E8. The cell suspension was distributed in one well of a 6-well plate (Sarsted 83.3920) which was coated with Matrigel (BD 354277) at RT 1h prior to the plating. Cells were treated with 10 μM ROCK inhibitor (Tocris 1254) to block apoptosis, kept 37 °C incubator with 5 % CO_2 and 95 % humidity. After 24 h, ROCK inhibitor was removed and cells were maintained in the E8 medium with daily medium changes.

Table 2.1: E8

Reagent	Distributor	Catalog no	Concentration
DMEM/F-12	Invitrogen	31330-095	1X
bFGF	PeproTech	100-18B	20 μg/ml
TGFβ	PeproTech	100-21	2 μg/ml
ITS	Table 2.2		50X
P/S	Invitrogen	15140-122	100X
Ascorbic acid	Sigma	A8960	221 mM

Table 2.2: ITS

Reagent	Distributor	Catalog no	Concentration
DMEM/F-12	Invitrogen	31330-095	1X
Insulin	Sigma	I1882	10 mg/ml
Holo-transferrin	Calbiochem	616424	20 mg/ml
Sodium selenite	Sigma	S5261	1.4 mg/ml

Passaging hiPS cells

iPS cells were cultured in the E8 medium under feeder-free conditions. iPSC colonies in one well of a 6-well plate were passaged with PBS without calcium and magnesium (PBS-/-) every 7 d. In short, cells were washed 2X with 1 ml PBS-/- and incubated for 12 min with PBS-/- and scraped by using cell spatula (Biochrom 99010). The cell suspension was collected in E8 medium and centrifuged at 118 g rpm for 1 min. The supernatant was removed and the cell pellet was resuspended in 9 ml fresh pre-warmed E8 medium and cells were plated in a new Matrigel coated 6-well plate. Cells were kept in a 37 $^{\circ}$C incubator with 5 % CO_2 and 95 % humidity.

Neuronal differentiation of hiPSC cells

Induction of neural lineage was initiated with a 6-day long small molecule directed differentiation: 6 μM SB-431542 (Tocris 1614) and 1 μM DM (Tocris 3093) in N2B27 medium (Table 2.3). This strategy, known as the dual SMAD inhibition, was used to induce neural lineage by inhibiting tumor growth factor beta (TGFβ) and bone morphogenic protein (BMP) signaling cascades which allows rapid differentiation of confluent, feeder free hiPSC cultures into early neurectoderm (Chambers et al. 2009). On day 7 colonies were detached by incubating with PBS-/- for 5 min and rounding up of the colonies from the edges was observed under the microscope. Cell aggregates were scraped gently and collected in N2B27 medium and centrifuged at 66 g for 1 min. After removing supernatant, the pellet was gently resuspended in N2B27 medium and transferred into T-25 flasks (Sarstedt 83.1810.002) and kept in a 37°C incubator with 5% CO_2 and 95% humidity for 2 weeks to obtain rounded embryoid bodies (EBs). On day 21 the EBs were plated onto a Matrigel-coated 100 mm culture dish (Sarstedt 83.1802) containing the fresh N2B27 medium. Cells were maintained in a 37°C incubator with 5%

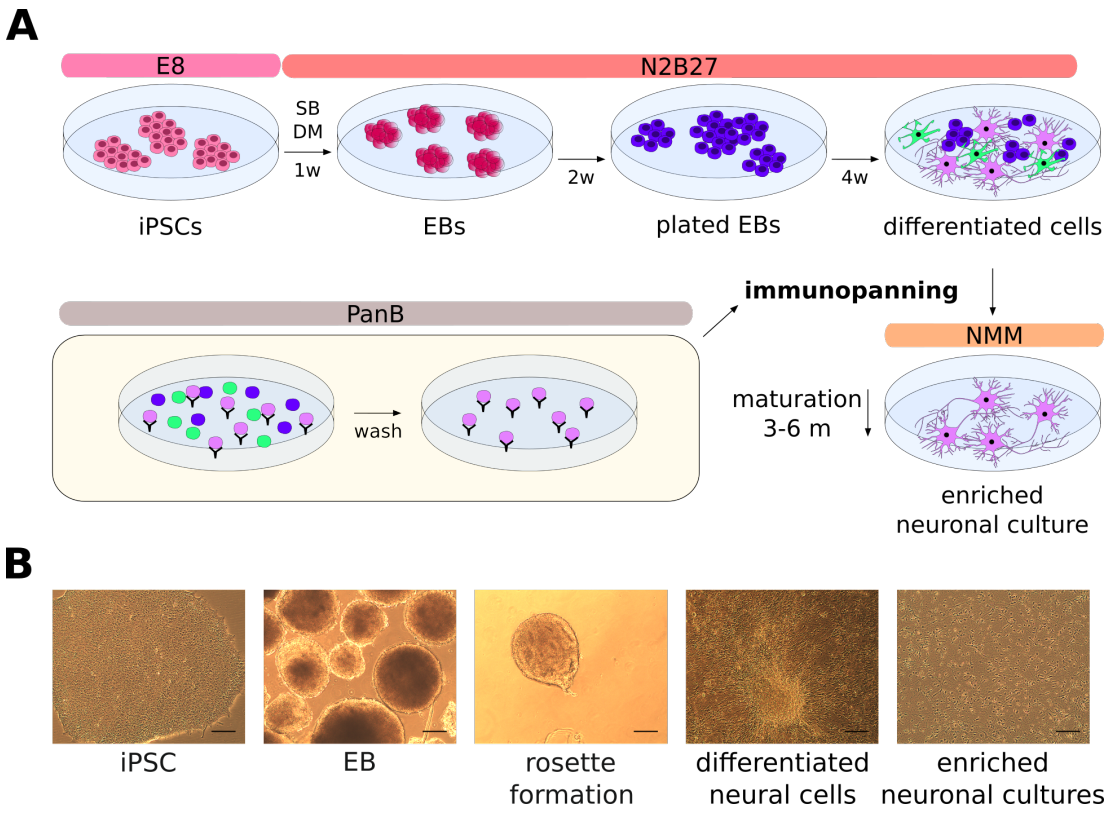

Figure 2.1: **Neuronal differentiation of iPSCs.** (A) iPSCs were maintained in E8 medium. Confluent iPSCs were treated with small molecules (SB-431542 and dorsomorphin) in N2B27 medium for 1 week. EBs were generated from detached colonies, and maintained in N2B27 medium for 2 weeks as non-adherent cultures and plated for further differentiation for 4 weeks. Differentiated cultures were enriched for neurons by anti-NCAM immunopanning. Further maturation of neurons was achieved by and incubated for 3-6 months of culture for further maturation in NMM medium. (B) Representative phase contrast images of neuronal differentiation of iPSC. iPSC: induced pluripotent stem cell, EB: embryoid body.

CO_2 and 95% humidity and the medium was changed weekly. After 4 weeks, differentiated cells with distinct processes were observed in the culture dishes and used for neuronal enrichment via the previously described method called immunopanning (Nieweg et al. 2015).

Immunopurification of hiPSC-derived neurons

To enrich the neuronal cultures by removing non-neuronal cells from the mixture, an immunopurification procedure so called immunopanning was performed. Culture dishes with bacterial quality (BD Falcon 351029) were used to prepare panning plates at least two day before the immunopanning. Plates were incubated with goat anti mouse IgG and IgM (Jackson labs, 115-005-068) in 50mM Tris/HCl, pH 9.5 (Sigma, T6066) at 4 °C ON for the attachment of the antibody to the plastic surface. On the following day,

Table 2.3: N2B27

Reagent	Distributor	Catalog no	Concentration
DMEM/F-12	Biochrom	FG4815	1X
NB	Invitrogen	21103	1X
B27 w/o RA	Invitrogen	12587-010	50X
Glutamax	Invitrogen	35050-038	100X
N2	Table 2.4		50X
P/S	Invitrogen	15140-122	100X
β-mercaptoethanol	Invitrogen	31350-010	50 mM
Heparine	Sigma	H3149	10 mg/ml

Table 2.4: N2

Reagent	Distributor	Catalog no	Concentration
DMEM/F-12	Biochrom	FG4815	1X
Insulin	Sigma	I1882	10 mg/ml
Holo-transferrin	Calbiochem	616424	20 mg/ml
Sodium selenite	Sigma	S5261	0.52 mg/ml
BSA	Sigma	S5261	10 mg/ml
Putrescine	Sigma	P5780	161 mg/ml
Progesteron	Sigma	P8783	0.62 mg/ml

antibody solution was removed, plates were washed with PBS-/-, and incubated with NCAM antibody (DSHB, VIN-IS-53) solution at 4 °C ON for the attachment of the primary antibody to the secondary antibody and kept until use.

On the day of immunopanning, NCAM solution was removed and kept at 4 °C. Plates were washed with PBS-/- and incubated with 0.2% BSA (Sigma A8806) containing PanB (Table 2.5) at RT to block antibody free areas. Cells were washed with PBS-/- and dissociated with accutase (Sigma A6964) at 37°C for 20 min. Detached cells were collected in a 15 ml tube (Greiner 188271) with 0.2% BSA containing PanB solution after scraping the plate gently and centrifuged at 223 g for 2 min. After removing the supernatant, cells were gently triturated with a P1000 plastic pipette tip. After each trituration step, the cell suspension was centrifuged at 30 g for 1 min to differentiate

Table 2.5: PanB

Reagent	Distributor	Catalog no	Concentration
Glucose	Merck	1083371000	0.1 %
Na-pyruvate	Invitrogen	11360	325 μM
PBS	Pan Biotech	P0436500	

single cells from the cell aggregates. Single cell-containing supernatants were collected in a separate tube. This process has been repeated until there was no visible pellet. The collected single cell suspension was centrifuged at 149 g for 13 min and supernatant was removed and the pellet was re-suspended in a 0.02% BSA containing PanB. Single cell suspension was further distributed onto previously prepared panning plates. Cells were kept on the panning plates for 8-10 min allowing only the attachment of neurons because of their highly expressed NCAM profiling. Unbound cells were immediately washed removed and weakly bound cells were removed at the end of the 20^{th} washing steps. After observing only the tightly attached cells under the microscope, cells were removed by forceful flushing and collected in a new tube. Cells were counted, centrifuged at 149 g for 13 min. The final pellet was re-suspended in NMM medium (Table 2.6) with the density of 5000 cell/μl) and plated on previously 1 mg/ml poly-l-ornitin (Sigma P3655)- and 10 μg/ml laminin (10 μl drop, Sigma L2020)-coated coverslips (Assistant 1001/12). Medium was added to the well after around 30 min, when cells had attached.

Maturation of hiPSC-derived neurons

Maturation of the cells was accomplished in NMM media enriched with 30 ng/ml BDNF (PeproTech 450-02) and laminin. 1 μM cAMP (Sigma D0260) was also used temporarily but did not result in an obvious improvement of neuronal maturation. For internal human astrocytic development, the cells were also treated with 1 μM DAPT (Cayman 13197) during the first week of maturation to stop proliferation and to allow further glial differentiation. Medium was replaced completely at the end of the first week and partially following weeks until experimental use of the networks.

To accelerate neuronal maturation, human neurons were co-cultured with primary rat cortical astrocytes (PCAs) in a ratio 10:1. PCAs were dissociated by washing with PBS-/-, incubating with trypsin, centrifuging at 184 g for 3 min, re-suspending in

Table 2.6: NMM

Reagent	Distributor	Catalog no	Concentration
NB	Invitrogen	21103	1X
B27	Invitrogen	12587-010	50X
Glutamax	Invitrogen	35050-038	100X
SATO	Table 2.7		50X
P/S	Invitrogen	15140-122	100X
Na-pyruvate	Invitrogen	31350-010	50 mM
BDNF	PeproTech	450-02	30 μg/ml

Table 2.7: SATO

Reagent	Distributor	Catalog no	Concentration
NB	Invitrogen	21103	1X
Insulin	Sigma	I1882	10 mg/ml
Holo-transferrin	Calbiochem	616424	20 mg/ml
Sodium selenite	Sigma	S5261	0.4 mg/ml
BSA	Sigma	S5261	20 mg/ml
Putrescine	Sigma	P5780	161 mg/ml
Progesteron	Sigma	P8783	0.62 mg/ml

astrocyte medium RCAM (Table 2.8), counting the cells, centrifuging at 184 g for 3 min, and again re-suspending in NMM to mix with human neurons. Co-cultures were treated with 1 μM DNA synthesis inhibitor Ara-C (arabinofuranosyl cytidine, Sigma C-6645) during the first week of maturation to kill proliferating cells. Cultures were checked regularly from 8-12 weeks on by calcium imaging and accepted as mature cultures only after observing synchronous activity.

2.1.2 Primary cortical neuronal (PCN) culture

Primary cortical neuronal cultures were prepared from embryonic day 18 (E18) Sprague-Dawley rats (Charles River Laboratories). Cortical neurons were cultured on coverslips or on 60 mm culture dishes, were maintained in NMM medium, and treated with 1 μM DNA synthesis inhibitor Ara-C (arabinofuranosyl cytidine) during the first 3-day of maturation to kill proliferating cells at 37 °C, 5 % CO_2. The medium was replaced completely to end

Ara-C treatment and partially following weeks until experimental use of the networks.

2.1.3 Primary cortical astrocyte (PCA) culture

Primary cortical astrocyte cultures were prepared from embryonic day 18 (E18) Sprague-Dawley rats (Charles River Laboratories). Cortical astrocytes were cultured in T25 culture flasks and were maintained in RCAM medium (Table 2.8) at 37 °C, 5 % CO_2. The next day, the medium was changed completely to remove all dead neurons and replaced regularly 3-4 days after they reached 50% confluence. For splitting and seeding for the cocultures, cells were washed once with PBS-/- to remove the growth medium completely and incubated with trypsin to detach the cells form the culture dish. For the cocultures, the procedure continued as described above and for splitting, 100 % confluent cultures were split in a 1:2-1:3 ratio, cultured in T25 culture flasks and were maintained in RCAM medium at 37 °C, 5 % CO_2. The following day, the medium was changed completely to remove cell debris and replaced regularly 3-4 days.

Table 2.8: RCAM

Reagent	Distributor	Catalog no	Concentration
DMEM High glucose	Invitrogen	11965-092	1X
FBS	PAA	A15-151	10X
L-glutamine	Invitrogen	25030081	100X
P/S	Invitrogen	15140-122	100X

2.1.4 CHO and 7PA2 cell culture

7PA2 cells, which stably express the V717F Alzheimer's disease mutation and the background Chinese hamster ovary (CHO) cells were cultured in CHOM (Table 2.9), in case of 7PA2 cells medium was supplemented with G-418 to select APP overexpressing cells. Every week cells were split in a 1:10-1:20 ratio. For splitting and seeding, cells were washed once with PBS-/- to remove the growth medium completely and incubated with trypsin (Gibco 25300-054) to detach the cells form the culture dish. To stop the protease activity of trypsin, fresh medium was used to dilute and the cell suspension was centrifuged at 184 g for 5 min. After discarding the supernatants, the pellet was resuspended in fresh medium, cells were counted and diluted for further plating. After 24 h of seeding, cells were used for further experiments.

Table 2.9: CHOM

Reagent	Distributor	Catalog no	Concentration
DMEM	Invitrogen	61965-026	1X
FBS	PAA	A15-151	10X
L-glutamine	Invitrogen	25030081	100X
P/S	Invitrogen	15140-122	100X

2.2 Amyloid-beta (Aβ)

2.2.1 Cell-derived Aβ

Soluble human Aβ oligomers were derived form 7PA2 conditioned medium. The supernatants of 7PA2 or CHO cells were collected after 72 h, centrifuged at 184 g for 3 min to remove cell debris, filtered, aliquoted, and kept at -80 °C until usage. For treatment, the 7PA2 conditioned medium was added directly to the iPSC-derived neural cultures and immunodepleted medium (incubating 7PA2-conditioned medium with IC16 antibody coupled to NHS-sepharose bead ON at 4 °C) used as a control for MEA experiments.

2.2.2 Synthetic Aβ oligomerization

Solubilization of monomeric Aβ was performed by dissolving lyophilized synthetic Aβ in HFIP (Fluka, 52517). Aβ_{1-42} was aliquoted at the end concentration of 8.576 μg/ 90 μl HFIP per tube. First 500 μl ice-cold HFIP was added in 1 mg Aβ_{1-42} (Bachem 4014447.1000) containing tube and incubated for 30 min at 37°C in the water bath. The solution was sonicated for 30 min at 37°C in the water bath and incubated for 30 min for final dissolving and cooled down on ice for another 30 min. Solution was transferred into an 8-ml glass vial (neoLab 2-7232). Original tube was rinsed 3X 500 μl HFIP and collected in the same glass vial. Then 2 ml HFIP was added and mixed. 2742 μl Aβ_{1-42} solution was transferred into a new glass vial for another mixture. The remaining solution was diluted further with 2036 μl HFIP, aliquoted in 2-ml glass vials (neoLab 2-7230) and kept at -80°C until usage. Pyroglutamylated Aβ_{3-42} ([Pyr3]Aβ_{3-42}, BioTrend BT-2987-01) was dissolved in HFIP at the final concentration of 8.19 μg/ 90 μl HFIP per tube. First 1000 μl ice-cold HFIP was added in 100 μg [Pyr3]Aβ_{3-42} containing tube and above-mentioned dissolving steps were performed. Next, 345 μl

[Pyr3]Aβ_{3-42} solution was transferred into a glass vial which were previously containing 2742 μl Aβ_{1-42} solution. The remaining solution was diluted further with 65 μl HFIP, aliquoted in 2-ml glass vials and kept at -80°C until usage.

For preparation of 95 % Aβ_{1-42} and 5 % [Pyr3]Aβ_{3-42} mixture (annotated as Aβ* in the rest of the thesis), the solution in the glass vial containing 2742 μl Aβ_{1-42} and 345 μl [Pyr3]Aβ_{3-42} was diluted with 4486 μl HFIP, mixed and aliquoted in 2-ml glass vials and kept at -80°C until usage. Vehicles were prepared by aliquoting 90 μl HFIP in 2-ml glass vials and kept at -80°C until usage.

To begin with the oligomerization protocol, vials were kept at RT to evaporate HFIP under a nitrogen stream for 30 min. Aβ and vehicle preparations were dissolved at the concentration of 5 μM in phenol free NB medium without supplements and incubated at 37 4°C or 4°C for 2 days. Oligomers were further analyzed by native, semi-native, and SDS PAGE followed by western blot to visualize the oligomerization profiling of different protocols. To treat the cells, prepared oligomers were further diluted to 2 μM concentration and media supplements were added. Treatments were done by adding prepared 2 μM Aβ oligomer solution following half medium removal from the culture dishes.

2.3 Patch-clamp recordings

Patch-clamp recordings were performed at RT to record electrophysiological characteristics of control, vehicle- and Aβ-treated cultures in whole cell mode. Coverslips were placed in the measuring chamber containing the standard extracellular solution (Table 2.10) under the phase contrast Axiovert 35M microscope (Zeiss). The patch pipette was prepared by pulling glass capillaries (Science Products GB150ETF-8P) using a horizontal programmable puller (Zeitz DMZ Universal Puller), filled with standard intracellular solution (Table 2.11) and had resistances of 5-7 MOhm. Electrophysiological data were filtered at 5 kHz and sampled at 20 kHz using Clampex Software (Axon Instruments) digitized a Digidata 1322A (Axon Instruments). Cells were approached via Narishige micro-manipulators (MHO-103) in presence of positive pressure. Thereafter, the pressure was released and negative pressure was applied along with a 3 mV stimulation pulse to obtain a Giga seal. Once the seal had been formed, the pipette was clamped at -60 mV and corrected for fast capacitance. After the pipette gained access to the cytosol, the cell capacitance contributed to the exponential decay in seal test (Figure 2.2).

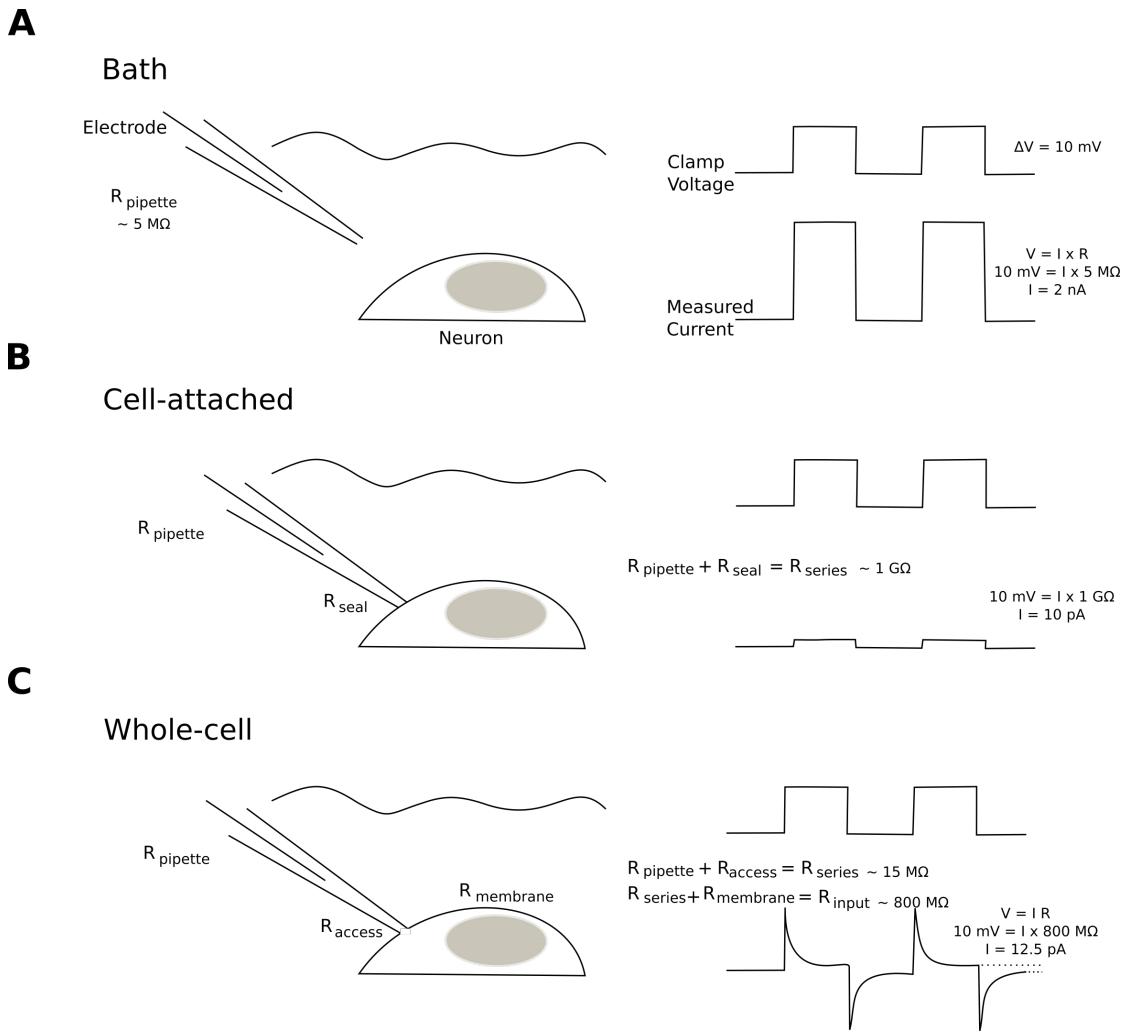

Figure 2.2: **Whole-cell patch clamp measurements.** According to application protocol of AxolBio (2016). (A) Micropipette with positive pressure in the bath solution. (B) Releasing the positive pressure helps the pipette to attach the neuron and resistance increases in the neuron attached form; therefore, current measured in oscilloscope decreases (middle). (C) Applying short pulsed suction to rupture the neuronal membrane allows the cell cytosol and the pipette solution to connect and increase in capacitive currents (bottom).

Table 2.10: Standard extracellular solution, pH 7.4

Reagent	Distributor	Catalog no	Concentration
NaCl	Sigma	S5886	130 mM
KCl	Roth	HN02.1	5 mM
$MgCl_2$	Roth	HN03.1	1 mM
$CaCl_2$	Roth	HN04.1	2.5 mM
HEPES	Roth	HN77.3	20 mM

Table 2.11: Standard intracellular solution, pH 7.4

Reagent	Distributor	Catalog no	Concentration
KCl	Roth	HN02.1	110 mM
KOH	J.T.Baker	0385	20 mM
$CaCl_2$	Roth	HN04.1	250 μM
HEPES	Roth	HN77.3	20 mM
EGTA	Merck	1.08435.0025	10 mM

2.3.1 Current clamp recordings

For current clamp recordings, the mode was switched to current-clamp, the resting membrane potential was noted at zero holding current, and then membrane potential was adjusted to -60 mV. For further analysis of the spiking properties and the passive membrane properties, 900 ms long current pulses (30 steps) were injected starting from -50 pA in a 10 pA increasing manner. Cells were classified according to their voltage responses including passive response, abortive response, single AP and repetitive AP. Input-output curves were plotted as the number of spikes versus the injected current. The amplitude was measured from the threshold to the maximum value for the first AP of 150 pA current injection. Maximum rising slope was calculated as the first time derivative of the amplitude. Half-width was determined as the duration of the AP at 50% amplitude. AHP was noted as the value after the AP peak to the threshold.

2.4 Calcium imaging

Calcium imaging was carried out by using Fura-2-AM (Sigma 47989), a cell membrane permeable, ratiometric calcium binding dye. The dye was de-esterified by cellular esterases to yield Fura-2 free acid. The ratio signal is independent of the dye concentration and illumination intensity which was the main advantage of using a ratiometric dye over a single wavelength probe. Fura-2 had an emission peak at 505 nm and changed its excitation peak from 340 nm to 380 nm in response to calcium binding. It exerts a high signal-to-noise ratio and allows to visualize neuronal activity (Smetters et al. 1999).

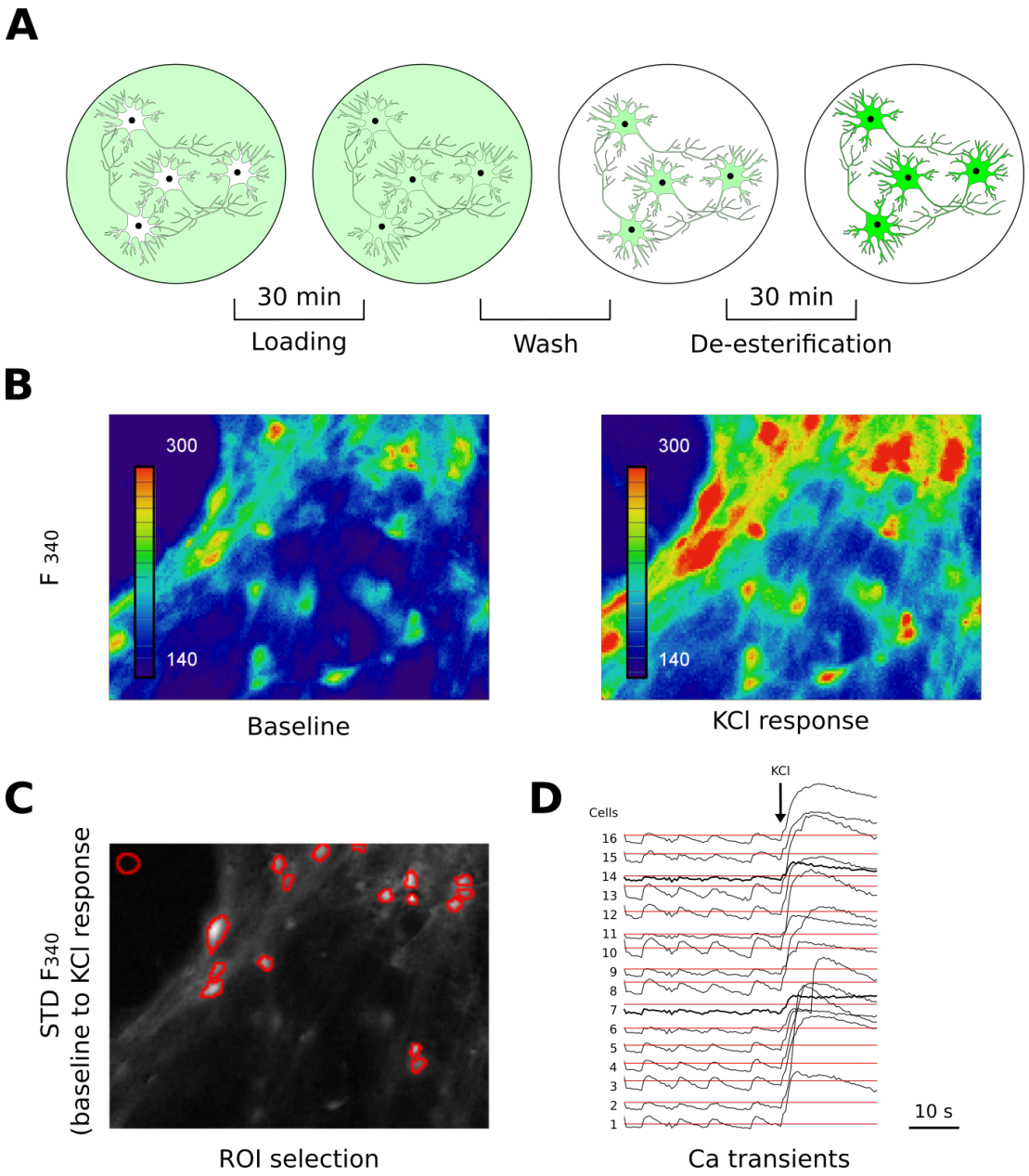

Figure 2.3: **Calcium imaging and analysis.** (A) For Fura-2 AM loading, cells were incubated in Fura-2 AM (green solution) for 30 min, the membrane-permeable acetylomethylester (AM) allows the dye to enter the cell. Extracellular dye was removed by washing. Incubation for 30 min for allowing de-esterification by cellular esterases to trap the dye in the cells (green cells). (B) Representative false color images of calcium bound Fura-2 AM at 340 nm excitation at baseline and 40 mM KCl response. (C) Standard deviation of 40 frames (25 frames before and 15 frames after the KCl treatment) at 340 nm excitation for the generation of regions of interest (ROI, red frames). (D) Time series analysis of calcium transients is plotted for the selected regions of interest. Red lines are the threshold values for each neuron calculated as the mean+5XSTD of the silent interval of each calcium transient.

To load the dye, cells were incubated with 3 μM Fura-2 AM in HEPES-Ringer buffer (Table 2.12) at 37°C for 30 min. The buffer was exchanged and cells were further incubated 20 min to allow for de-esterification of the dye (Figure 2.3). Fura-2-loaded

cells were placed under the microscope using 20x objective lens (Table 2.13). Calcium imaging was performed at 37°C. Fluorescent images at 340 nm and 380 nm were taken every 500 ms. 960 frames were recorded per coverslip, of which the first 400 frames represented baseline recordings, followed by 500 frames after acute 4AP (Tocris 0940) stimulation. Finally, 40 mM KCl was added to distinguish neurons from non-neuronal cells. Each coverslip was regarded as a single network and as an independent n.

Table 2.12: HEPES-ringer buffer (HRB), pH 7.4

Reagent	Distributor	Catalog no	Concentration
NaCl	Sigma	S5886	136.4 mM
KCl	Roth	HN02.1	5.6 mM
$MgCl_2$	Roth	HN03.1	1 mM
$CaCl_2$	Roth	HN04.1	2.2 mM
HEPES	Roth	HN77.3	10 mM
Glucose	Sigma	G70021	5 mM

Table 2.13: Equipments for Cal

Equipment	Distributor
IX70 Microscope	Olypmus, Hamburg, Germany
20 x Objective (oil)	Olympus, Hamburg, Germany
Immersion oil	Olympus, Hamburg, Germany
Polychrome IV lamp	TILL Photonic's, Gräfelfing, Germany
Lambda 10-2 optical filter changer	Sutter Instruments, Novato, CA, USA
TILLvisION software	TILL Photonic's, Gräfelfing, Germany

The data analysis was done with ImageJ. Regions of interest (ROI) were selected based on standard deviation of time projection images at 340 nm before (25 frames) and during (15 frames) KCl addition, followed by 2.5 % RenyiEntropy thresholding. The background was selected manually in a cell free region. Selected ROIs were analyzed for mean fluorescent intensities from 340 and 380 images and imported in Excel. Furthermore, the ratio of images were calculated after the background subtraction. Individual traces were off-set by their minimal value in the first 50 frames. Active cells were defined as cells showing at least one peak above the calculated threshold (Mean+5XSTD of a

manually selected silent part of the transient ratio for each ROI. Transient amplitudes were calculated from ratio traces of active cells. For the amplitude, 3 maximum values of ratio traces before, during, and post 4AP treatments were calculated and normalized to the pre-treatment condition. Transient frequencies were extracted from AOIs of the 340 nm / 380 nm ratio images of a field, which contained several neurons. Peaks were manually counted in the respective traces, representing the mean ratio intensity of an AOI.

2.5 Multi electrode array (MEA)

The MEA system (USB-MEA256-System) and the arrays used in this study were purchased from Multichannel Systems. They are standard arrays (8X8 conformation, 59 + 1 internal reference electrodes, W x D x H : 49 mm x 49 mm x 1 mm) with a 12 mm high glass rings. In-house built glass lids with plastic rings were used to keep cultures sterile during measurements. For the experiment, MEAs were washed, autoclaved, covered with 1 mg/ml PO and 10 µg/ml laminin (20 µl drop). iPSC-derived mature neuronal cultures were plated by removing the cultures from the glass coverslip and transferring them on the MEAs, directly on the laminin drops. After incubating several hours, NMM was added gently on the MEAs and incubated for 3 days.

Table 2.14: NB-Extra, pH 7.4

Reagent	Distributor	Catalog no	Concentration
NaCl	Sigma	S5886	65 mM
KCl	Roth	HN02.1	5 mM
$MgCl_2$	Roth	HN03.1	0.8 mM
$CaCl_2$	Roth	HN04.1	0 or 1.8 mM
NaH_2PO_4	Sigma	71505	0.9 mM
$NaHCO_3$	Sigma	S5761	26.2 mM
HEPES	Roth	HN77.3	10 mM
Glycine	Roth	3908.2	0.4 mM
Glucose	Merck	1083371000	25 mM
Na-pyruvate	Invitrogen	31350-010	1.2 mM
Glutamine	Invitrogen	25030081	1X
Phenol red	Sigma	P0290	0.0005 %

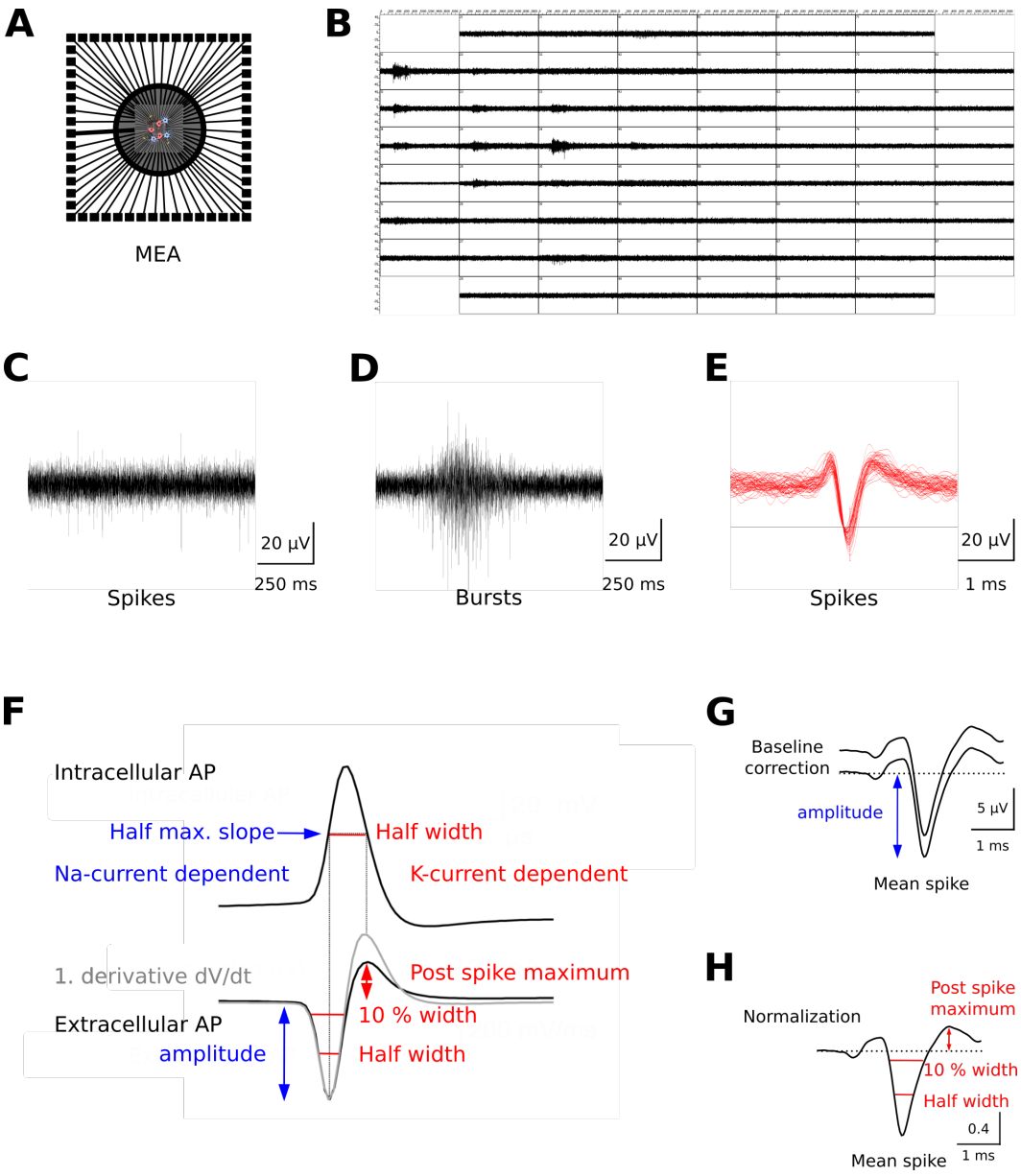

Figure 2.4: **Extracellular recording on multi electrode arrays (MEA).** (A) Illustration of standard MEA chip. (B) Data stream of synchronously burst firing network. Examples of (C) spike and (D) burst firing individual electrode. (E) Detected extracellular spike waveforms from an individual electrode. (F) The correlation of intracellular AP and extracellular AP. The first time derivative of the intracellular trace is superimposed on the extracellular trace (bottom trace, gray line). The half-maximal rising slope and the half-width of the intracellular AP (horizontal line) is represented on the extracellular spike (Bugaysen et al. 2010). (G) Baseline correction of the mean extracellular spike. (H) Normalization of the spike amplitude to 1 for extraction of widths and post spike maximum values.

Spontaneous electrical activity was recorded from MEAs at 37 °C (head stage heating) with constant 5 % CO_2 for 3 min. Signals were sampled at 25 kHz and stored on hard disc. Offline spike and burst detection were carried out by MC-Rack (Multi Channel systems) software. Measurements were done in NMM medium. For the calcium

dependent network activity measurements, the NB-extra solution (Table 2.14) was used.

2.5.1 Spike and burst detection

To detect spikes, a threshold of minus 5 times the standard deviation (-5XSD) of the mean noise amplitude was set. The detection threshold was run over 200 Hz high-pass Butterworth 2nd order filtered data stream which allowed to remove field potential since the threshold method for spike detection was used. An active channel was defined as channel which have fifty or more spikes per 3 minutes. Bursts were defined using the three criteria: min 5 spikes/burst, 100 ms minimum burst duration, 10 ms inter-spike-interval to count a spike in a burst. Data were presented as normalized mean spike or burst rate by calculating individual spike or burst rate in Hz for each array.

2.5.2 Extracellular spike parameters

The shape of the extracellular spike closely resembles the first time derivative of an intracellular action potential (Heinricher 2004) and therefore, the amplitude of a an extracellular spike represents the maximum rising slope of an intracellular action potential and thus correlates with the density of Na^+ channels on the axonal membrane (Bugaysen et al. 2010) (Figure 2.4F). On the other hand, alterations in the spike width (Bugaysen et al. 2010) and the post-spike maximum (Speckmann et al. 2015) of the extracellular spike correlate with K^+ conductance. Quantification of extracellular spike parameters like spike amplitude, half-width, 10 %-width, and post-peak maximum could give hints on changes in neuronal excitability (Na^+ and K^+ channel densities) as part of the homeostatic plasticity. In order to extract single spikes, raw data were filtered with Butterworth 2nd order low-pass 2000 Hz filter and spikes were detected by identifying the times of negative voltage deflections which drop below a threshold of minus 5 times the standard deviations of the mean noise amplitude (-5XSD), saving the -2 to +2 ms around the threshold crossing time. Up to 50 spikes per channel were selected from all active channels by placing the selection tool at the threshold crossing lane (Figure 2.4E), selecting all traces that pass at this point. The extracted spikes were sorted using visual basic for applications (VBA) editor in Excel (see Scripts and Macros). Excel macro imported .dat files extracted from a single channel in different time points and calculated the mean for the first 0.5 s to off-set the spike (Figure 2.4G). As the distance between electrode and cell as well as the electrode impedance affect the spike amplitude, amplitudes are highly variable between different MEAs and even electrodes of the same MEA. Therefore, each channel was analyzed separately. The amplitude

was extracted as the minimum value of the spike (Figure 2.4G). After each spike amplitude had been normalized to -1, half width, 10 %-width and post spike maximum values were extracted from each spike (Figure 2.4H) and compared between before, during and after treatment conditions for each active channel.

2.6 Immunocytochemistry

Immunocytochemistry was carried out according to the standard protocol. hiPSC-derived neurons grown on coverslips were washed once with PBS and fixed with 4 % paraformaldehyde (PFA, Table 2.15) for 13 min at RT.

Table 2.15: PFA

Reagent	Distributor	Catalog no	Concentration
PFA	Polysciences	18814	4%
PBS	Pan Biotech	P0436500	

Table 2.16: Permeabilization buffer

Reagent	Distributor	Catalog no	Concentration
Glycine	Sigma	50045	100 mM
Triton-X100	Sigma	X100	0.25 %
PBS	Pan Biotech	P0436500	

Table 2.17: Antibody buffer

Reagent	Distributor	Catalog no	Concentration
BSA	Sigma	A3059	2 %
Sucrose	Merck	10176871000	5 %
PBS	Pan Biotech	P0436500	

Cells were washed three times with PBS and permeabilized in permeabilization buffer (see Table 2.16) for 10 min at RT and blocked with 30 % goat serum (Invitrogen, 16210064) for 1 h at RT. Cells were incubated with primary antibody (primary antibodies used in Table 2.18) solutions ON at 4°C with gentle rocking. The next day cells were

washed three times with PBS and secondary antibody (secondary antibodies used in Table 2.19) solutions were added to the wells for 1h at RT. Optionally, DNA staining using DAPI (Sigma, D9542) was carried out during the first PBS washing step after the removal of secondary antibodies. After two more washing steps with PBS, the coverslips were rinsed with ddH2O, mounted on microscope slides using Fluor Safe Reagent (Calbiochem, 345789), dried ON at RT, and kept at 4°C until imaging.

Table 2.18: Primary antibodies for ICC

Reagent	Distributor	Catalog no	Concentration
Tbr1	Abcam	ab31940	1:500
Ctip2	Abcam	ab18465	1:200
GAD67	Millipore	MAB5406	1:500
Map2	Abcam	ab92434	1:1000
4G8	Covance	SIG-39220	1:1000
Satb2	Abcam	ab51502	1:50
Rest	Bethyl	IHC-00141	1:300

Table 2.19: Secondary antibodies for ICC

Reagent	Distributor	Catalog no	Concentration
anti-Ms-555	Invitrogen	A21424	1:1000
anti-Rb-488	Invitrogen	A11029	1:1000
anti-Rb-555	Invitrogen	A21429	1:1000
anti-Ch-488	Invitrogen	A11034	1:1000
anti-Ch-AMCA	JIR	103-155-155	1:1000

Imaging was performed using Axiovert 200 M inverted fluorescence microscope (Zeiss) equipped with a 12-bit monochrome CoolSNAP ES2 CCD camera (Photometrics). Four images per coverslip were taken with 20X objective for each wavelength with constant exposure times and the number of positive nuclei per total DAPI nuclei was calculated. n represents the number of coverslips.

For the REST staining, imaging was performed using LSM700 confocal microscope (Zeiss) equipped with a 63X, 1.4 NA oil objective. Five images per coverslip were taken with 63X oil objective. Maximum intensity projections of each image were calculated

with ImageJ. In case of MAP2 co-staining, MAP2 positive DAPI nuclei were selected and mean nuclear and cytosolic REST immunofluorescence intensities were extracted in ImageJ. Background was selected from the cell-free area. After background subtraction of REST channel, nuclear versus cytoplasmic ratio was calculated. n represents the number of cells.

2.7 Cell viability assay

The 3-[4,5-dimethylthiazol-2-yl]-2,5-diphenyl tetrazolium bromide or in short MTT (Sigma M2128) was used to measure cell viability in different conditions. The viable cells converted MTT substance into purple colored formazan salt which was dissolved in DMSO and measured by a spectrophotometer at a wavelength of 570 nm. The optical density of the dissolved substance indicated the amount of viable cells and the degree of cytotoxicity of the compound of interest.

Primary rat cortical neurons were isolated as described before and seeded on a 96-well plate. After treatments of the cells with compounds such as different Aβ preparations, 7PA2 conditioned medium, LiCl (Sigma L4408), X5050 (Millipore 5.06026.0001), and CHIR (Tocris 4423) to observe their effects on cell viability, cells were treated with 20 μM MTT (500 μg/ml) and incubated at 37 °C for 30 min to allow cells to convert MTT substrate to colored formazan crystals. After gently removal of the solution, the plate was shock-frozen at -80 °C. To dissolve the colored crystals, 150 μl DMSO added into each well of the plate and the absorbance was measured by a spectrophotometer (Fluostar OPTIMA, BMG Labtech) at a wavelength of 570 nm.

2.8 Protein analysis

2.8.1 Total protein lysates

Protein lysates were prepared by two different methods. Human iPSCs were collected directly in pre-boiled 2X sample buffer with fresh 50 mM DTT (Sigma D9779) by re-suspending and post-boiling for 5 min at 95 °C. CHO, 7PA2 cells and rat neuronal cultures were lysed by using RIPA buffer (Sigma R0278). Culture dishes were handled on ice during the procedure. Cells were washed 2X with 2 ml ice-cold PBS. 200 μl RIPA buffer with protease inhibitor cocktail (Roche 05892970001) and phosphatase inhibitor (Roche 04906845001) was added to the cells and incubated for 5 min. Cells were scraped and collected in microfuge tubes. Lysates were sonicated Branson Digital

Sonifier (102c, Branson Ulstrasonic Corporation) 50% pulse for 10 s with 500 ms on/off steps, centrifuged for 1 min at 2000 g to remove cell debris and the supernatant was collected for further protein concentration quantification.

2.8.2 Nuclear fractionation

Nuclear fractionation was performed to investigate the translocation of REST protein from cytosol to nucleus. For each condition, two PO-coated 6-cm tissue culture dishes covered with 2.5 million PCN isolated from rats. Cells were treated with an inhibitor (X5050) and activator (CHIR) of REST at the DiV 20 after spontaneous activity had been confirmed by calcium imaging. 2 days after, medium was removed, cells were washed twice with ice-cold PBS. Cells were collected by adding 200 µl of 0.1% NP-40 (+protease inhibitors) in PBS gentle scraping. Cell lysates were triturated, collected and gently pipetted into microcentrifuge tubes. 100 µl of each lysate was removed and kept in new microcentrifuge tubes as whole cell fractions. The rest of the lysates were centrifuged at 17000 g for 1 min a 4°C. The supernatant was transferred into a new tube as the cytoplasmic fraction. To remove remaining cytoplasmic proteins from the nuclear pellet, the remaining pellet was resuspended with 500 µl of 0.1% NP-40 (+protease inhibitors), centrifuged, and the supernatant was removed. Finally, the pellet was resuspended with 100 µl of 0.1% NP-40 (+protease inhibitors) and sonicated for 10 seconds. All fractions were stored at -80°C until use.

2.8.3 Quantification of protein concentration

To determine the protein concentration, Pierce BCA Protein Assay Kit (Thermo Scientific 23225) was used according to the manufacturer's instructions. A set of protein standards were prepared in RIPA which were containing 0-200 µg / 100 µl bovine serum albumin (BSA) for the standard curve. 10 µl of each standard and sample was pipetted into a 96-well plate (Nunc). 1:50 mixture of reagent B: reagent A were prepared and 200 µl mixture was pipetted into each well of the 96-well plate. The plate was incubated at 60 °C for 30 min. Absorption was measured at 590 nm using a microplate reader (Fluostar OPTIMA, BMG Labtech). Sample concentrations were calculated according to the standards and diluted with RIPA to ensure the equal amount of proteins in the samples.

2.8.4 SDS PAGE

Sodium dodecyl sulfate polyacrylamide gel electrophoresis (SDS-PAGE) was used to separate proteins due to their molecular weight in an electrical field. After protein

concentrations had been determined, 10 – 15 µg protein was mixed with 4x loading buffer (Laemmli buffer with 100 mM DTT) and heated for 5 min at 95 %C. Samples were loaded on 4 % stacking gel (prepared with 125 mM buffer Table 2.20, 4 % acrylamide, 0.1 % APS, 0.1 % TEMED) separated on a 10-12 % polyacrylamide gel (prepared with 375 mM buffer Table 2.8.4, 10 % acrylamide, 0.1 % APS, 0.1 % TEMED). Protein-Marker IV Prestained (Peqlab 27-2110) was used to determine the size of the proteins. Electrophoresis was performed initially at 80 V for 20 min to allow samples to reach the separation gel and increased later to 120 V for 1.5-2 h in running buffer (Table 2.22).

Table 2.20: Stacking gel buffer

Reagent	Distributor	Catalog no	Concentration
Tris	Roth	0188.2	0.5 M
HCl	Roth	4625.2	to set pH 6.8
ddH_2O			

Table 2.21: Separation gel buffer

Reagent	Distributor	Catalog no	Concentration
Tris	Roth	0188.2	1 M
HCl	Roth	4625.2	to set pH 8.8
ddH_2O			

Table 2.22: Running buffer

Reagent	Distributor	Catalog no	Concentration
Tris	Roth	0188.3	25 mM
Glycine	Roth	3908.2	192 mM
SDS	Roth	0183.2	0.1 %
ddH_2O			up to 1 l

2.8.5 Native and semi-native tris-tricine PAGE

Semi-native tris-tricine PAGE was established to separate and visualize oligomeric forms of Aβ by using Biorad Mini-PROTEAN system. In order to sustain high molecular weight oligomers of Aβ, 0.1% SDS was only added to the electrophoresis buffer (Table 2.23). 150 - 200 ng Aβ oligomers were mixed with 4x native loading buffer (125 mM Tris-HCl pH 6.8, 40 % Glycerol, 0.01 % Bromophenol blue) and the mixture was loaded on a 4 % stacking gel (prepared with 125 mM buffer Table 2.22, 4 % acrylamide, 0.1 % APS, 0.1 % TEMED) separated on 18% polyacrylamide gel (prepared with 1 M buffer Table 2.22, 4 and 18 % acrylamide, 0.1 % APS, 0.1 % TEMED). SeeBlue Plus2 Pre-stained Protein Standard (Invitrogen LC5925) was used to determine the size of the oligomers. Electrophoresis was performed initially at 80 V for 20 min to allow samples to reach the separation gel and increased later to 120 V for 2.5 - 3 h in semi-native running buffer (Table 2.23). Furthermore, native tris-tricine PAGE was perfomed as semi-native except that the running buffer did not include any SDS.

Table 2.23: Semi-native gel buffer

Reagent	Distributor	Catalog no	Concentration
Tris	Roth	0188.2	3 M
HCl	Roth	4625.2	to set pH 8.45
ddH_2O			

Table 2.24: Semi-native running buffer

Reagent	Distributor	Catalog no	Concentration
Tris	Roth	4855.2	100 mM
Tricine	Roth	6977.2	100 mM
SDS	Roth	0183.2	0.1 %
ddH_2O			up to 1 l

2.8.6 Western blot

After electrophoresis, separated proteins were transferred either to polyvinylidene fluoride (PVDF) or nitrocellulose Amersham membranes (GE Healthcare 10600021, 10600002, respectively) according to the sizes of separated proteins. For analysis of

Aβ, oligomers were blotted to a PVDF membrane. All other proteins were blotted to nitrocellulose membranes. PVDF membranes were first activated in ethanol and then incubated for 10 min in 1 x transfer buffer (Table 2.24) before blotting. All other materials such as Whatman papers, sponges, and gels were incubated for 5 min in transfer buffer. Blotting apparatus (BioRad) was filled with the membrane to the anode and gel to the cathode in between Whatman paper and sponge layers. Blotting was performed either 25 V and 4 °C ON or 100 V at RT for 2 h in transfer buffer.

Table 2.25: Transfer buffer

Reagent	Distributor	Catalog no	Concentration
Tris	Roth	0188.3	25 mM
Glycine	Roth	3908.2	192 mM
Ethanol	Roth	5054.4	200 ml
ddH_2O			up to 1 l

Table 2.26: Blocking buffer

Reagent	Distributor	Catalog no	Concentration
Roti-Block	Roth	A151.1	10X
ddH_2O			up to 20 ml

Table 2.27: TBST

Reagent	Distributor	Catalog no	Concentration
Tris	Roth	AE15.2	50 mM
NaCl	Roth	3957.1	150 mM
Tween 20	Sigma	P1379	0.1 %
ddH_2O			up to 1 l

The membrane was blocked with blocking buffer (Table 2.25) under gentle shaking at RT for 1 h. Primary antibody dilutions were prepared in blocking buffer. Membranes were incubated with antibody solutions ON at 4 °C. control. The next day, membranes were washed three times with TBST (Table 2.26) for 10 min and incubated with the appropriate HRP-conjugated secondary antibody (diluted in blocking buffer, Table 2.8.6)

Table 2.28: Primary antibodies for WB

Reagent	Distributor	Catalog no	Concentration
4G8	Covance	SIG-39220	1:1000
6E10	Covance	SIG-39320	1:1000
βIII tubulin	Covance	PRB-345P	1:30000
GAPDH	Calbiochem	CB1001	1:20000
Rest	Millipore	09-019	1:1000
SNAP25	SynSys	111011	1:1500
Lamin	Abcam	ab16048	1:1000

Table 2.29: Secondary antibodies for WB

Reagent	Distributor	Catalog no	Concentration
anti-Ms-HRP	SantaCruz	sc-2055	1:4000
anti-Rb-HRP	SantaCruz	sc-2054	1:10000

for 1 h at RT. Membranes were washed three times with TBST and once with TBS before developing with Western Bright Quantum ECL reagent (Biozym 541015) according to manufacturer's instructions.

2.8.7 myc-REST overexpression in HEK cells

The plasmids, msREST-myc and empty vector (kindly provided by Pietro Baldelli), were recovered by cutting the DNA-containing circles from the filter paper and immersing the circles in 50 µl of ddH_2O in microcentrifuge tubes (Sarsted 72.706.200). After centrifuging for 1 min at 17000 g, 1 µl plasmid was used to transform competent bacteria. In short, 100 µl competent bacteria was mixed with 20 µl 5X KCM (Table 2.30), 80 µl ddH_2O, and 1 µl plasmid DNA on ice. Mixture was incubated on ice for 20 min, at RT for 10 min and following 1 ml LB (10 % trypton, 5% yeast extract, 10 % NaCl, pH 7.5) addition, at 37 °C for 50 min at 850 rpm on the thermomixer (Eppendorf 22331). 100 µl mixture was scraped on LB-agar plates (10 % trypton, 5% yeast extract, 10 % NaCl, 15 % agar, pH 7.5). The next day selected colonies were inoculated in 5 ml LB containing tubes.

Plasmids were purified using the QIAGEN Plasmid Plus Mini Kit (Qiagen) according to the manufacturer's protocol. Plasmid DNA-concentrations were measured with a

Table 2.30: KCM Buffer, 5X

Reagent	Distributor	Catalog no	Concentration
KCl	Roth	HN02.1	500 mM
$CaCl_2$	Roth	HN04.1	150 mM
$MgCl_2$	Roth	HN03.1	250 mM

NanoVue Plus Spectrophotometer (Implem, GE Healthcare). HEK cells were seeded in 6 cm dishes (83.3901) and after they reached 90 % confluence, cells were transfected with Lipofectamine 2000 (Invitrogen 11668019). 3 µg of DNA plasmid were diluted in 300 µl Opti-MEM (Invitrogen 31985070) and 6 µl of Lipofectamine 2000 were diluted in 300 µl Opti-MEM. Two dilutions were mixed by pippeting and the mixture was incubated for 20 min at RT. The medium of the HEK cells were refreshed and the 600 µl mixture were added dropwise to the dishes. Empty vector was prepared in the same way and used as control vector. Cells were incubated for transfection for 5 h. Medium was replaced completely. Transfection was monitored by fluorescence microscope (GFP expression) and cells were lysed for further WB analysis.

2.9 Softwares

Softwares used in this study according to experimental set-ups:

Immunocytochemistry images were taken by ZEN software (ZEISS) and imported into ImageJ (National Institutes of Health) for cell counting or intensity measurements.

Western blot membranes were developed by using Chemidoc-XRS software (Bio-Rad), exported images were modified and quantified in ImageJ.

Patch clamp data acquisition was carried out using Clampex (Axon Instruments). Data was imported in Clampfit (Axon Instruments) for extraction of parameters.

Calcium imaging data acquisition and extraction were done with TILLvisION software (TILL Photonic), ROI selection and image processing was done by ImageJ.

MEA data acquisition and data extraction were carried out with MC_Rack (MultiChannel systems), calculations were performed in Excel with VBA editor (Microsoft).

The data from all experiments were calculated in Excel, figures and statistical tests were made in GraphPad Prism 6 software (GraphPad Software), Figures were combined in

Inkscape and imported in TeXstudio.

2.10 Statistics

GraphPad Prism 6 software was used for statistical analysis. Statistical tests used in each figure were stated in respective figure legends. Error bars represented standard errors of the mean (SEM).

3. Results

3.1 Generation and characterization of human iPSC-derived neuronal networks

3.1.1 Generation of human iPSC-derived neuronal networks

To generate mature human neuronal networks, human induced pluripotent stem cells were differentiated via triggering neural induction by inhibiting TGFβ and BMP pathways (Chambers et al. 2009) with small molecules such as SB-431542 and DM. Embryoid bodies (EBs) were generated from induced cells for further neural differentiation in this well-established three dimensional cell aggregate. After two weeks in suspension culture, EBs were attached to matrigel coated dishes for further proliferation of neurogenic progenitors and final differentiation of neurons. Differentiated neural cultures were purified by anti-NCAM immunopanning to obtain enriched neuronal cultures (Figure 2.1). In order to obtain functionally mature neuronal networks, neurons had to be further cultured for three to six months (network maturation). In the first week after immunoisolation, proliferation of persisting, NCAM-positive neural stem cells (NSCs) was inhibited and their differentiation was induced by treatment with DAPT (10 μM for 7d). DAPT is a gamma-secretase inhibitor, which prevents notch cleavage and thus NSC maintenance (Imayoshi et al. 2010). Eventually, these cells differentiated into astrocytes, as after 1-2 months of maturation, neurons, as well as astrocytes, could be detected in the immunopurified cultures. The developing cultures were evaluated by their firing characteristics by using different strategies such as multi electrode array and calcium imaging. Maturation of synaptically connected neural networks required a culture time of three to six months. As maturation of the endogenous human neuron-astrocyte cocultures was not very reliable, the culture system was optimized for accelerated network maturation. Therefore, freshly immunoisolated neurons were plated together rat cortical astrocytes and treated with ARAC (1 μM for 7d), in order to eliminate proliferating NSCs. These cultures showed a higher reproducibility and developed mature networks within 8 weeks.

3.1.2 Characterization of neuronal subtypes

3.1.2.1 Immature neurons express deep layer cortical markers

In order to characterize the generated human neuronal networks, iPSC-derived human neurons were immunostained for cortical markers of different layers markers, one day after immunopanning. Tbr1 (T-box, brain, 1) and Ctip2 (chicken ovalbumin upstream promoter transcription factor-interacting protein 2) are expressed in early-born deep layer neurons, whereas Satb2 (special AT-rich sequence-binding protein 2) is an upper layer marker. GAD67 (glutamic acid decarboxylase 67) was used to identify GABAergic interneurons. MAP2 (microtubule-associated protein 2), which is abundant in soma and dendrites (Caceres et al. 1984), served as the pan-neuronal marker (Figure 3.1A). In three independent experiments, the percentage of MAP2 positive neurons, expressing each marker was quantified. Due to the early developmental stage of the cultures, excitatory neurons exhibited mainly deep layer cortical characteristics (Figure 3.1B). Only 15% of the neurons were GABAergic interneurons.

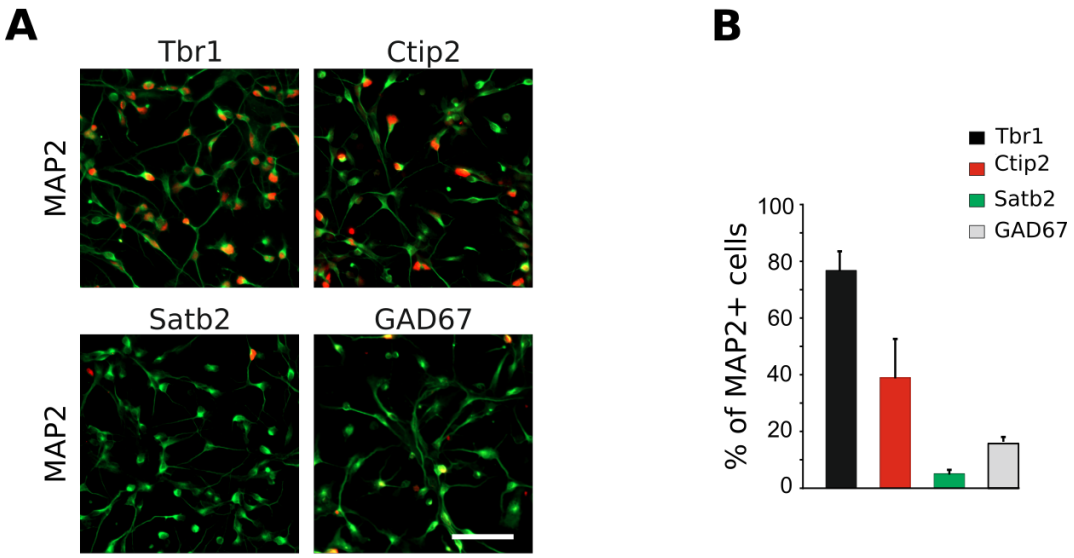

Figure 3.1: **Characterization of human iPSC-derived immature neurons.** (A) Fully differentiated neurons express pan-neuronal marker MAP2 (green) and cortical markers Tbr1, Ctip2 (deep-layer markers), and Satb2 (upper-layer marker), as well as GABAergic marker GAD67 (red). (B) Quantification of neurons expressing Tbr1 (black bar; 76.7±3.9), Ctip2 (red bar; 40±7.9), Satb2 (green bar; 5±0.8) and GAD67 (grey bar; 15±0.9), n=3. Scale bar represents 50 μm. All values are represented as mean, error bars show standard error of mean (SEM).

3.1.2.2 Interneurons remain functionally immature

To investigate whether interneurons present in the human cortical-like neuronal networks gained functional maturity, I performed gabazine treatments in combination with multi electrode array (MEA) measurements after 5 months of network maturation.

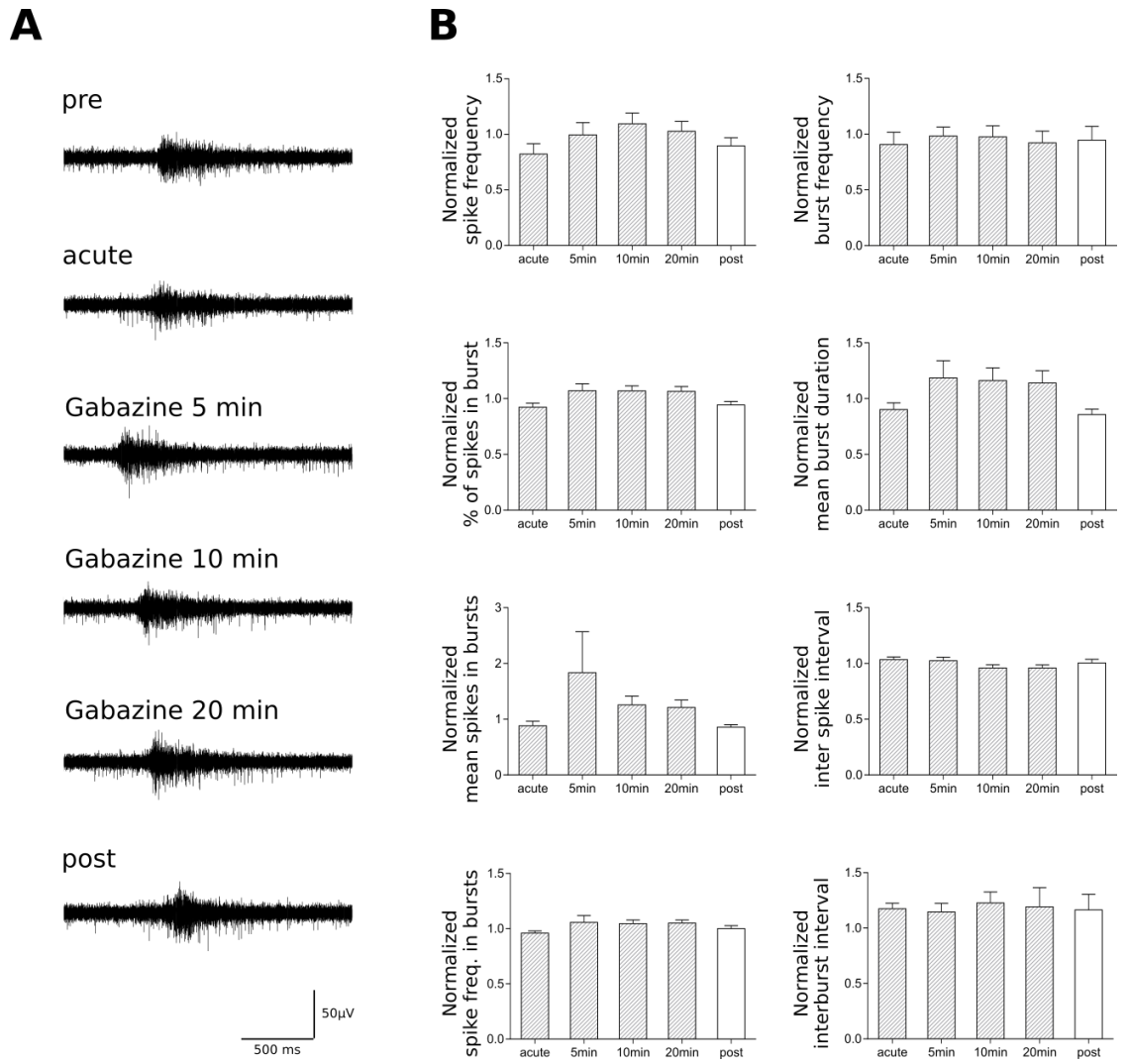

Figure 3.2: **Analysis of interneuron function in cortical-like actively firing neuronal networks.** Neuronal cultures that had reached a maturity stage, where synchronous bursting was detectable, were tested for the presence of functional interneurons by treatment with the GABA-A receptor antagonist gabazine. (A) Representative voltage traces recorded on MEAs before, during and after washout of 20 µM gabazine. (B) Bar graphs represent normalized (mean±SEM) activity parameters measured by MEA recording of neuronal cultures incubated for 5, 10 and 20 min with gabazine and after washout. Each measurement was normalized to the baseline value, recorded before the gabazine treatment (pre). No significant differences were observed (one-way ANOVA followed by Bonferroni's test), n=5 MEAs.

At this stage, networks showed an activity pattern with synchronous burst firing. MEA

cultures were incubated with the GABA-A receptor antagonist for up to 20 min and recorded before, during and after treatment. Although 15% of GABAergic interneurons were present in the immature cultures immediately after panning, no significant change in firing rate nor any of the other activity parameters was detected (Figure 3.2).

In the immature brain, GABA is excitatory and only becomes inhibitory after delayed expression of a chloride exporter, which leads to a shift in the reversal potential for chloride ions (Ben-Ari 2002). Thus, depending on the developmental stage of the cultures, gabazine was expected to either decrease or increase the network activity. The absence of any response indicated non-functional GABAergic synapses or the elimination of interneurons during network maturation.

In conclusion, hiPSC-derived neuronal networks mainly consisted of deep layer excitatory neurons, without any functional interneurons.

3.1.3 Characterization of network parameters by MEA analysis

In order to select useful parameters for the characterization of network activity recorded by MEAs, synaptic transmission in mature human neuronal networks was blocked by inhibition of postsynaptic glutamate receptors (Figure 3.3) and by reducing the extracellular calcium concentration to block presynaptic vesicle release (Figure 3.4). Neuronal excitability was manipulated by inducing calcium concentration-dependent changes (Figure 3.4).

To determine synaptic connectivity-dependent parameters from extracellular MEA recordings, glutamatergic synapse transmission in mature human neuronal networks was blocked by exposure to saturating concentrations of the NMDA receptor antagonist APV (50 μM) and the AMPA receptor antagonist DNQX (10 μM). A partially reduced spike frequency was observed upon APV and DNQX treatments (Figure 3.3A and C), however, bursts and burst-dependent parameters were no longer detectable (Figure 3.3B and D). This suggests that the occurrence of bursts completely depends on glutamatergic synaptic transmission. Individual action potentials, on the other hand, may be caused by spontaneous (non-synaptic) depolarization of individual neurons.

In an alternative approach, I manipulated synaptic connectivity as well as neuronal excitability by decreasing extracellular calcium concentrations. A decrease in external calcium concentration leads to a reduced saturation of negative surface charges and thus a reduction of the membrane potential towards a more depolarized state. Hence, an initial decrease of extracellular calcium increases neuronal excitability (Speckmann

et al. 2015). Further lowering of external calcium below a certain threshold leads to the inhibition of calcium-dependent presynaptic vesicle release and thus synaptic connectivity in neuronal networks.

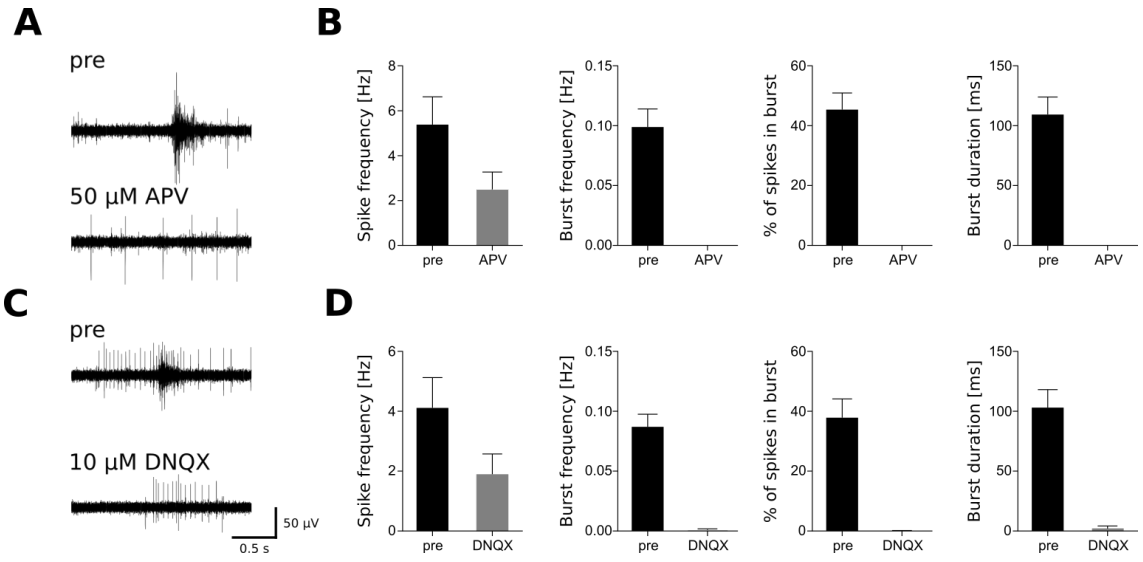

Figure 3.3: **Synapse dependent network activity.** To determine which of the activity parameters correlated with synaptic connectivity, iPSC-derived neural networks were recorded on MEAs before and after application of postsynaptic glutamate receptor inhibitors. Representative voltage traces recorded upon treatment of (A) APV (50 µM) and (C) DNQX (10 µM). Quantification of the network parameters of (B) APV and (D) DNQX treatment. Bar graphs represent activity parameters (mean±SEM). n= 10 electrodes from 1 MEA.

To this end, mature human iPSC-derived neuronal networks were subjected to decreasing concentrations of extracellular calcium (1.8 mM to 0 mM) in an artificial Neurobasal-like solution and the network activity was monitored by MEA recordings (Figure 3.4). All recordings were normalized to baseline activity, measured in NeurobasalTM containing culture medium (NMM) with a $CaCl_2$ concentration of 1.8 mM. In the mammalian brain, external calcium concentrations range from 1.5 to 2.0 mM (Egelman & Montague 1999). As expected, the initial decrease of extracellular calcium led to an elevation of overall network activity due to increased neuronal excitability. Both spike and burst parameters reacted in a similar way (Figure 3.4B). When approaching 0 mM external calcium, the overall activity strongly declined. Spike frequency (Figure 3.4B) reached a level comparable to baseline activity. The fact that synaptic bursts were still present at the lowest calcium concentration may be explained by the lack of calcium chelators and thus, residuals of the ion, sufficient to allow synaptic transmission. However, the parameter “percentage of spikes in bursts” was reduced below baseline

levels, indicating an increase of synapse-independent spikes, due to increased neuronal excitability.

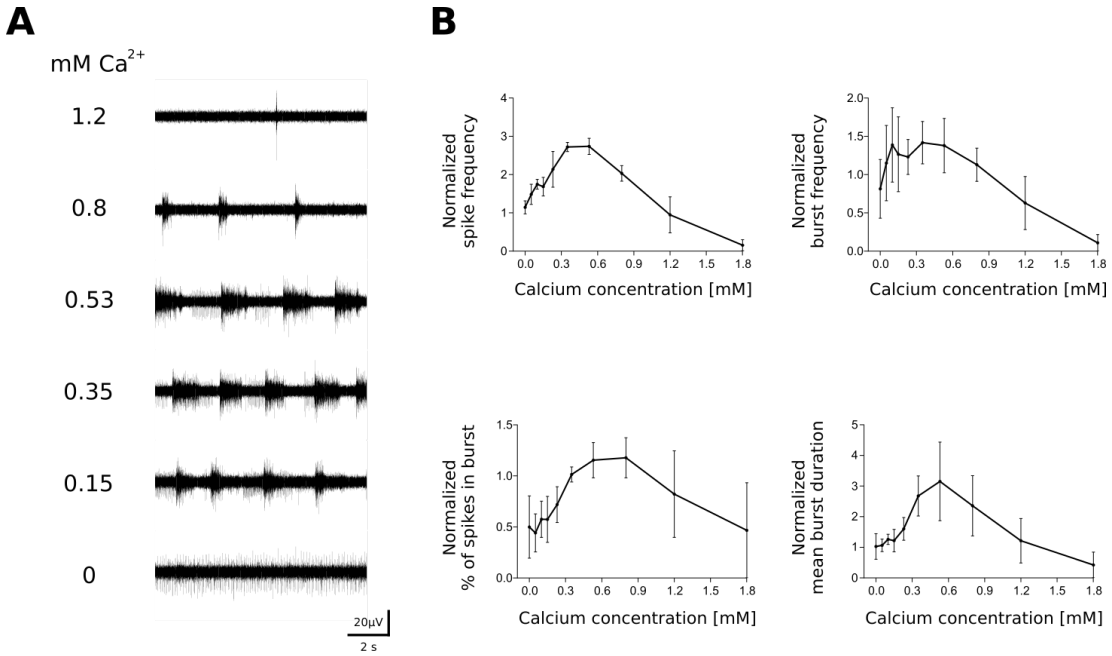

Figure 3.4: **Ca^{2+}-dependent network activity.** To analyze the effects of blockage of presynaptic vesicle release on overall network activity, a calcium dose-response curve was performed in iPSC-derived neural networks, recorded on MEAs, showing bursting activity. Therefore, NMM was replaced by a defined extracellular solution (Table 2.14) containing 1.8 mM Ca^{2+} and Ca^{2+} was then reduced in defined steps. (A) Representative voltage traces recorded on MEA at different Ca^{2+} concentrations. (B) Concentration dependent changes in different neuronal activity parameters (mean$\pm$SEM). Each measurement was normalized to the baseline value recorded before the treatment (neurons recorded in NMM). No significant differences was observed (one-way ANOVA followed by Bonferroni's test), n=3 MEAs.

Taken together, characterization of activity parameters showed that spike and burst frequency parameters are differentially influenced by changes in the network connectivity and neuronal excitability, where the frequency of synchronous bursts and the percentage of action potentials appearing within bursts correlate with synapse function. Changes in these parameters may thus give the first hint on underlying mechanisms when analyzing treatment responses in human neuronal networks.

3.1.4 Characterization of network parameters by calcium imaging analysis

Calcium imaging is another method to monitor network connectivity, whereby synchronous calcium oscillations of individual neurons represent synaptic activity across neurons (Figure 3.5). To determine that the occurrence of Ca^{2+} transients was

exclusively the outcome of synaptic activity, human iPSC-derived neuronal networks (5 months of network maturation), showing synchronous calcium transients were treated with inhibitors of postsynaptic receptors (30 μM DNQX, 5 μM APV and 20 μM gabazine). Spontaneous synchronous calcium transients were completely eliminated which indicates that their occurrence depends on the synaptic communication (Figure 3.5B). At the end of measurements, KCl (40 mM) was added to select and quantify the results only from neuronal ROIs (Figure 3.5B), which showed immediate sharp increases in the signal. Cells were determined as firing or silent as described in methods (2.5). Before application of inhibitors around 80% of the neurons were active, whereas all neurons were silenced after the treatment (Figure 3.5C).

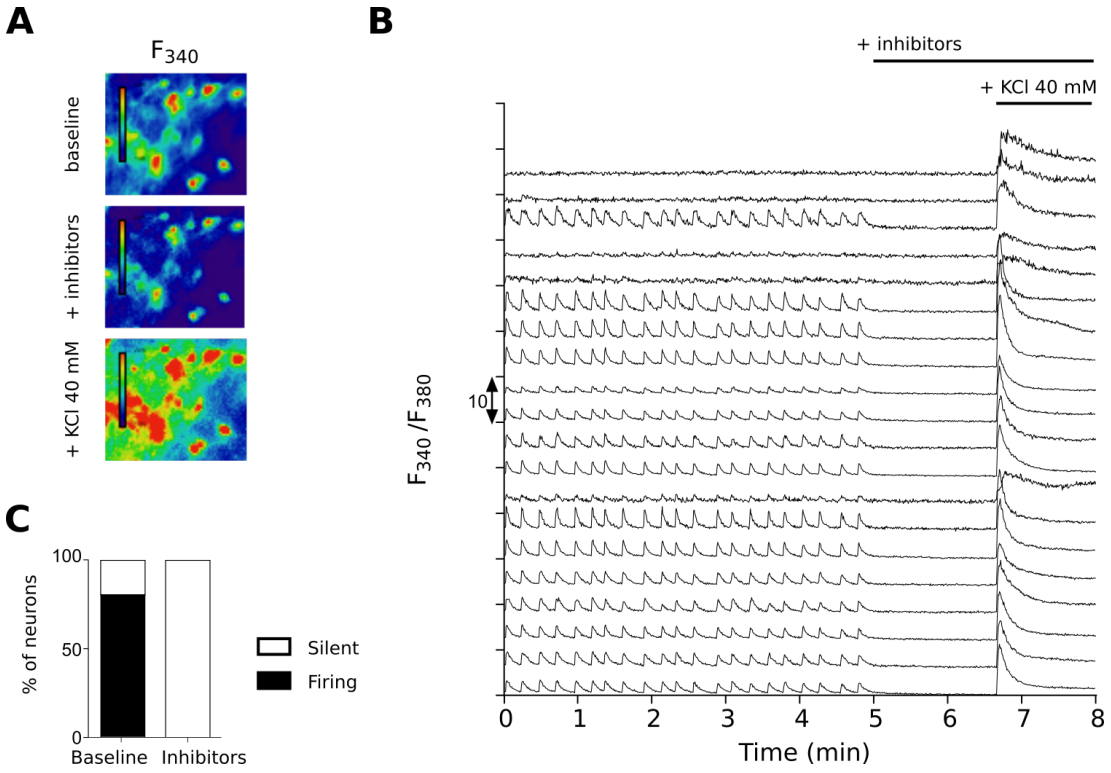

Figure 3.5: **Synchronous calcium oscillations in mature iPSC-derived neuronal networks.** (A) Representative false color images of intracellular calcium concentrations visualized at 340 nm. Blue and red showing low and high calcium concentrations, respectively. Images were taken at baseline, after application of synaptic inhibitors (30 μM DNQX, 20 μM gabazine and 5 μM APV), and KCl (40 mM). (B) Calcium transient traces imaged from one field. Each trace was offset-corrected and represents the ROI of a single neuron. Neurons were identified by their KCl responsiveness at the end of each measurement and ROIs were generated as described under 2.4. (C) Percentage of silent and synchronously firing neurons before (baseline) and during (inhibitors) inhibitor treatment. n = 1 coverslip

In conclusion, it was confirmed that calcium imaging is a valuable method to monitor

human iPSC-derived neuronal network activity to support MEA recordings and investigate the changes in the network activity.

3.1.5 Assay development using human iPSC-derived neuronal networks for synaptotoxicity testing

To develop assays using human iPSC-derived neuronal networks to test synaptotoxicity, botulinum neurotoxin type A (recombinant BoNT/A, toxogen GmbH, Hannover, Weisemann et al. (2015)) treated networks were subjected to calcium imaging (Figure 3.6) and SNAP25 cleavage assay (Figure 3.7). To see if the two methods gave the same results, the effects of BoNT/A exposure were compared in a dose- and time-dependent manner.

3.1.5.1 Time- and dose-dependent effects of BoNT/A on calcium transients of human neuronal networks

To investigate the effects of BoNT/A on spontaneous network activity (spontaneous synchronous calcium transients) in human cultures, iPSC-derived neuronal networks co-cultured with rat primary astrocytes (3 months of network maturation) were treated for 2, 4 and 6 days with different concentrations of BoNT/A.

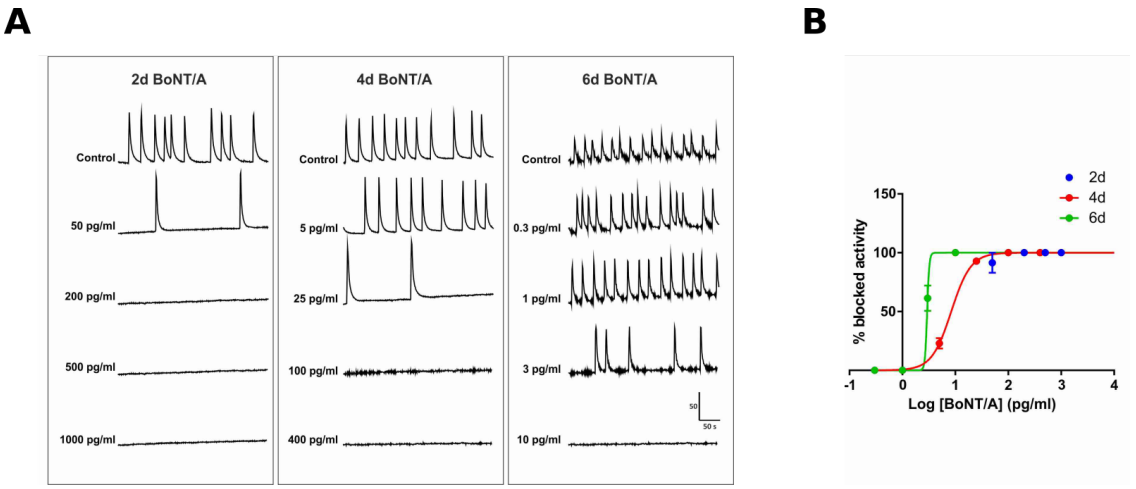

Figure 3.6: **Inhibition of spontaneous synchronous network activity by BoNT/A.** Synchronously active iPSC-derived neural networks were incubated with different concentrations of recombinant BoNT/A for 2, 4, 6 days and analyzed by Fura-2-based calcium imaging. (A) Example calcium transient traces imaged from coverslips at different concentrations and treatment times. Each trace represents the mean fluorescent intensity from one AOI including all neurons in the field. (B) Dose-response relations of the blocked spontaneous calcium transient frequency for 2, 4, 6 days BoNT/A incubation. n = 3 cultures per data point.

Under control conditions (without toxin incubation), all investigated cultures showed spontaneous synchronous calcium transients (Figure 3.6A, control), the frequency of which was quantified and set as 0%-blocked activity. Incubation with BoNT/A led to dose-dependent reduction of the calcium transient frequency (Figure 3.6). Calcium imaging showed a complete loss in the synchronous calcium transient rate for BoNT/A concentrations of 200 pg/ml, 100 pg/ml, and 10 pg/ml for 2, 4, and 6 day of BoNT/A treatments, respectively (Figure 3.6).

3.1.5.2 Dose-response-curve for BoNT/A in human and rat neurons according to SNAP25 cleavage

The SNAP25 cleavage assay is the most frequently used in vitro efficacy test method for BoNT/A and is also used by the BoNT/A manufacturers (Cai, Singh & Sharma 2007).

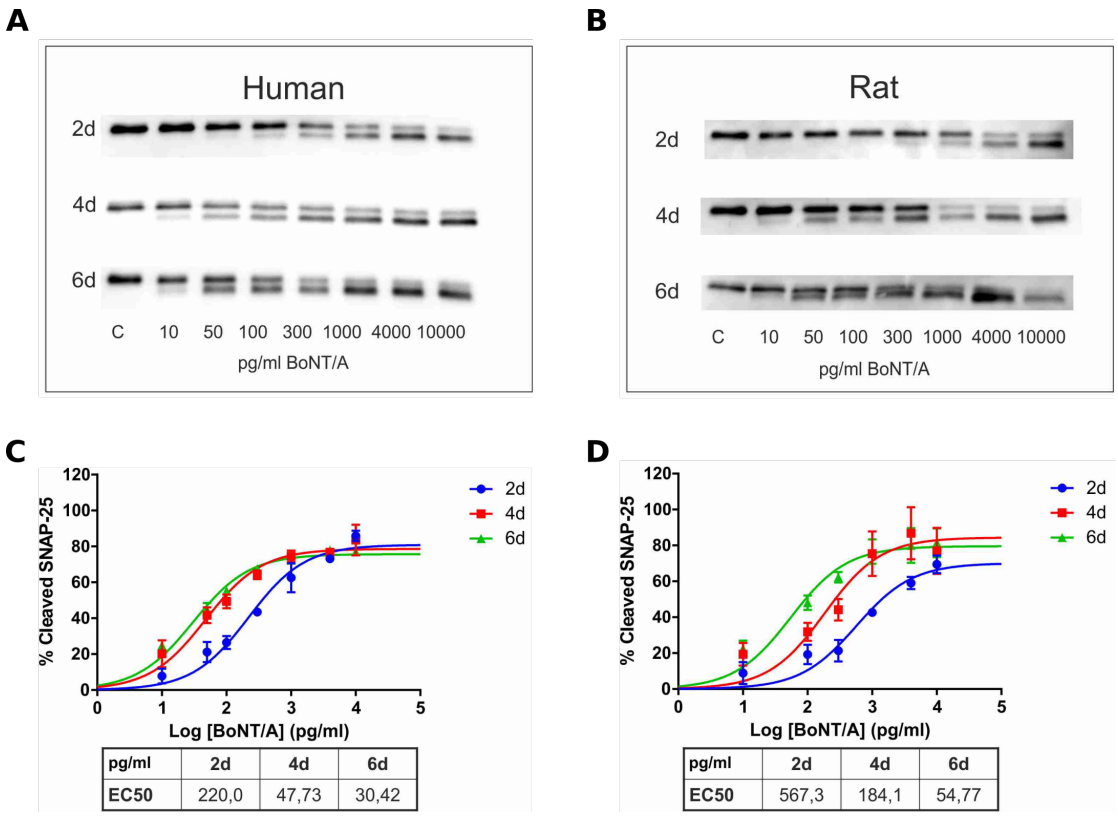

Figure 3.7: **SNAP25 cleavage in human and rat neurons upon BoNT/A treatment.** Human iPSC-derived and primary rat cortical neurons were incubated with increasing concentrations of BoNT/A for 2, 4 and 6 days and cell lysates were analyzed for SNAP25 and its cleavage products by western blotting. Example blots showing (A) human and (B) rat SNAP25 immunoreactivity at different time points and concentrations. Corresponding dose-response curves for SNAP25 cleavage in (C) human and (D) rat neurons. EC50 (pg/ml) values are shown in the tables. Data represent mean±SEM, n = 3 biological replicates per data point.

To replicate the method and compare the results, human immunopurified iPSC-derived neurons (2 months of network maturation) and rat primary cortical neurons (14 div) were treated with different concentrations of BoNT/A for 2, 4, and 6 days and western blots were quantified by calculating the ratio of cleaved to non-cleaved SNAP25 protein (Figure 3.7). Exposure to BoNT/A for 2d resulted in a significant increase in SNAP25 cleavage in human compared to rat cortical neurons at much lower concentrations (Figure 3.7 C and D, tables). Human neurons showed higher sensitivity to BoNT/A during 2 and 4 days treatment; however, species-specific differences were eliminated after prolonged incubation (6 days). These results might be explained by the fact that the BoNT/A receptors responsible for internalizing the toxin might have different structures in rat and the human neurons since The duration of the effects varies extensively depending on dose, animal species (Pirazzini et al. 2017). Therefore, human neurons have higher sensitivity to the toxin in early time-points. Overall, the dose-response curves obtained from calcium imaging and SNAP25 cleavage assays using human neurons differentiated from iPSCs showed different results, showing that the synchronous calcium transient-based assay has higher sensitivity compared to the SNAP25 cleavage assay. This difference in sensitivity might be explained by that BoNT/A is taken up at the synapses and thus cleave synaptic SNAP25 first. This would then have an effect on network activity. The total pool of SNAP25 is probably much higher and also contains non-synaptic SNAP25, which is relevant for the SNAP cleavage assay, but not the activity assay.

3.2 Modeling homeostatic plasticity in human neuronal networks

Neuronal networks have the ability to regulate activity in order to maintain their firing rates at basal levels. The existing body of research on homeostatic plasticity was done primarily in vivo and in vitro murine models (Desai 2003). It is still not known whether human iPSC-derived neuronal networks share similar properties. Therefore, the first set of questions aimed to investigate the homeostatic plasticity abilities of human iPSC-derived neuronal networks. Their firing rates were manipulated by either blocking action potentials with tetrodotoxin (TTX), a voltage-gated Na^+ channel blocker (Figure 3.8) to silence network activity or prolonging action potentials with 4-aminopyridine (4AP), a specific blocker of outward K^+ current (Figure 3.10) to enhance network activity. The changes in firing rates were monitored by MEA recordings and calcium imaging. (Figure 3.16). Furthermore, the involvement of REST in 4AP-mediated homeostatic plasticity was investigated by immunocytochemistry (Figure 3.18). REST (or NRSF), a transcription repressor of neuronal genes, was recently described as a mediator of homeostatic plasticity in hyperactive mouse hippocampal neurons (Pozzi et al. 2013). Possible attempts to manipulate REST expression were examined by western blot using primary rat cortical neurons (Figure 3.19).

3.2.1 Homeostatic plasticity in TTX-silenced mature human neuronal networks

To examine the response of human iPSC-derived neuronal networks to TTX, which is the mostly used homeostatic plasticity model (Turrigiano 2012), the MEA system was used, as it enables longitudinal, non-invasive monitoring of network activity (Figure 3.8). Endogenous cocultures of human neurons and astrocytes were extracellularly recorded before (pre), during (acute, 1d, 2d, and 3d) and after (post 3h) TTX (1 μM) or control treatments (Figure 3.8A, B). For quantification, the spike and burst frequency values were normalized to pre values of each culture. The network activity of the control cultures was stable during the course of the measurement (Figure 3.8C and D, black line). However, cultures that underwent TTX treatment maintained a suppressed activity profile in the presence of TTX and showed an increase in spike (Figure 3.8C, blue line) and burst frequency (Figure 3.8D, blue line) after removal of TTX, with an average increase of around 2 fold above the baseline. These results showed that human cultures have the capability to alter network properties as a result of their homeostatic plasticity response.

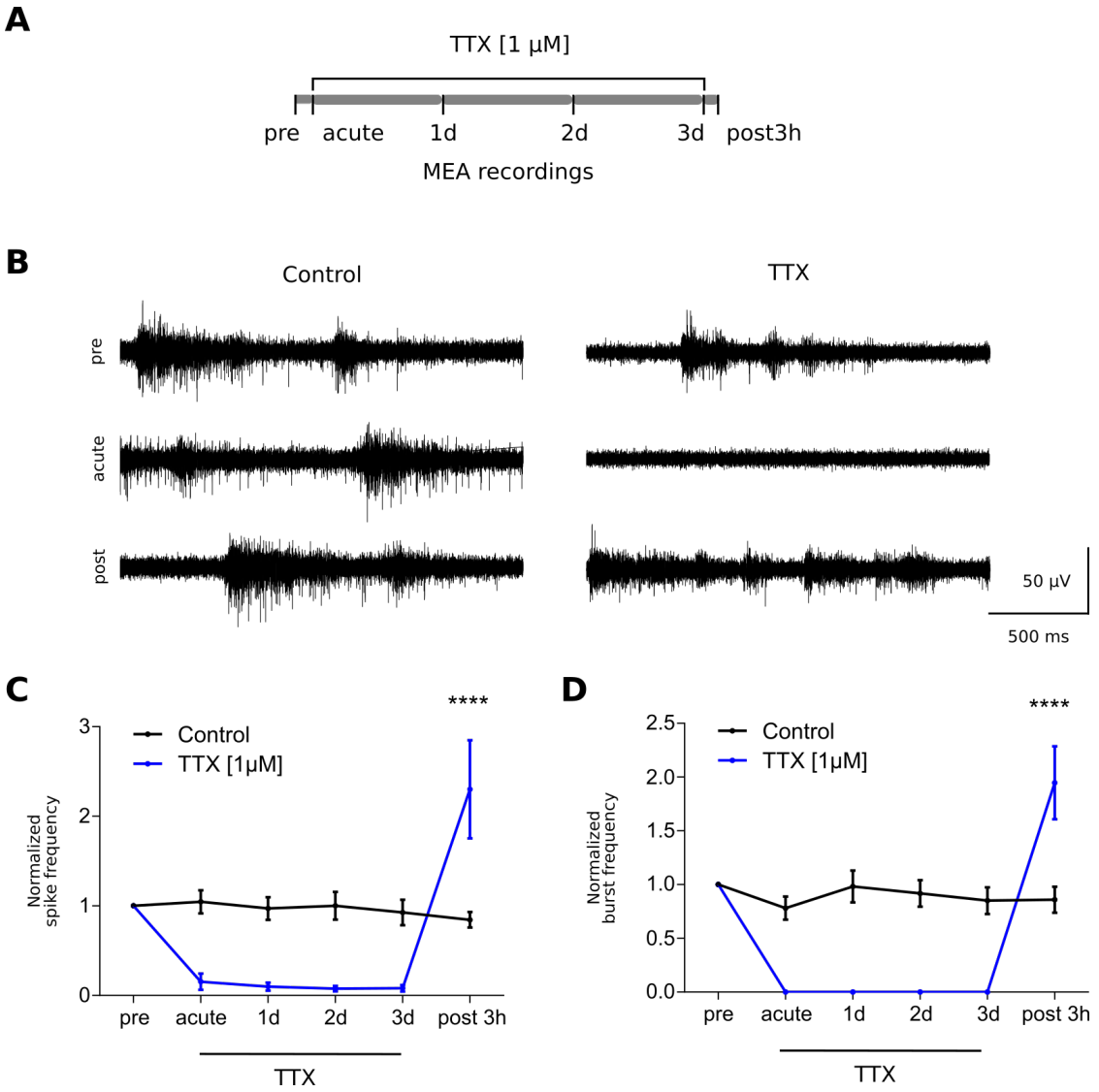

Figure 3.8: **Homeostatic plasticity in TTX-silenced mature human neuronal networks.** (A) Schematic treatment and measurement protocol. d: day, h: hour. (B) Representative extracellular voltage traces recorded from MEAs with hiPSC-derived mature neuronal networks incubated without (left) or with 1 µM TTX (right) before (top), during (middle) and after (bottom) TTX treatment. Time-course of normalized mean (C) spike and (D) burst frequencies before (pre), during (indicated by bottom line, 1 µM for 72 h) and after (post 3h) TTX treatment. Each value was normalized to baseline activity (pre value). Data points represent mean±SEM, n = 3 MEAs. (Two-way ANOVA followed by Tukey's multiple comparison test **** $p < 0.0001$). Normalized mean spike and burst frequencies were increased after the removal of TTX.

3.2.2 Changes in spike parameters after TTX silencing

To analyze the homeostatic response mechanism to TTX treatment at the level of a single neuron, the recorded data from MEA experiments were further processed to extract single action potentials (spikes). The shape of the extracellular spike closely resembles the first time derivative of an intracellular action potential and the width of the

intracellular and extracellular action potential are highly correlated (Henze et al. 2000, Bugaysen et al. 2010) (Figure 2.4E). Therefore, the amplitude of a spike represents the maximum rising slope of an action potential and thus correlates with the density of Na^+ channels on the axonal membrane. On the other hand, alterations in the width (Bugaysen et al. 2010) and the post-spike maximum (Speckmann et al. 2015) (Figure 2.4E) of the extracellular spike correlate with K^+ conductance. Hence, quantification of parameters like spike amplitude, half-width, 10%-width and post-peak maximum could give hints on changes in neuronal excitability (Na^+ and K^+ channel densities) as part of the homeostatic plasticity.

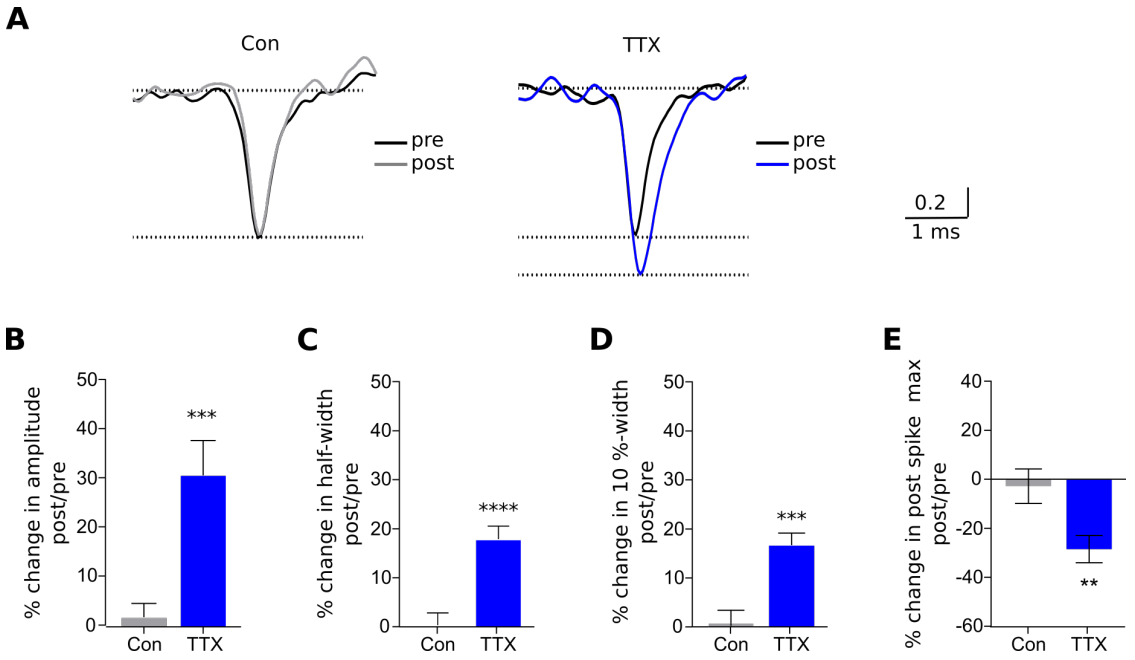

Figure 3.9: **Changes in spike parameters after TTX silencing.** (A) Representative mean extracellular spikes extracted from one electrode of MEA recordings before (pre, black spikes; normalized to 1) and after (post; normalized to pre) treatment in control (gray spike, left) and TTX (blue spike, right) treated cultures. Effect size, shown as percent change in (B) amplitude, (C) halfwidth, (D) 10%-width, and (E) post spike max. Mean±SEM, n > 20 electrodes from 3 MEAs. (Unpaired two-tailed t test ****p < 0.0001, ***p < 0.001, **p < 0.01).

In order to extract single spikes, raw data were filtered with a low-pass 2000 filter and spikes were detected by the 5XSTD method. Spikes were sorted and extracted from control and treated cultures before (pre) and after (post) treatment. Spike curves were imported into Excel for further analysis. The in-house written macro (see Scripts and Macros) was used to detect the mentioned parameters from each spike. As the distance between electrode and cell as well as the electrode impedance affect the spike

amplitude, amplitudes are highly variable between different MEAs and even electrodes of the same MEA. Therefore, mean spike amplitudes and post-spike maximum from one electrode were normalized to the baseline (pre, before the treatment) amplitude of the corresponding electrode. Plasticity-dependent changes were investigated by comparing spike parameters between before (pre) and after (post) the treatment and data are shown as effect size (percent change). The same procedure was used for all experiments dealing with the investigation of spike parameters.

After three days of TTX treatment, the spike amplitude was increased by 30% (Figure 3.9A and B), indicating that the density of axonal Na^+ channels was increased during homeostatic plasticity in silenced networks. Notably, in control treated cultures, no changes could be observed, suggesting that medium changes did not affect spike. Furthermore, half-width and 10%-width (Figure 3.9C and D) were significantly increased and the post-spike maximum was significantly decreased (Figure 3.9E) suggesting a reduction of K^+ channels.

Taken together, changes in spike and burst frequency and the different spike parameters indicated, that mature human iPSC-derived neural networks upregulate neuronal excitability as homeostatic plasticity response to prolonged silencing of network activity.

3.2.3 Effect of 4AP on network activity in immature human neuronal networks

Another significant aspect of homeostatic plasticity is that increasing network activity leads to a decrease in neuronal excitability to come back to basal firing rates for preventing excitotoxicity. To this end, as previously described (Pozzi et al. 2013), 4AP was used to induce hyperactivity by blocking voltage-dependent K^+ channels which affects repolarization, prolongs action potentials, and leads to increased neurotransmitter release. First, immature human neuronal networks (2 months of network maturation), showing only spike firing (Figure 3.10B, pre) were treated with 4AP (100 μM) or with vehicle for 72 h and the activity was recorded by MEA (Figure 3.10A). Surprisingly, the networks showed no detectable change in spike frequency (Figure 3.10B). Also, 4AP treatment did not lead to the induction of bursting activity (Figure 3.10B, acute 4AP, post 1d) suggesting that the synaptic connectivity within the network was not well developed. These results might also suggest that 4AP targets, members of the Kv1 (Shaker, KCNA) family of voltage-activated K+ channels, were not yet expressed by developmentally immature human neurons.

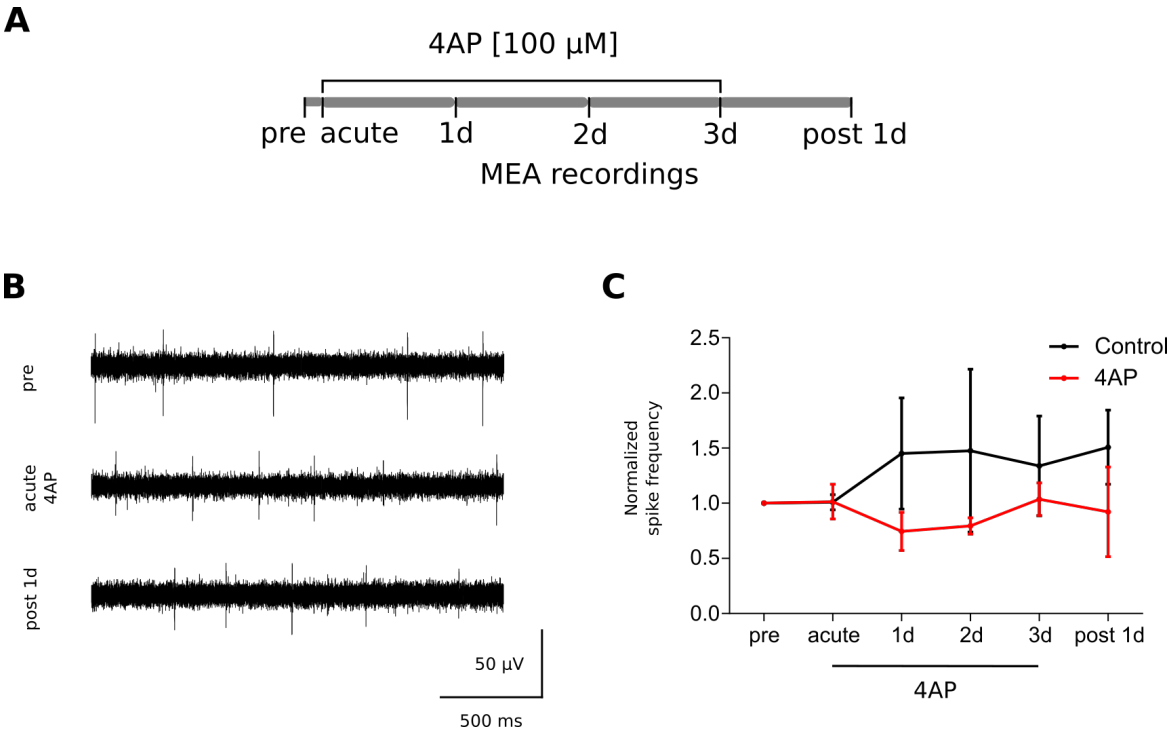

Figure 3.10: **Effect of 4AP on network activity in immature human neuronal networks.** (A) Schematic treatment and measurement protocol. d: day. (B) Representative extracellular voltage traces recorded from MEAs with hiPSC-derived immature neuronal networks incubated before (top), during (middle) and after (bottom) 4AP treatment. (C)Time-course of spike frequencies recorded from neuronal cultures before (pre), during (indicated by bottom line, 100 µM for 72 h) and one day after 4AP treatment (post 1d). Each value was normalized to baseline activity (pre). Data points represent mean±SEM, n = 3 MEAs. (Two-way ANOVA followed by Tukey's multiple comparison test). Normalized mean spike frequencies showed no changes during and after the 4AP treatment.

3.2.4 Acute 4AP effects on spike parameters in immature human neurons

Immature human neuronal cultures showed no increase in the network activity upon 4AP stimulation. 4AP was described to prolong action potential duration and thus increase spike width, by blocking voltage-dependent K^+ channels (Lin 2012). To investigate whether 4AP affects the spike form in immature neurons, extracellular spikes were analyzed before and during 4AP treatment in control and 4AP-treated cultures (Figure 3.11A). Quantitative analysis showed, that 4AP-treatment did not significantly affect spike amplitude (Figure 3.11B), half-width (Figure 3.11C), 10% width (Figure 3.11D), and post-spike maximum (Figure 3.11E), compared to control cultures. These data implicated that 4AP targeted K^+ channels were not expressed by developmentally immature human neurons.

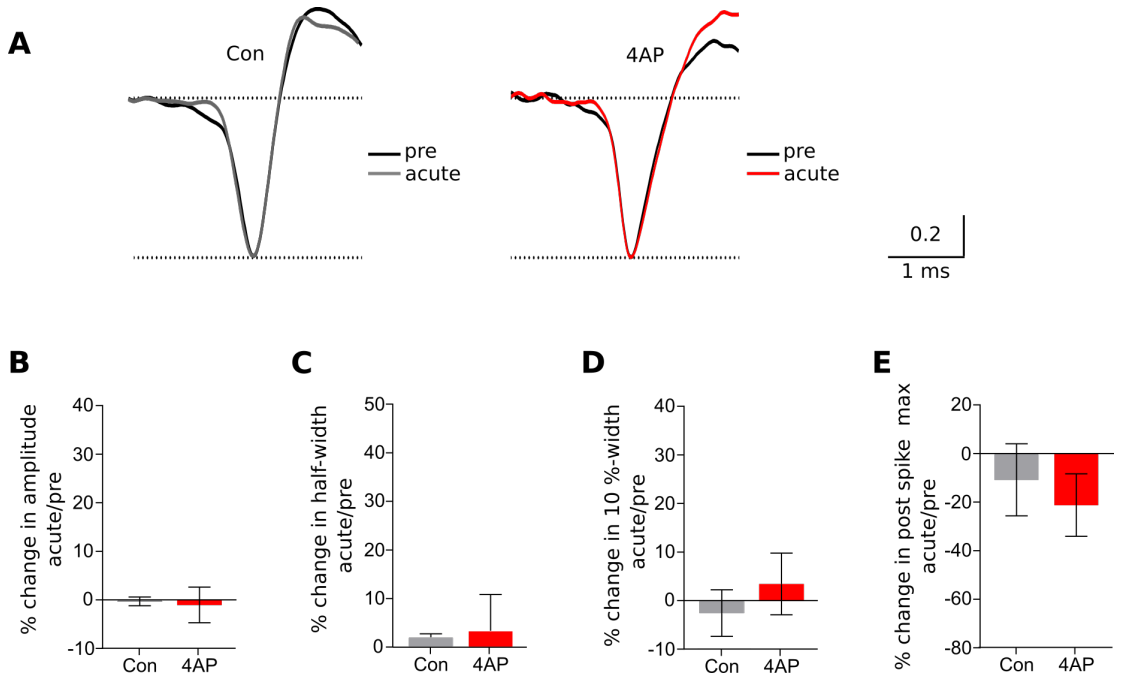

Figure 3.11: **Spike parameters of 4AP-treated immature human neurons.** (A) Representative normalized mean extracellular spikes extracted from one electrode of MEA recordings before (pre, black spikes) and during treatment in control (gray spike, left) and 4AP (red spike, right) treated cultures. Effect sizes, shown as a percent change in (B) amplitude, (C) half-width, (D) 10%-width, and (E) post spike max. Mean±SEM, n > 5 electrodes from 3 MEAs. (Unpaired two-tailed t test). No changes were observed.

3.2.5 Homeostatic plasticity in 4AP-treated mature human neuronal networks

In order to investigate hyperactivity-induced homeostatic plasticity in human neural networks, the maturation time of cultures was increased, until the synchronous burst firing activity was observed, which was shown to be reliable parameter for synaptically well-connected networks. Human neurons were then treated with vehicle (control) or 4AP (100 μM) for up to 96 h. Longitudinal changes in network activity were monitored by MEA recordings before (pre), during (acute, 1d, 2d, 3d, and 4d), and after (post 4d) 4AP treatment or control treatments (Figure 3.12A). Mature networks showed spikes and bursts during pre-measurements (Figure 3.12B, pre) and upon 4AP treatment, networks increased the firing activity dramatically (Figure 3.12B, acute, right). Control networks showed no change in activity pattern (Figure 3.12B, acute, left). Although individual networks showed variable magnitude of response, the pattern of the response was similar for the same type of treatment (Figure 3.12C). After 24 h in 4AP, the networks displayed decreased spiking and bursting rates (Figure 3.12D and E, 1d, red line). The firing returned to basal values at the end of 96 h (Figure 3.12D and E, 4d, red line).

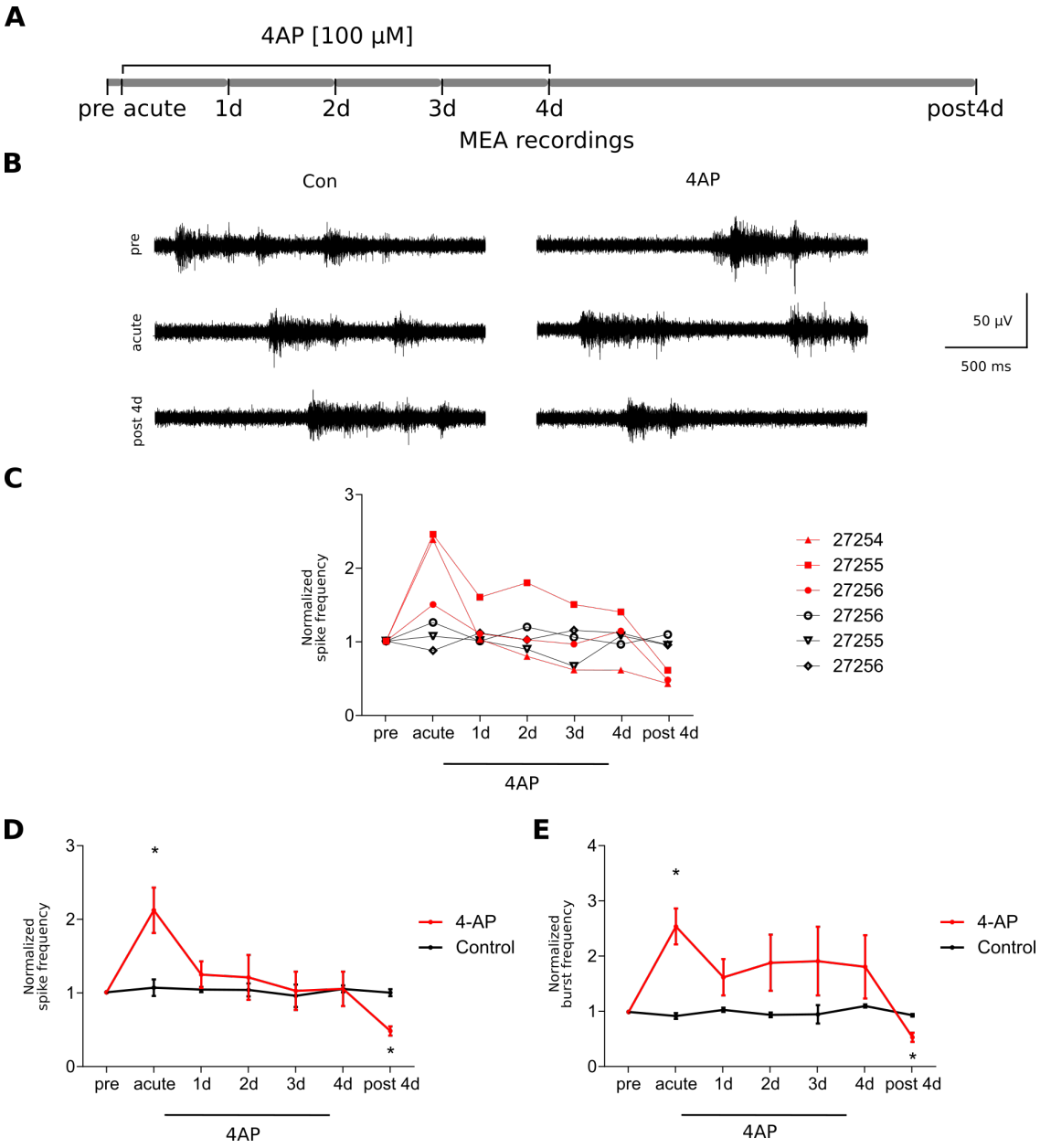

Figure 3.12: **Homeostatic plasticity in 4AP treated mature human neuronal networks measured by MEA.** (A) Schematic treatment and measurement protocol. d: day. (B) Representative extracellular voltage traces recorded from MEAs with hiPSC-derived mature neuronal networks incubated without (left) or with 4AP (right) before (top), during (middle) and after (bottom) treatment. (C) Time-course of normalized spike rates from single MEA recordings before (pre), during (indicated by bottom line, 100 µM 4AP for 96 h) and after (4 days post) 4AP (red) and control (black) treatment. Each value was normalized to the baseline activity (pre value). (D) Time-course of normalized mean spike and (E) burst frequencies. Data points represent mean ±SEM, n = 3 MEAs, * indicates significant difference between 4AP and control (Multiple t test *$p < 0.05$). The normalized mean spiking rate was increased by acute 4AP treatment. After removal of 4AP, the firing rate was decreased.

Notably, 4 days after the removal of 4AP, networks still showed decreased firing rates (Figure 3.12D and E, post 4d, red line) compared to baseline activity (pre), indicating

that neurons have changed their properties during 4AP treatment. In conclusion, maturity of neuronal networks was required to study homeostatic plasticity in human neuronal networks.

3.2.6 Acute 4AP effects on spike parameters in mature human neurons

Mature human neuronal networks responded to the 4AP treatment by increasing firing rates (Figure 3.12). To further elucidate the changes in the cellular level, extracellular spike waveforms were extracted from each active channel and analyzed after normalizing the amplitudes to 1 before (Figure 3.13A, pre, black spikes) and during control (Figure 3.13A, pre, gray spike) and 4AP (Figure 3.13A, pre, red spike) treatments.

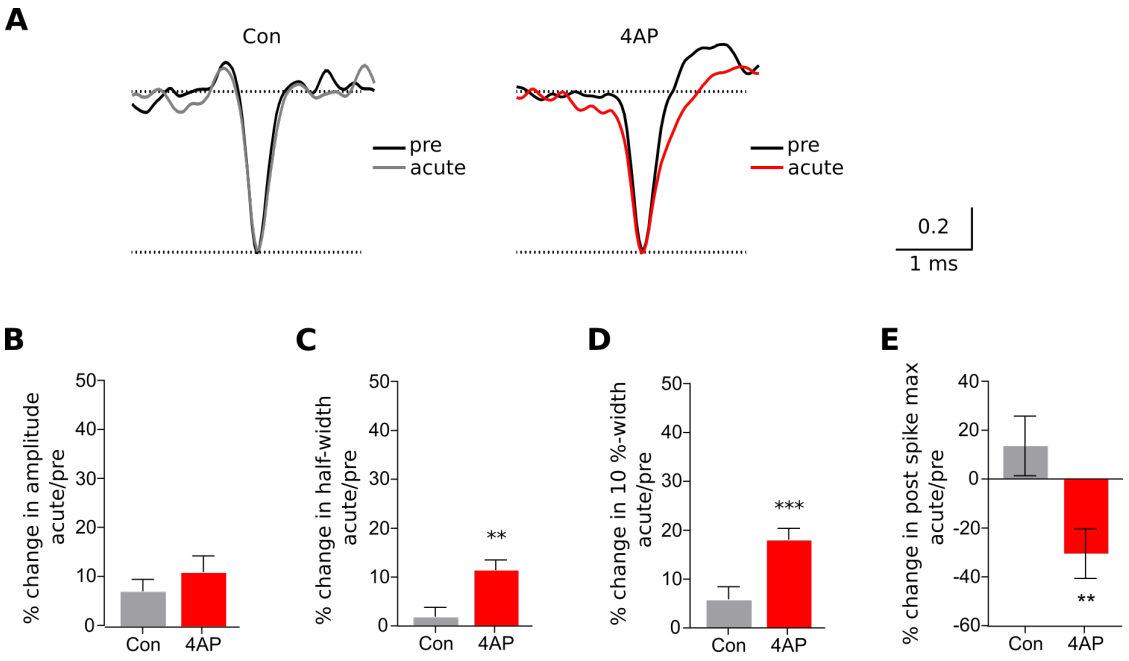

Figure 3.13: **Acute 4AP treatment affects spike parameters in mature human neurons.** (A) Representative normalized mean extracellular spikes extracted from one electrode of MEA recordings before (pre, black spikes, normalized to 1) and during (acute, normalized to pre) treatment in control (gray spike, left) and 4AP (red spike, right) treated cultures. Effect size, shown as a percent change in (B) amplitude, (C) half-width, (D) 10 % -width, and (E) post spike max. Mean±SEM, n > 20 from 3 MEAs. (Unpaired two-tailed t test, **p<0.01 ***p<0.001).

Blocking potassium channels with 4AP did not affect the extracellular spike waveform amplitude (Figure 3.13B). Since action potential width is modulated by potassium channels, blocking them with 4AP showed an increase in half-width (Figure 3.13C) and 10 % width (Figure 3.13D). On the other hand, blocking potassium channels also

affected the afterhyperpolarization of the action potential which is represented as the post spike maximum of the extracellular spike waveforms and the second maximum values were decreased upon 4AP treatment (Figure 3.13E).

3.2.7 Spike parameters of immature and mature human neurons

Mature (burst firing) and immature (spike firing) networks responded to the 4AP treatment differentially both in network (Figure 3.12 and 3.10) and cellular (Figure 3.13 and 3.11) level. To investigate whether these differences were dependent on the differences in spike properties and could be investigated by the spike waveform analysis, extracellular spike waveforms were compared without any treatment (Figure 3.14A). Since alterations in the width of the extracellular spike waveform represented the changes in K^+ channels, half-width (Figure 3.14B) and 10 % width (Figure 3.14C) values of immature and mature neurons were compared without normalizing. Both half-width and 10 % -width values were smaller in mature cultures suggesting that smaller spike width was a correlate of maturation and might indirectly suggest the presence of increased number of K^+ channels on the neuronal membrane.

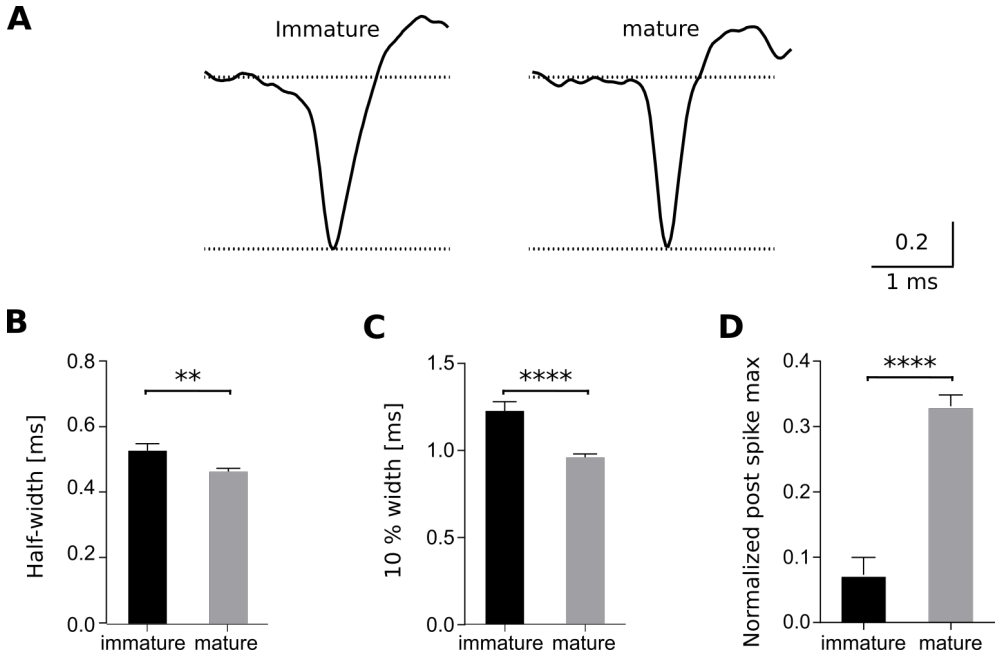

Figure 3.14: **Spike parameters of immature and mature human neurons.** (A) Representative normalized mean extracellular spikes extracted from one electrode of MEA recordings from immature (left) and mature (right) neurons. Quantification of the (B) spike half-width, (C) 10%-width, and post spike maximum (normalized to spike amplitude). Mean n±SEM, n > 20 electrodes from 3 MEAs. (Two-tailed t test, **p< 0.01, ****p < 0.0001).

3.2.8 Changes in spike parameters after 4AP induced hyperactivity in mature human neurons

To investigate the long-term effect of 4AP on spike waveforms, single spike analysis was performed after the removal of 4d 4AP treatment (Figure 3.15). To this end, the recorded data from MEA experiments were further processed as previously described. Extracellular spike waveforms were extracted from each active channel and analyzed after normalizing the amplitudes to 1 before (Figure 3.15A, pre, black spikes) and 4 d after the control (Figure 3.15A, post, gray spike) and 4AP (Figure 3.15A, post, red spike) treatments. Blocking potassium channels with 4AP triggered homeostatic mechanisms and the extracellular spike waveform amplitude was significantly reduced (Figure 3.15B). Furthermore, 4AP treated neurons also showed a decrease in both in half-width (Figure 3.15C) and 10 % width (Figure 3.15D). However, second maximum values were not affected (Figure 3.15E).

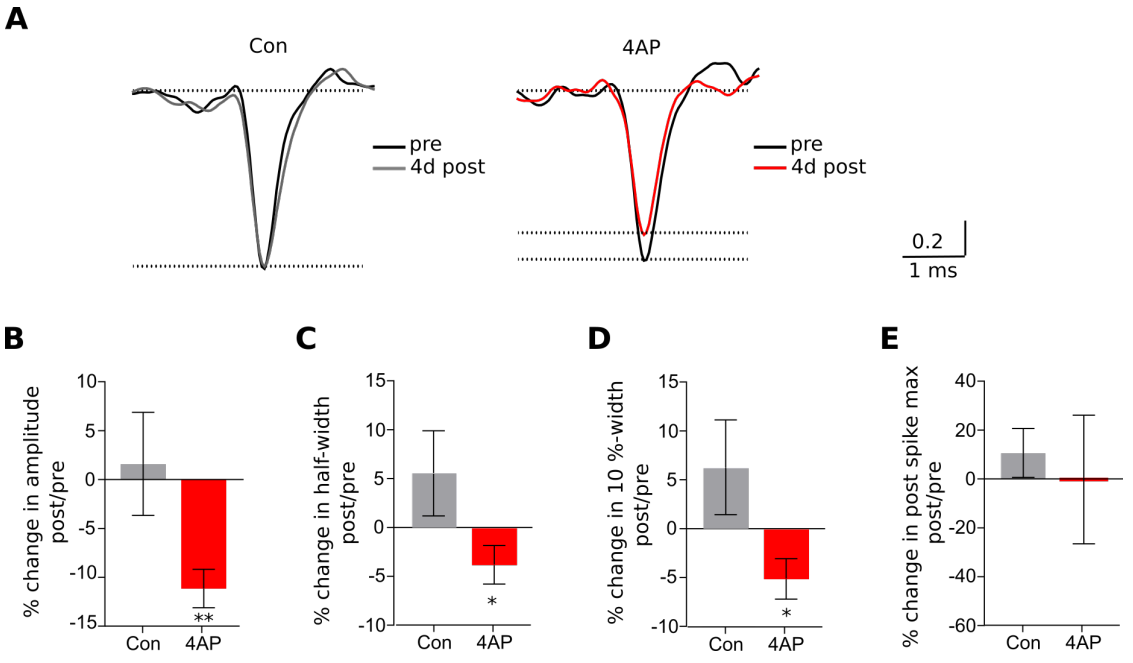

Figure 3.15: **Change of spike parameters after 4AP induced hyperactivity in mature human neurons.** (A) Representative normalized mean extracellular spikes extracted from one electrode of MEA recordings before (pre, black spikes) and 4 d after treatment in control (gray spike, left) and 4AP (red spike, right) treated cultures. Effect size, shown as a percent change in (B) amplitude, (C) half-width, (D) 10%-width, and (E) post spike max. Mean±SEM, n > 20 electrodes from 3 MEAs. (Two-tailed t test, *p<0.05, **p<0.01).

Taken together, these results suggest that mature human-iPSC-derived neurons were

able to change their membrane properties which could be detected by extracellular spike waveform analysis to modulate their network activity via homeostatic plasticity mechanisms.

3.2.9 Calcium imaging

The second method in this study which was used to identify the long term changes in the global network activity was the calcium imaging with Fura-2AM.

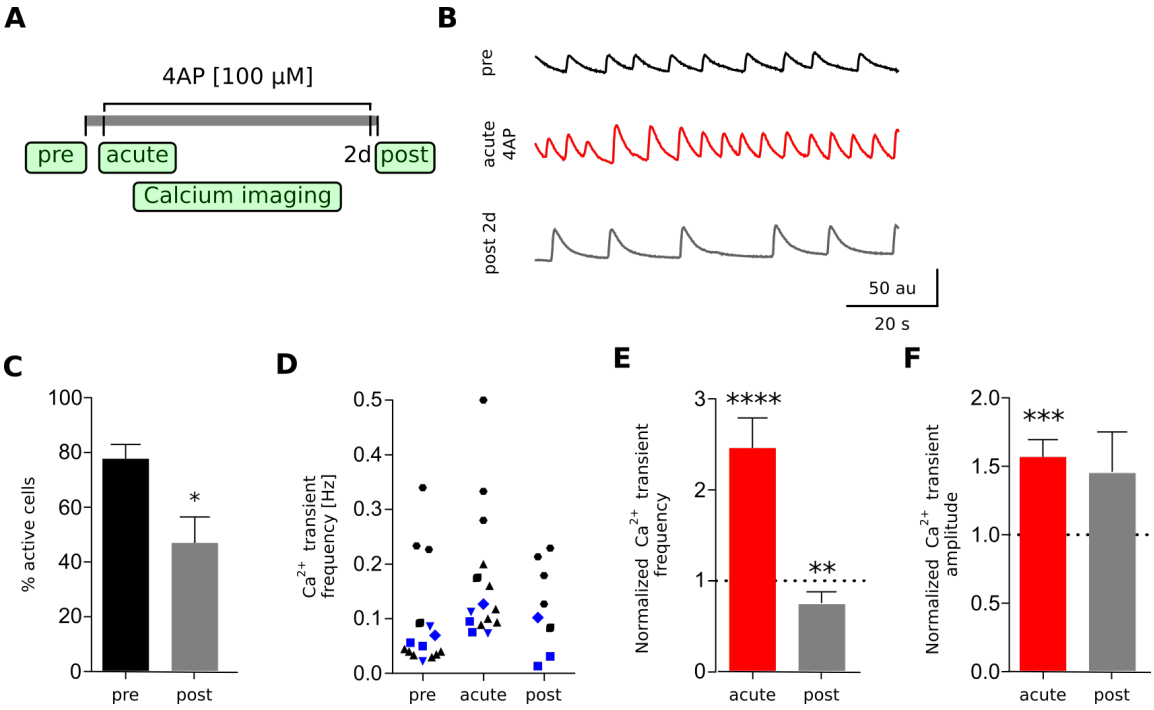

Figure 3.16: **Homeostatic plasticity in 4AP treated mature human neuronal networks measured by calcium imaging.** (A) Schematic treatment and measurement protocol. d: day. (B) Representative traces of calcium transients before (top), during (middle), and after (bottom) 4AP treatment extracted from one AOI with several neurons. (C) Percentage of synchronously firing cells before and after 4AP treatment (n = 5 coverslips from 3 different preparations). (D) Distribution of calcium transient frequencies. Sister coverslips are indicated by symbol shape. Cultures with human astrocytes are in blue and with rat asytrocytes in black. Normalized calcium transient (E) frequency (n > 8 coverslips from at least 4 different preparations) and (F) amplitude (n > 25 cells from 3 different preparations) during (acute) and after (post) 4AP treatment. Each value was normalized to the baseline value (pre) of sister coverslips and represents mean±SEM (Two-tailed t test *p < 0.05, **p < 0.01, ***p < 0.001, ****p<0.0001). After removal of 4AP, the spontaneous synchronous calcium transient rate was decreased.

It has been previously described that synchronous calcium transients represent burst activity of MEA recordings (Shew et al. 2010). Since the downregulation of the network activity have already been observed with MEA recordings after 48 h, calcium transient

measurements were performed before (Figure 3.16A, pre) during (Figure 3.16A, acute 4AP), and after removal of 2 d 4AP treatment (Figure 3.16A, post 2d). 4AP treatment affected synchronous calcium transients (Figure 3.16B). The 4AP treatment resulted in a decrease in the percentage of active cells joining the network activity (Figure 3.16C). Acute 4AP treatment increased the calcium transient frequency and amplitude (Figure 3.16E and F, red bars). Furthermore, after removal of 2d 4AP treatment, sister cultures from each experiment were normalized to pre values. Calcium transient frequency was reduced below the baseline levels (Figure 3.16E, gray bar). However, transient amplitudes varied compared to the baseline values. Overall, homeostatic response was possible to monitor by using calcium imaging.

3.2.10 Evaluation of cell viability upon LiCl, CHIR and X5050 treatment

REST is a translational repressor known to regulate neuronal genes and also homeostatic plasticity as recently described (Pozzi et al. 2013). Before monitoring REST levels directly, to test the neurotoxicity of the substances which might moduate REST levels such as LiCl, CHIR, and the inhibitor X5050 (Charbord et al. 2013), MTT assays were performed using primary rat cortical neurons along with the glutamate treatment to ensure the assay quality which resulted in reduced cell viability to 50 %. The safe concentrations of used substances were indicated as 0.5 mM for LiCl (Figure 3.17A), 100 nM for CHIR (Figure 3.17B), and 10 μM for X5050 (Figure 3.17C).

3.2.11 Changes in REST expression upon 4-AP treatment

To unravel the role of REST in 4AP-induced homeostatic plasticity, mature human iPSC-derived neurons were stained with REST antibody and nuclei were identified with DAPI (Figure 3.18A). REST expression levels varied cell-to-cell even without any treatment ((Figure 3.18A, control). Upon 4AP stimulation, increase in nuclear REST levels and nuclear to cytosolic REST ratio were observed first after 24 h, compared to controls (Figure 3.18B, C, and D, 24h). This data was in line with the findings of MEA recording which showed reduction in the network activity after 24 h. 48 h 4AP treatment also showed increase nuclear REST levels and nuclear/cytosolic REST ratio (Figure 3.18B and D, 48h). However, cytosolic REST levels were comparable to control condition at this time point (Figure 3.18C). CHIR increased both nuclear and cytosolic REST levels, as well as the the ratio between them (Figure 3.18A,B,C, and D, CHIR). Surprisingly, TTX treated cells showed increased REST levels both in cytoplasm and nucleus. However, the nuclear/cytoplasmic ratio was not different compared with the

control. In conclusion, for 4AP-related REST changes, the nuclear/cytosolic REST ratio at 24 hours was selected as valuable read-out for the further experiments.

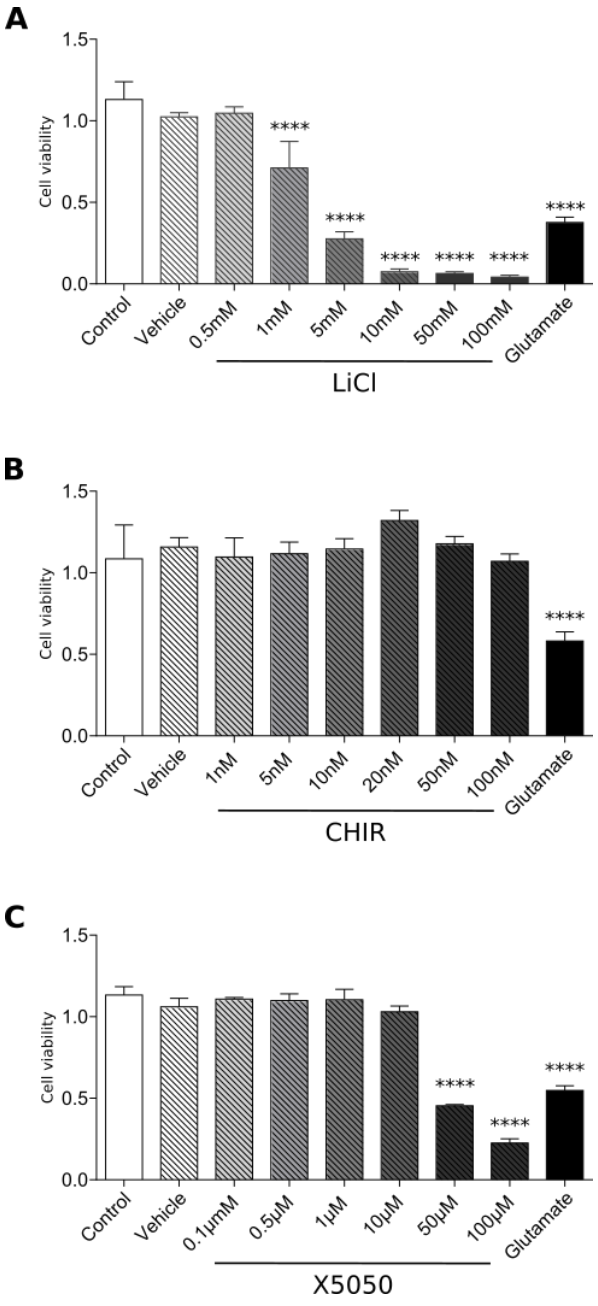

Figure 3.17: **Decrease of cell viability upon LiCl, CHIR, and X5050 treatment.** MTT assay of primary rat cortical neurons, treated for 48 hours with different concentrations of (A) LiCl, (B) CHIR, and (C) X5050. 100 µM glutamate treatment for 15 min (and further incubation for 1.5 h) served as a positive control. All values were normalized to control and represent mean±SEM, n=6 wells. (One-way ANOVA Tukey's multiple comparisons test ****p < 0.0001). LiCl caused toxicity at 1 mM, CHIR did not show toxicity, X5050 decreased the cell viability at 50 µM and glutamate caused a 50 % reduction of cell viability parameters.

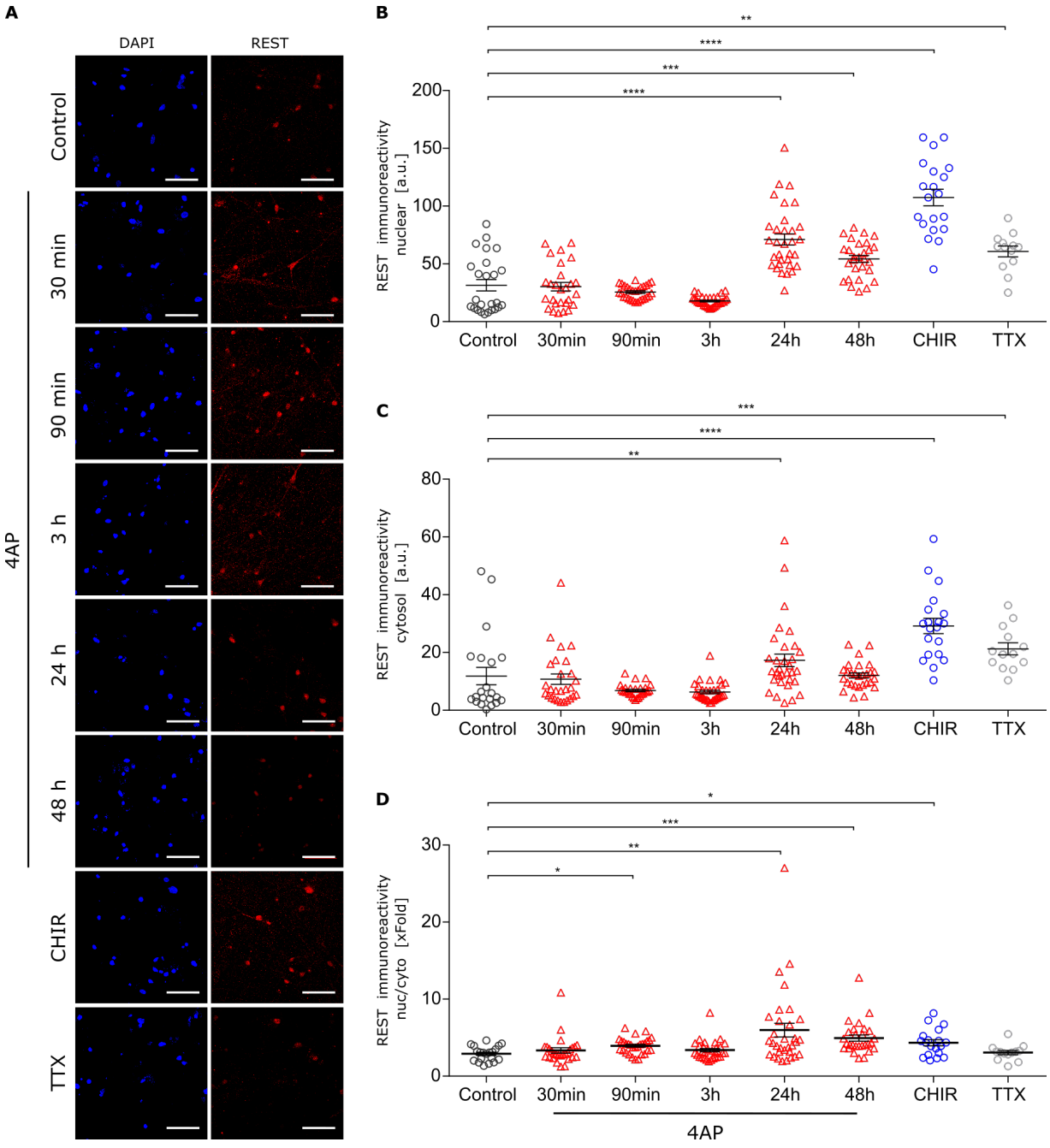

Figure 3.18: **Changes of REST expression in 4AP-treated human neurons upon manipulation of network activity.** Neurons were treated with 4AP (100 μM) to increase and TTX (1 μM) to silence network activity. CHIR is known to upregulate REST expression and was used as a positive control (100 nM). (A) Example confocal micrographs of control, 4AP (30 min, 90 min, 3 h, 24 h, and 48 h), CHIR (24h), and TTX (3h) treated human neurons, immunocytochemically stained for REST (red). Nuclei were stained with DAPI (blue). Quantification of mean fluorescent intensity of (B) nuclear and (C) cytosolic REST at the indicated treatment timepoints. (D) Nuclear vs cytosolic REST ratio. Data are represented as single data points, representing values from one neuron, and mean, n > 20 neurons from two coverslips. (One-way ANOVA Dunn's multiple comparisons test *p < 0.05, **p < 0.01, ***p < 0.001). Scale bar, 50 μm.

3.2.12 Manipulation of REST expression levels in primary rat cortical neurons

To further confirm the REST expression changes with another method, western blot analysis of nuclear and cytosolic fractions was performed. In this case, primary rat cortical neuronal cultures were used, since human networks include astrocytes and excluding astrocytic REST levels in western blots was not possible. To investigate the changes in REST expression levels, western blot analysis was performed using X5050 (10 μ)- and CHIR (100 nM)-treated PCNs and untreated control PCNs after fractionating nuclei and cytosol. Since several splice variants of REST were described, mouse REST overexpressing HEK cell lysate was used as a positive control to identify the REST band (Figure 3.19A). Nuclear fractions were identified and REST levels were normalized to Lamin, whereas cytosolic REST expression levels were normalized to GAPDH. Quantification of the upper band showed no changes in REST immunoreactivity (Figure 3.19B, upper panel). However, CHIR treated cells showed increased nuc/cyto REST ratio in the lower band (Figure 3.19B, lower panel).

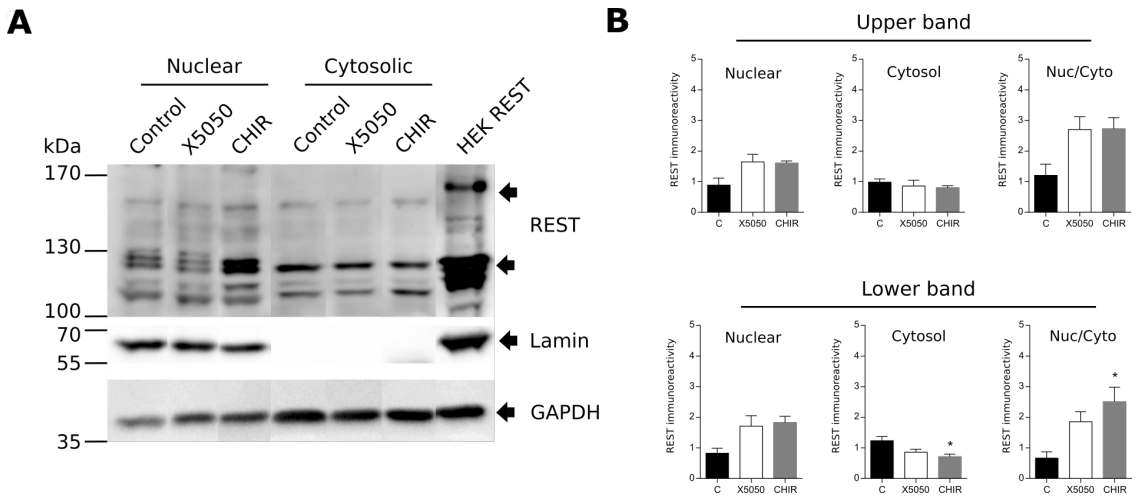

Figure 3.19: **Manipulation of REST expression levels in primary rat cortical neurons.** (A) Representative WB of fractionated lysates from control, X5050 (10 μM, 48h), and CHIR (100 nM, 48h) treated primary rat cortical neurons probed with REST antibody. Total cell lysate from myc-tagged-REST overexpressing HEK cells were run on the same gel and probed with anti-myc antibody. Arrows indicate potential REST immunoreactivity, due to molecular weight, treatment responsiveness and nuclear/cytosolic distribution. Lamin and GAPDH are markers for nuclear and cytosolic fractions, respectively. (B) Quantification of REST immunreactivity in nuclear and cytosolic fractions and their ratios. Data represent mean$\pm$SEM, n = 4 biological replicates. (One-way ANOVA Dunn's multiple comparisons test *p < 0.05).

Taken together, a homeostatic plasticity model, based on 4AP-induced hyperactivity in

mature and spontaneously active human neuronal networks differentiated from iPS cells was established and the REST protein was identified as a potential player in this mechanism. The model was ready to use for further investigations of disease-related alterations and evaluations of potent therapeutic strategies.

3.3 Characterization of different Aβ preparations

After characterizing human iPSC-derived neuronal networks and establishing homeostatic plasticity models, these cultures were ready to be employed for modeling certain aspects of Alzheimer's disease. In order to investigate AD-related changes, studying the effect of amyloid beta (Aβ) in human iPSC-derived neuronal networks was the first approach since the increased amount of this peptide is found in cerebrospinal fluid (CSF) of preclinical AD patients and it represents the central player in the amyloid cascade (Figure 1.6), triggering early events like synaptic dysfunction.

3.3.1 Effects of cell-derived Aβ

For the generation of cell-derived Aβ species, conditioned medium was collected from control CHO and 7PA2 (CHO:V717F in the APP751) cells. for obtaining cell-derived Aβ species. Overexpression of APP in stably transfected 7PA2 cells was confirmed by immunocytochemistry with the 4G8 antibody (Figure 3.20A) and 8% SDS-PAGE followed by western blot with the 6E10 antibody (Figure 3.20B). Both methods showed a clear APP overexpression in 7PA2 cells compared to control CHO cells.

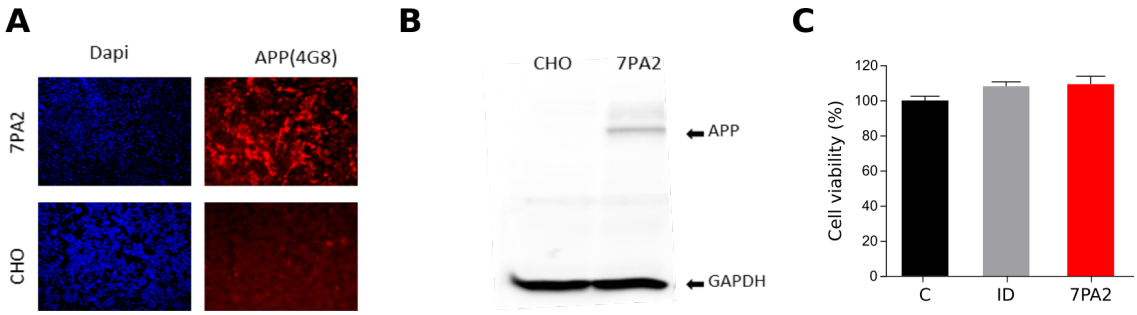

Figure 3.20: **7PA2 cells and the conditioned medium on cell viability** (A) Representative images of 7PA2 and CHO cells immunostained with 4G8 antibody for APP (red) and DAPI for nuclei (blue). (B) Western blot analysis of 7PA2 and CHO cells immunolabelled with GAPDH and 6E10 antibody for APP. (C) Primary rat cortical cells were exposed to control (black bar), ID (grey bar) or 7PA2 (red bar) conditioned medium for 48 h. Cytotoxicity was measured by MTT assay at an absorbance of 545 nm using a microplate reader. Data are presented as a mean±SEM, n = 6.

To test the effects of 7PA2 conditioned medium on cell viability, an MTT assay was performed using primary rat cortical neurons. As control, 7PA2, immunodepleted for Aβ (ID) by incubating 7PA2-conditioned medium with IC16 antibody coupled to NHS-sepharose bead ON at 4 °C, was used. 7PA2 conditioned medium and the

immunodepleted control medium did not show any changes in cell viability (Figure 3.20C). Since no change in cell viability was observed, the next step was to evaluate the cell-derived Aβ dependent effects on network activity in human iPSC-derived networks.

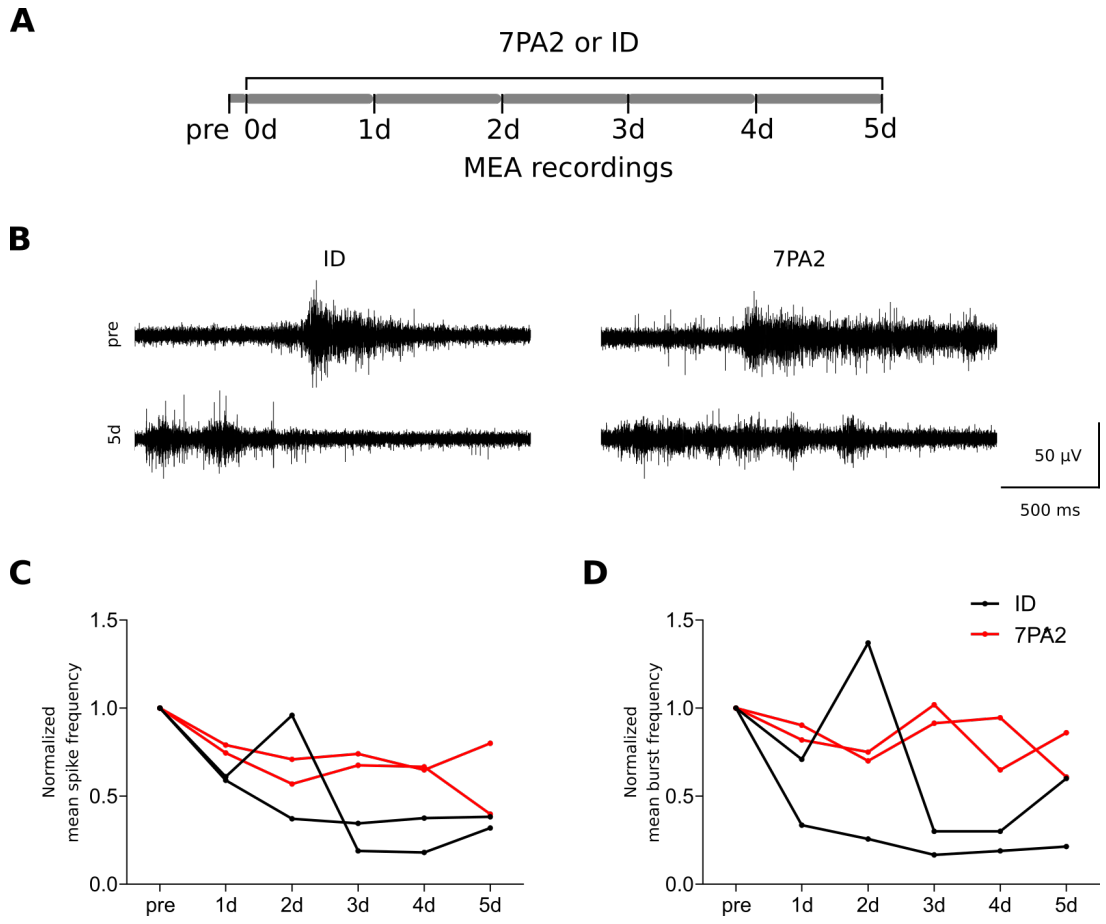

Figure 3.21: **Effects of cell-derived Aβ on network activity.** (A) Schematic 7PA2 od ID treatment protocol on mature human networks. d: day. (B) Representative extracellular voltage traces recorded from hiPSC-derived mature neuronal networks incubated with 7PA2 conditioned medium (right panel) or immunodepleted 7PA2 conditioned medium as control (left panel). Time-course of normalized (each culture to respective basal value) spike (B) and burst (C) frequencies of neuronal networks before (pre) and during (1-5 d) 7PA2 or ID treatment. n = 2.

To this end, the activity of mature human networks was monitored by MEA recordings before and during Aβ treatment (Figure 3.21A). Spike and burst frequencies of different cultures were normalized to baseline activity (pre). Both Aβ and ID treatment induced a trend towards reduced network activity (Figure 3.21C and D). However, immunodepleted control conditioned medium showed an even stronger effect indicating unspecific effects derived from components introduced by the immunodepletion procedure. Thus, cell-derived Aβ and its ID control were not suitable to serve as a proper

treatment/control group and next steps opted for a more defined Aβ preparation.

3.3.2 Generation and characterization of synthetic Aβ oligomers

To obtain more defined and consistent disease-related Aβ preparations, I aimed at generating low molecular weight oligomers (Selkoe 2001) of synthetic Aβ. Another type of Aβ was used additionally since it has been described that N-terminal truncated and pGlu-modified Aβ species (Pyroglutamylated $A\beta_{3-42}$ ([Pyr3]$A\beta_{3-42}$,) are present in AD brains in large quantities (Saido et al. 1995). The preparation of a mixture of $A\beta_{42}$:[Pyr3]$A\beta_{3-42}$ (95%:5%) was prepared according to the published protocol (Nussbaum et al. 2012). First a main issue with visualizing Aβ oligomers had to be solved, as some polyacrylamide gel electrophoresis (PAGE) types alter the oligomer profile. Therefore, different PAGE conditions were tested (Figure 3.22). Subsequently, synthetic $A\beta_{42}$ was subjected to different oligomerization protocols with varying oligomerization temperature, time and solvent used to dissolve $A\beta_{42}$ (Figure 3.23).

3.3.2.1 Western blot analysis of synthetic Aβ oligomers with different PAGE conditions

SDS, used in conventional SDS-PAGE is known to solubilize Aβ fibrils or aggregates until the dimer state, thus changing the initial oligomer profile. Therefore, native and semi-native PAGE protocols were performed to observe the full-range oligomer profile (Figure 3.22A).

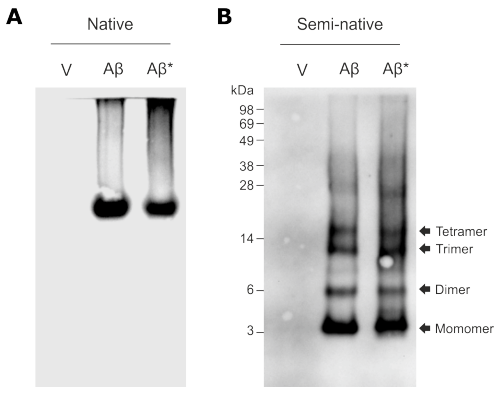

Figure 3.22: **Western blots of synthetic Aβ oligomers with different PAGE conditions** (A) Native and (B) semi-native PAGE contained 0.1 % SDS in the electrophoresis buffer and allowed identification of Aβ monomer and low molecular Aβ oligomers such as dimer, trimer, and tetramer by conventional SDS-PAGE molecular weight markers. V = vehicle, Aβ = $A\beta_{1-42}$, Aβ* = 95 % $A\beta_{1-42}$ + 5 % [Pyr3]$A\beta_{3-42}$.

Native PAGE did not contain any SDS. Semi-native PAGE contained SDS only in the running buffer to facilitate the running of the peptides in the 18% gel (Figure 3.22B). The vehicle sample which was used as a negative control and did not show any signal. The semi-native condition resolved low molecular weight oligomers such as dimer, trimer, and tetramer and monomers (Figure 3.22B) and single bands could be detected by conventional SDS-PAGE molecular weight markers. However, in native conditions, all different bands were observed as a single band and undefined smear (Figure 3.22A). Overall, semi-native PAGE was a useful method to monitor oligomeric Aβ species and was used routinely for the rest of the study to check the oligomer profile of Aβ preparations.

3.3.2.2 Synthetic Aβ* oligomerization and oligomer stability

To establish stable low molecular weight oligomer preparations, synthetic Aβ* was first solubilized in HFIP to generate a purely monomeric sample. Aβ* was aliquoted in glass vials to reduce loss of the sticky peptide during resolubilization. For oligomerization, HFIP was evaporated and Aβ* was dissolved and incubated at different conditions (Figure 3.23A).

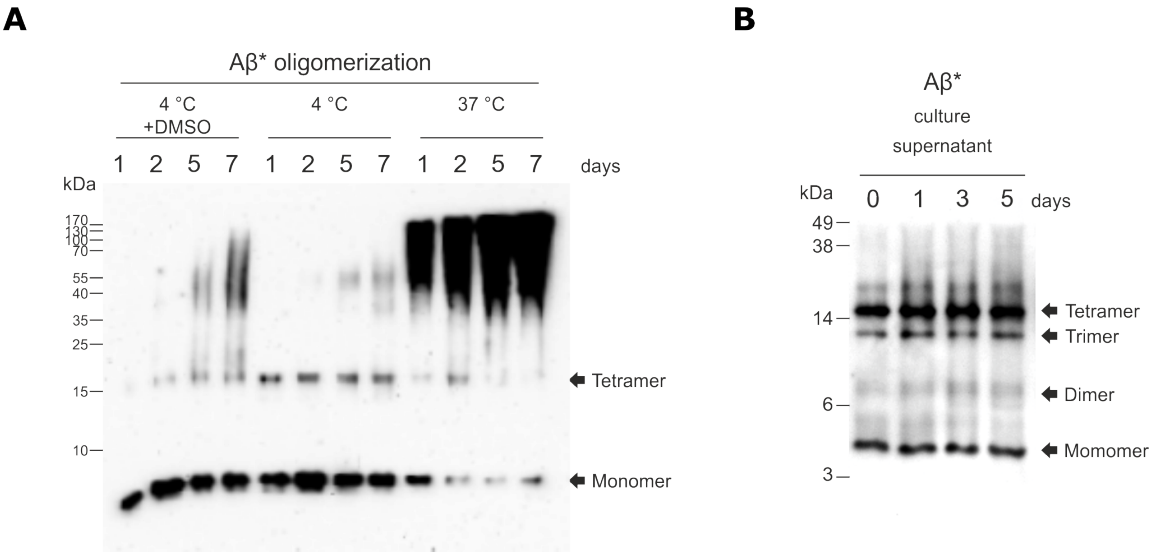

Figure 3.23: **Synthetic Aβ* oligomerization and oligomer stability during cellular incubation time.** Semi-native WBs were probed with the 6E10 antibody. (A) Synthetic Aβ* oligomers, prepared with or without DMSO in phenol-free Neurobasal medium, were incubated at (5 μM) for up to 7 d (1, 2, 5, and 7 d) either at 4 °C or 37 °C. (B) Western blot analysis of collected culture supernatant from primary rat cortical neurons, treated with 1 μM Aβ* (oligomerized with the DMSO-free protocol for 2d at 4 °C) for up to 5 d (0, 1, 3, and 5 d). This shows, that oligomer profiles were stable during 5 days of incubation at 37 °C.

Mostly, Aβ is dissolved in DMSO, which stabilizes the monomeric form (Shen & Murphy 1995). However, the presence of DMSO might cause synaptic alterations (Hanslick et al. 2009, Götte et al. 2010). Therefore, synthetic Aβ* was oligomerized at 5 μM in aqueous solutions (phenol free neurobasal solution) or in DMSO + NB (Aβ was first dissolved in DMSO at 5 mM briefly and further diluted in NB to 5 μM) for up to 7 d (1, 2, 5, and 7 d) at 4 °C or 37 °C. Oligomerization products were the analyzed by a semi-native western blot. This showed, that Aβ* oligomer profiles of DMSO+NB and only NB preparations (DMSO with more smear-like) performed at 4 °C were similar (Figure 3.23A, first 8 lanes), however, the DMSO-free condition contained more low molecular weight oligomers at any time point. It was also observed that temperature alters the oligomer profiles of Aβ* preparations immensely (Figure 3.23A, last 8 lanes). 37 °C resulted in more high-molecular weight aggregates in comparison to 4 °C. On the contrary, monomeric Aβ* was the most abundant species at 4 °C, followed by tetramers. To be able to observe the dimers and trimers in the preparations, longer exposure of the membranes was necessary (data not shown). Furthermore, high molecular weight oligomers were only observable in 5 d and 7 d preparations at 4 °C. Therefore, 4 °C preparations of Aβ* which gave rise to low-molecular weight oligomers were used for the rest of the study. Surprisingly low-molecular weight synthetic Aβ oligomers prepared in this method were very stable, media collected from cells, incubated with 1 μM Aβ* over 5 days showed no decrease in Aβ* and no change in the oligomer pattern (Figure 3.23B). Taken together, the Aβ preparation used in the following experiments contained mainly monomers and low-molecular weight Aβ oligomers.

3.3.3 Effects of synthetic Aβ* on neuronal cell viability

To test the effects of Aβ, Aβ* oligomer preparations on cell viability, an MTT assay was performed using untreated controls or HFIP-vehicle, Aβ, Aβ* oligomer-treated PCNs for 3d and 7d (Figure 3.24A and B, respectively). No change in cell viability was observed. To further investigate whether Aβ* oligomer-treatment alter the effect on cell viability in less enriched medium, SATO supplement was omitted from the medium and MTT assay was performed with 8 d long Aβ* oligomer-treated primary rat cortical neurons (Figure 3.24C). There was no change in cell viability neither in regular nor in less-enriched conditions (Figure 3.24C).

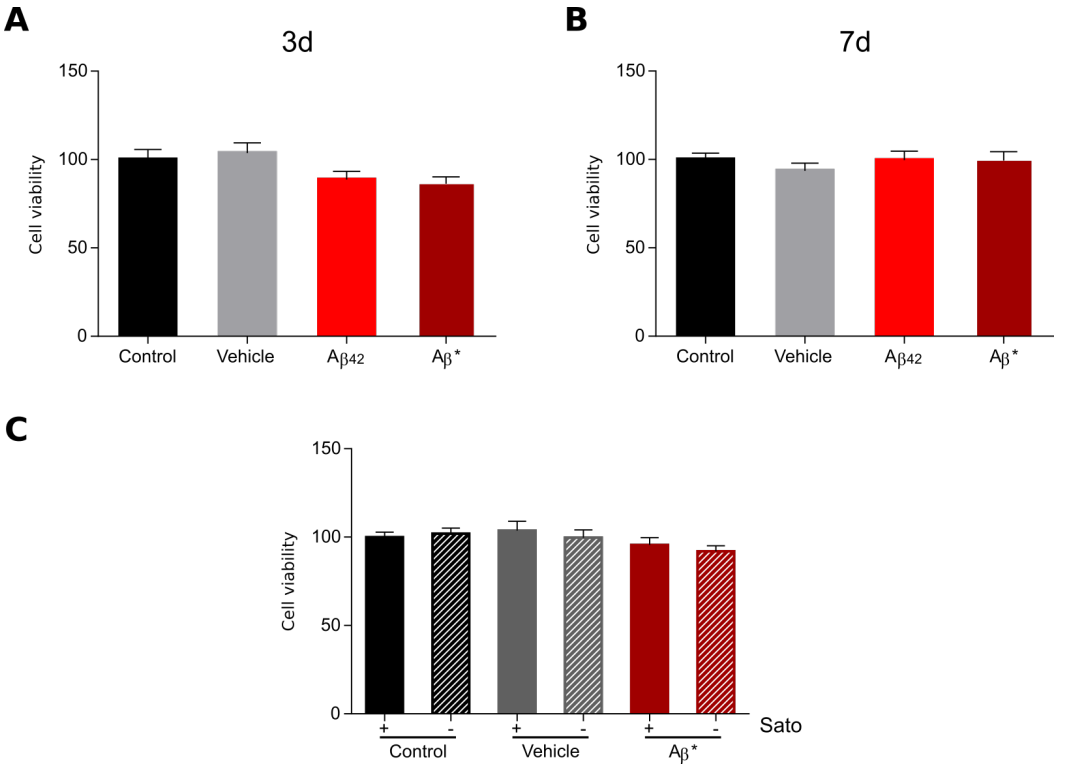

Figure 3.24: **Effect of synthetic Aβ species on cell viability.** Rat cortical cells were exposed to control medium (black bar), HFIP-vehicle (grey bar), 1 μM Aβ (red bar) or 1 μM Aβ* (dark red bar) oligomers for (A) 3d and (B) 7d. (C) Cell viability in presence and absence (dashed bars) of SATO supplement (Table 2.7) along with control (black bar), vehicle (grey bar), or 1 μM Aβ * oligomer (dark red bar) treatments. Cytotoxicity was measured by an MTT assay. Data are presented as a mean ±SEM, n = 6 wells (One-way ANOVA) No evidence of impaired cell viability was detected.

3.3.4 Effects of synthetic Aβ on electrophysiological properties of human neurons

To investigate the effects of the Aβ oligomers on the excitability and firing behavior of human iPSC-derived neurons, single-cell patch-clamp recordings were performed with mature cultures treated with vehicle and Aβ (for this experiment Aβ was oligomerized by incubation for 24h at 37°C) and compared to control cultures with no treatment (Figure 3.25). Injected current pulses resulted in depolarization and repetitive firing in almost all cells and representative evoked spike trains are shown for selected current steps (10, 50, 100, 150, and 200 pA current injection) of control, vehicle, and Aβ oligomer-treated cultures (Figure 3.25A). Repetitive firing patterns of Aβ oligomer-treated neurons were different for 50 and 100 pA current injection steps between vehicle and control neurons.

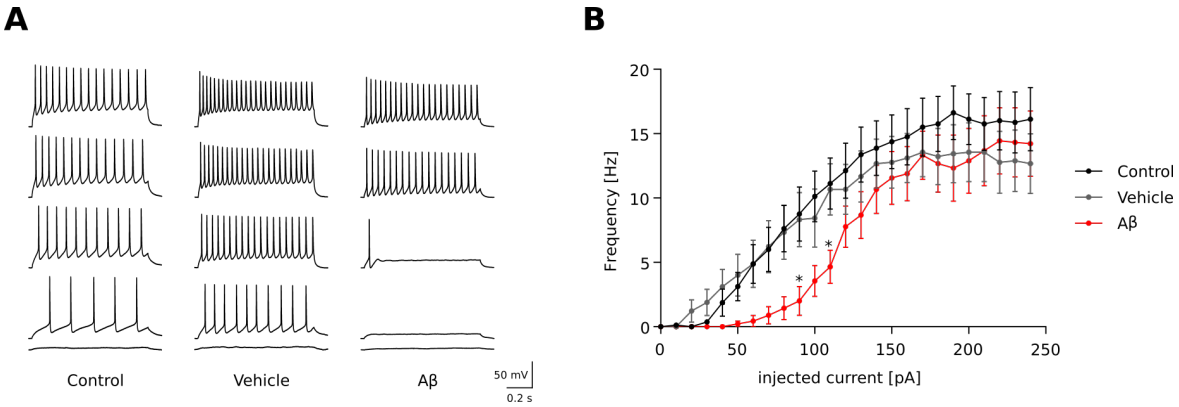

Figure 3.25: **Effects of synthetic Aβ oligomers on excitability.** (A) Representative current-clamp recordings of spike trains evoked by current injections of 10, 50, 100, 150, and 200 (bottom to top) under control, vehicle, or Aβ conditions. (B) Action potential (AP) frequency response to depolarizing current injections of untreated control (black), and vehicle- (gray) or Aβ- (red) treated neurons. (Two way ANOVA, Tukey's multiple comparison test *p < 0.05) n = 9.

All injected current pulses (-50 pA to 240 pA, 10 pA/step) were plotted against the corresponding firing rates (input-output curve, Figure 3.25B). Firing frequency showed reduction in 90 pA and 110 pA current injection steps in Aβ treated cultures compared to control and vehicle (Figure 3.25B, red line).

The shape of the first AP occurring upon 150 pA current injection was characterized from the patch clamp recordings of control, vehicle and Aβ oligomer-treated human iPSC-derived neuronals (Figure 3.26). APs of all human neurons showed a fast rise time to peak amplitude followed by a fast drop in voltage into afterhyperpolarization (AHP), which then slowly recovered to resting membrane potential (Figure 3.26A). The threshold for firing an AP was not different between treatments (Figure 3.26B). The initial phase of AP represented by AP amplitude and maximum rising slope, which are predominantly regulated by Na^+ channels, were not changed upon long term vehicle and Aβ oligomer treatment compared with control (Figure 3.26C and D). Furthermore, half-width, maximum rising slope, and AHP, which are predominantly regulated by K^+ channels, were not significantly different between treatments. These data suggest that there was no difference in AP parameters between neurons upon Aβ treatment.

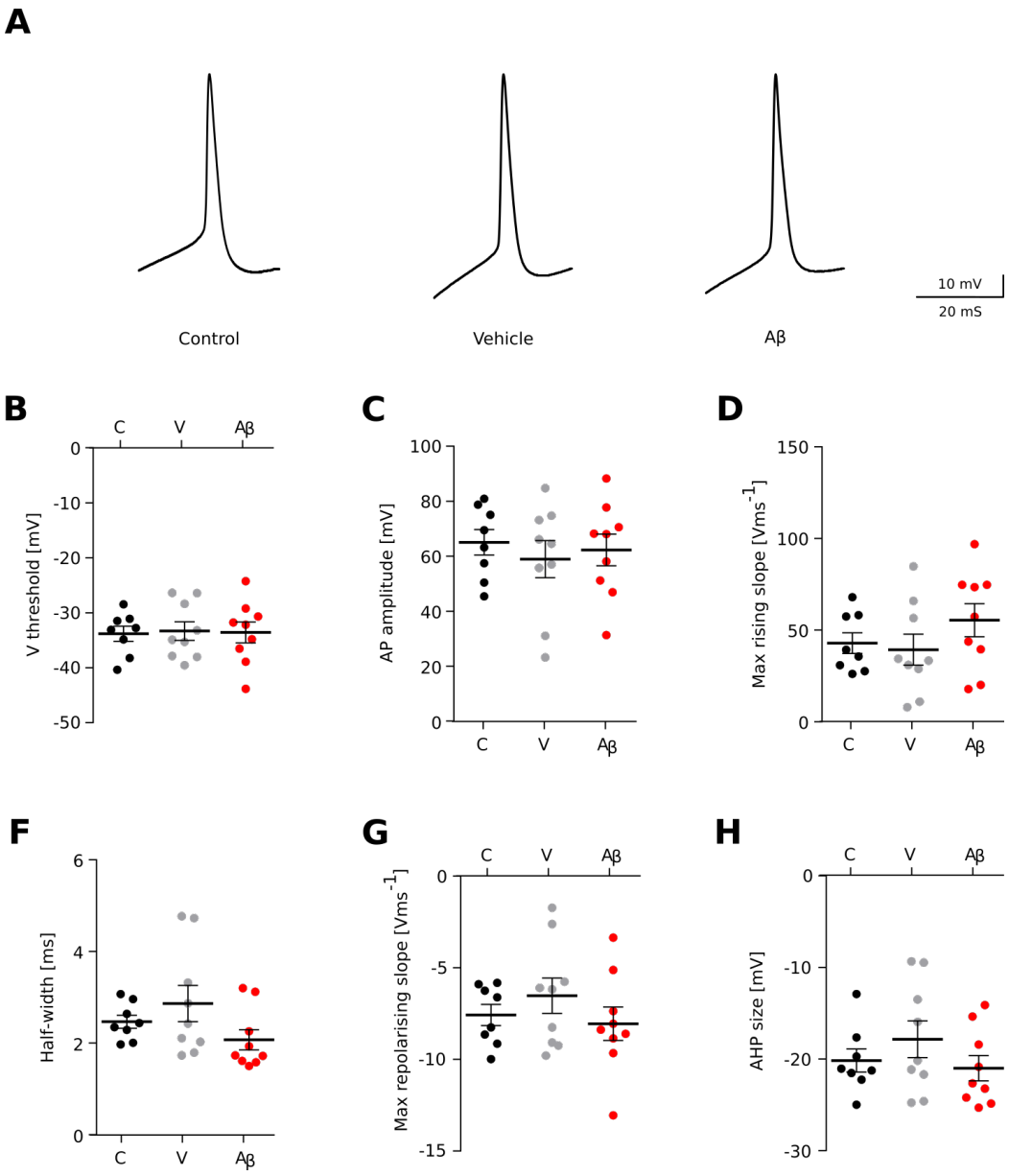

Figure 3.26: **Effects of synthetic Aβ oligomers on AP properties.** The shape of the first AP occurring upon 150 pA current injection was characterized. (A) Representative AP trace of control, vehicle, or Aβ treated neurons. (B) V threshold, (C) AP amplitude, (D) maximum rising slope, (E) half-width, (F) maximum repolarising slope, and (G) afterhyperpolarization of control (black), vehicle- (gray), and Aβ- (red) treated cultures. No changes were observed (One-way ANOVA followed by Tukey's multiple comparison test). n = 9.

3.3.5 Effects of synthetic Aβ* on spontaneous network activity of human neurons

In order to examine the effects of synthetic Aβ* oligomers on spontaneous activity, mature human iPSC-derived networks were treated with HFIP-vehicle or Aβ* and were extracellularly recorded by MEA. Firstly, to be able to use the vehicle-treated cultures as a control for the rest of the experiments, the network activity alterations were

investigated in vehicle-treated human iPSC-derived neuronal cultures and compared to the network activity of control cultures (Figure 3.27). Since the vehicle was prepared by evaporating HFIP (in which Aβ* was monomerized) under N2 stream for 30 min and followed by addition of phenol-free neurobasal medium to the tube, evaluation of traces of HFIP on the network activity was necessary to exclude vehicle effects. MEA recordings revealed that treatment of vehicle did not alter spike and burst frequency (Figure 3.27A and B), burst duration (Figure 3.27C), as well as the spike rate in bursts (Figure 3.27), compared to control cultures. Therefore, HFIP-vehicle was used for the rest of the study as a control for the synthetic Aβ* oligomer-related MEA recording experiments.

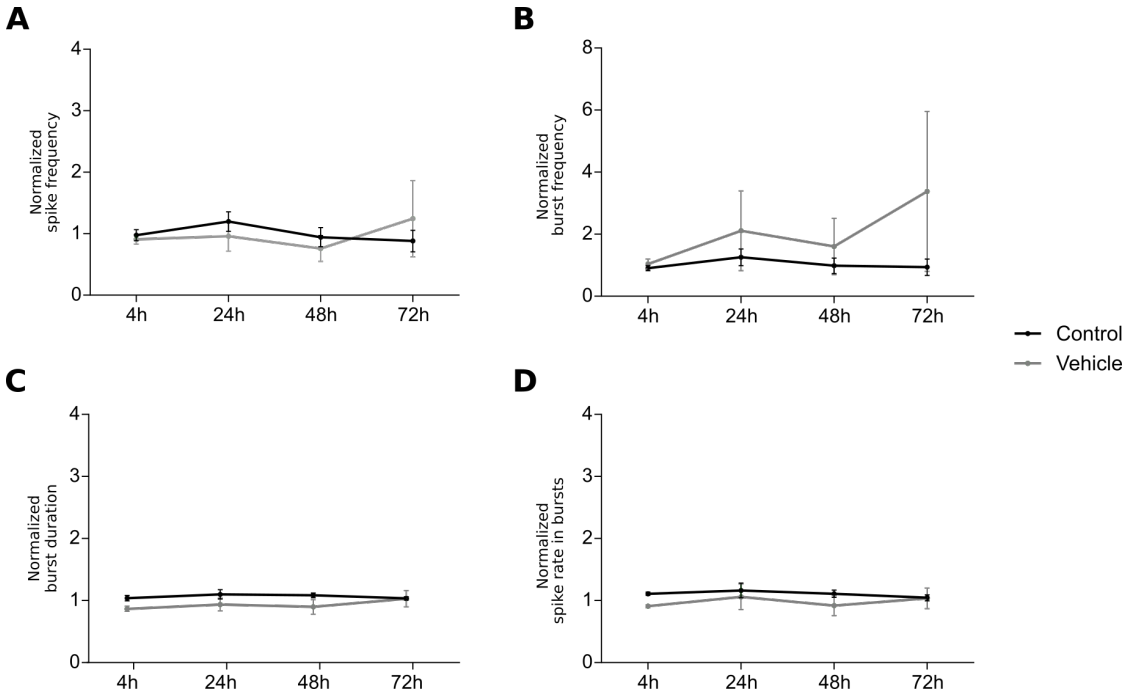

Figure 3.27: **Effects of vehicle HFIP treatment on spontaneous activity in mature human neuronal networks.** HFIP vehicles were prepared according to the Aβ oligomerization protocol and MEA cultures were treated by replacing half of the medium with vehicle containing fresh medium. Time-course of the normalized (A) spike frequency, (B) burst frequency, (C) burst duration, and (D) spike rate in bursts extracted from MEA recordings of human neuronal cultures, incubated for 4, 24, 48, and 72 h in the absence (control, black lines) and presence of vehicle (gray lines). Each value was normalized to the baseline value (before treatment). Data represent normalized mean±SEM, n = 3 MEAs.

Next, synthetic Aβ* oligomer-dependent effects were studied. Long-term changes in network activity upon synthetic Aβ* oligomer treatment were monitored for up to 8 days of treatment (1d, 2d, 3d, 4d, 5d, and 8d) (Figure 3.28A). Mature networks showed spike

and burst activity during pre measurements (Figure 3.28B, pre). Both vehicle- and synthetic Aβ* oligomer-treated networks showed no change in activity pattern (Figure 3.28B, 4d and 8d). Time-course analysis also revealed that synthetic Aβ* oligomer-treated networks showed no detectable changes in spike (Figure 3.28C) and burst (Figure 3.28D) rates compared to vehicle-treated control networks. Overall, synthetic Aβ* oligomers did not alter network activity in human neuronal networks.

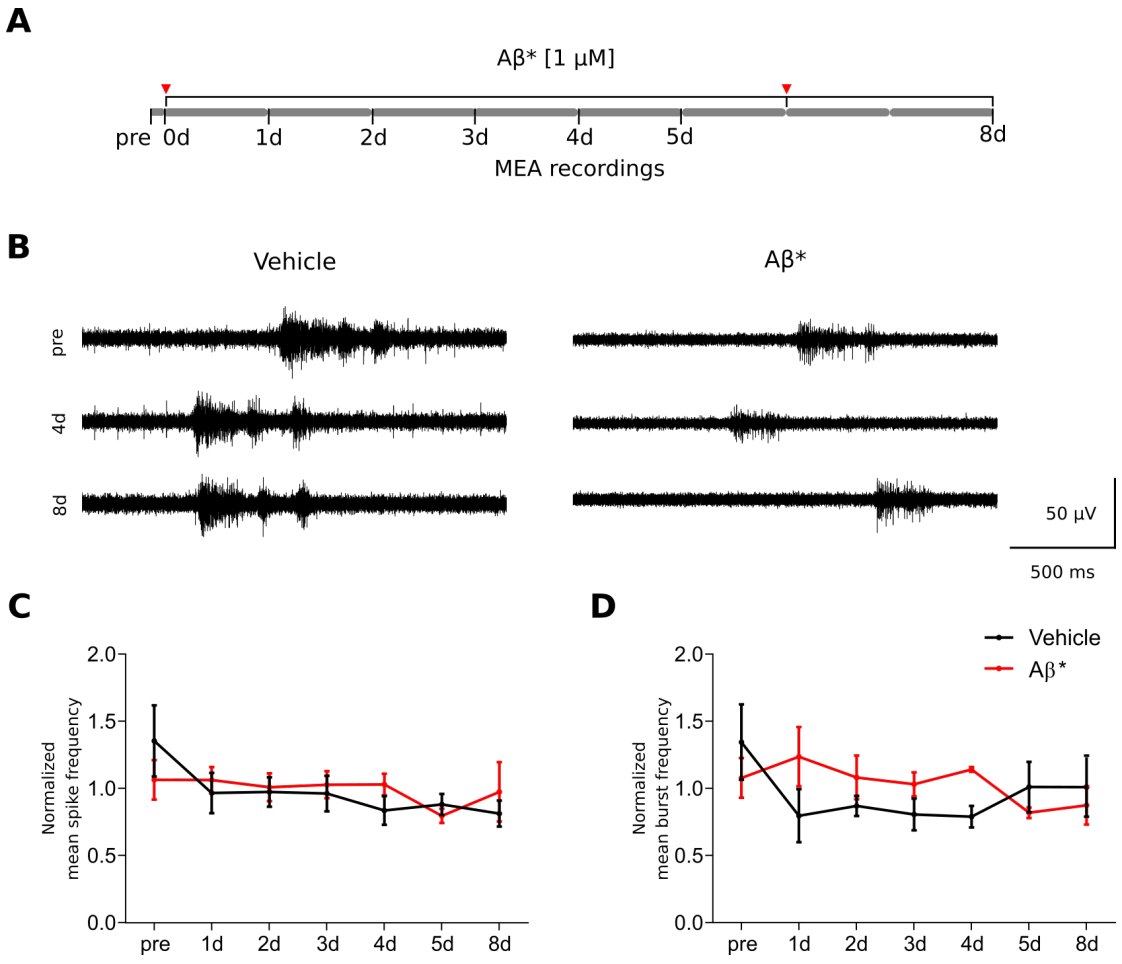

Figure 3.28: **Effects of synthetic Aβ* oligomers on spontaneous activity in mature human neural networks.** (A) Schematic Aβ* treatment and measurement protocol. d: day. Red arrowheads indicate the half medium changes with Aβ* treatments. (B) Representative extracellular voltage traces recorded from MEAs with vehicle (left) or Aβ* (right) treated cultures. Time-course of normalized (C) spike and (D) burst frequencies before (pre) and during (1, 2, 3, 4, 5, and 8 d) vehicle or Aβ* treatment. Each value was normalized to the baseline activity (pre). Data represent normalized mean±SEM, n = 3 MEAs. (Two-way ANOVA followed by Tukey's multiple comparison test). Normalized mean spike and burst frequencies showed no changes during Aβ* treatment.

Finally, to examine the long-term effect of synthetic Aβ* oligomers on spike properties, single spike analysis was performed before, at 1 d and 5 d of Aβ* treatment (Figure

3.29). To this end, the recorded data from MEA experiments were further processed as described before. Extracellular spikes from each active channel were normalized to the mean spike amplitude from the same electrode measured before the treatment (Figure 3.29A, -1d, black spikes. Quantification of spike parameters such as amplitude, half-width, 10 %-width and post-spike peak did not show any significant changes after 1 d and 5 d Aβ* treatment, compared to vehicle treated cultures (Figure 3.29B-E).

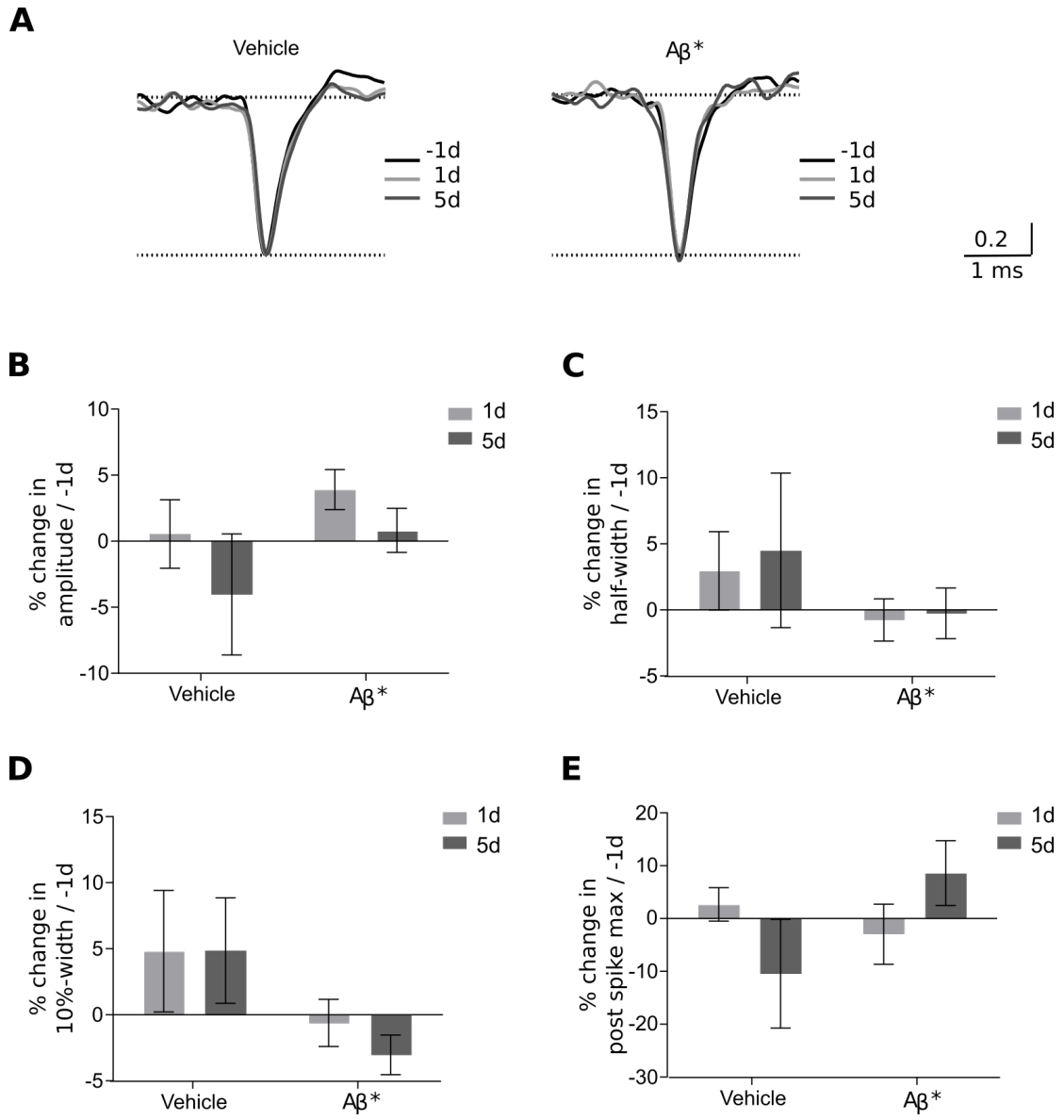

Figure 3.29: **Spike parameters of synthetic Aβ* oligomer-treated mature human neurons.** (A) Representative normalized mean extracellular spikes extracted from one electrode of MEA recordings before (-1d, black spikes) and during (1d, light gray spikes and 5d, dark gray spike) vehicle or Aβ* oligomer treatment. Effect size, shown as percent change in (B) amplitude, (C) spike half-width, (D) 10 % -width, and (E) post spike maximum. Data represent mean±SEM, n > 20 electrodes from 3 MEAs.

The results in this chapter indicated that high molecular weight or aggregated synthetic Aβ did not impair neuronal excitability (Figure 3.25 and Figure 3.26) and low molecular weight Aβ * oligomers did not affect the overall network activity (Figure 3.28) or spike properties (Figure 3.29) in human iPSC-derived neuronal networks. The lack of changes in burst activity suggested, that synapse number or efficiency were not affected by synthetic Aβ * oligomers. The next chapter, therefore, moves on to investigate alteration in homeostatic plasticity alterations upon synthetic Aβ* oligomer treatment.

3.4 Effect of synthetic Aβ* on 4AP-induced homeostatic plasticity

After establishing a hyperactivity-based homeostatic plasticity model in human iPSC-derived neuronal networks and characterizing Alzheimer disease-related Aβ* oligomers, the next step was to combine these approaches to study potential homeostatic plasticity alterations in AD. To this end, mature human iPSC-derived neuronal networks underwent long-term synthetic Aβ* oligomer exposure and later they were subjected to 4AP stimulation. Their ability to induce homeostatic plasticity in response to 4AP stimulation was monitored by MEA recording and calcium imaging (Figure 3.30 and Figure 3.33). Their response to acute and long-term 4AP stimulation and the ability to change the firing properties were investigated by spike analysis (Figure 3.31 and Figure 3.32). The involvement of REST was studied using immunocytochemistry and calcium imaging (Figure 3.34 and Figure 3.35).

3.4.1 Changes in homeostatic plasticity upon synthetic Aβ* treatment in mature human neuronal networks

To investigate the effect of Aβ* oligomers on hyperactivity-induced homeostatic plasticity, mature hiPSC-derived neurons, which were pre-treated with Aβ* oligomers (oligomer preparation: 5 μM for 2 d at 4 °C) or vehicle for 8 days, were subjected to 4AP stimulation and the network activity was monitored by MEA recordings (Figure 3.30A). Networks showed burst pattern activity before 4AP treatment (Figure 3.30B, pre). Both vehicle and Aβ* oligomer-treated networks displayed increased activity upon 4AP stimulation (Figure 3.30B, acute 4AP). After 24 h in 4AP, vehicle-treated networks showed decreased spike rates which continued decreasing until 96 h. After removal of 4AP, the spike frequency was reduced, compared to baseline levels. Low activity levels sustained for at least 72 h after 4AP removal (Figure 3.30B, post1d and Figure 3.30C, black lines). Aβ* treated networks were also able to decrease their firing rates; however, the initial decrease was lower and even after 96 hours, the plasticity response was only partial and did not reach the levels of vehicle-treated networks (Figure 3.30B, post1d and Figure 3.30C, red lines). To conclude, Aβ* treatment leads to an impaired homeostatic network response to induced hyperactivity in human iPSC-derived neuronal networks.

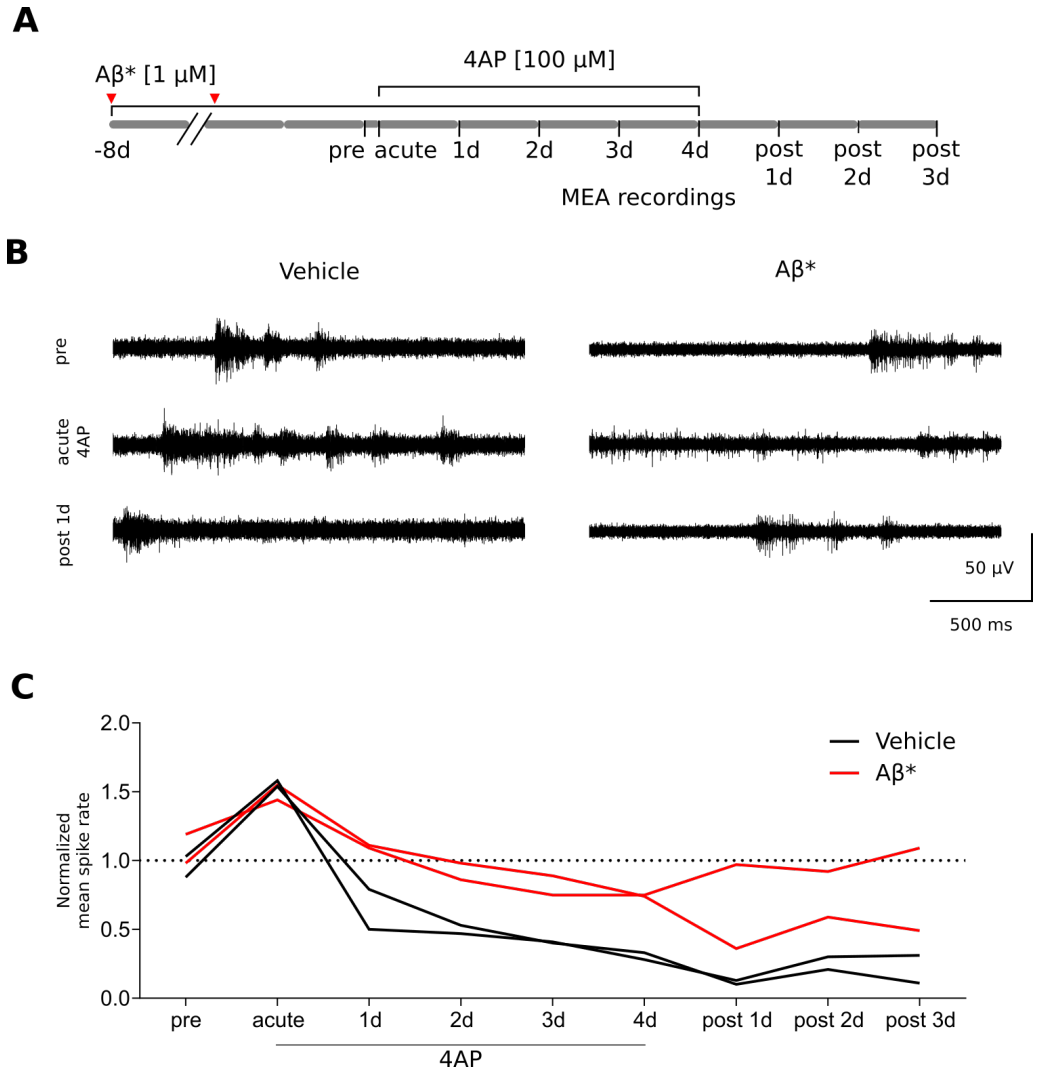

Figure 3.30: **Effect of Aβ* oligomers on homeostatic plasticity in mature human neuronal networks.** (A) Schematic treatment and measurement protocol. Human neurons were pretreated with vehicle and oligomeric Aβ* for 8 days, with a half medium change and Aβ* refreshment after 6 days. Red arrowheads represent the medium changes. Homeostatic plasticity was then induced by 4AP treatment for 4 days. Network activity was analyzed before, during and after 4AP treatment. (B) Representative voltage traces from MEA recordings before (top), during (middle) and after (bottom) 4AP treatment in vehicle (left) and Aβ* (right) treated cultures. (C) Time-course of normalized spike frequencies from single MEAs before (pre), during (bottom line, 100 µM for 96 h) and after (post 1d, 2d, 3d) 4AP treatment. Each value was normalized to the baseline activity (pre value).

3.4.2 Effects of Aβ* oligomers on 4AP-induced changes in spike properties

To evaluate the effects of Aβ* oligomers on homeostatic plasticity, spike properties were investigated during acute treatment and after the removal of Aβ*. First, it was tested, whether both vehicle and Aβ*-treated cultures responded to 4AP stimulation in a similar manner (Figure 3.31). Representative normalized extracellular spikes of vehicle and

Aβ*-treated neurons before and during 4AP stimulation are shown in Figure 3.31A. Quantification of spike parameters revealed that the spike amplitude (Figure 3.31B) was not changed by 4AP treatment in vehicle and Aβ* pre-treated cultures. Acute 4AP stimulation resulted in increased spike half-width (Figure 3.31C) and 10 % width (Figure 3.31D) and decreased post-spike maximum (Figure 3.31E) in both conditions. However, the increase in 10 % width was slightly lower in Aβ*-treated cultures (Figure 3.31D, red bar).

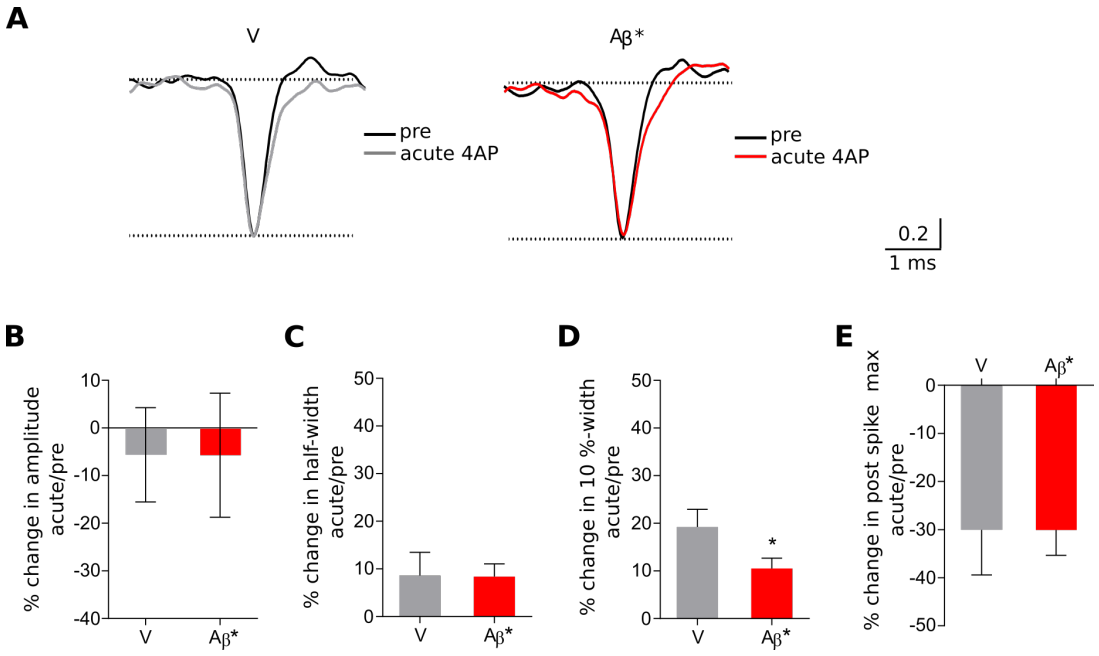

Figure 3.31: **Effects of Aβ* oligomers on 4AP-induced acute changes in spike parameters.** (A) Representative normalized mean extracellular spikes extracted from one electrode of MEA recordings before (pre, black spikes, normalized to 1) and during (acute, normalized to pre) 4AP treatment in vehicle (gray spike, left) and Aβ* (red spike, right) treated cultures. Effect size, shown as percent change in (B) amplitude, (C) half-width, (D) 10 %-width, and (E) post spike max. Mean±SEM, n > 20 electrodes from 2 MEAs. (Two-tailed t test, *p<0.05).

Once it was confirmed that vehicle and Aβ* oligomer-treated human neurons responded to the acute 4AP stimulus in a similar manner, plasticity-dependent changes were investigated by comparing spikes before and after 4AP treatment (Figure 3.32). Extracellular mean spike amplitudes from one electrode of vehicle and Aβ*-treated neurons were normalized to the mean spike amplitude before 4AP treatment (Figure 3.32A). As expected, blocking potassium channels with 4AP triggered homeostatic mechanisms and the amplitude of vehicle-treated neurons was decreased in the post 4AP condition compared to the values before treatment (Figure 3.32A, post 4AP, gray

spike). However, this change was significantly diminished in Aβ*-treated neurons (Figure 3.32A, post 4AP, red spike and Figure 3.32B). In both conditions, 4AP-treated neurons showed a decrease in half-width (Figure 3.32C) and 10 %-width (Figure 3.32D) and the post-spike maximum was not affected (Figure 3.32E). Overall, indicated by the data on spike properties, Aβ*-treated human iPSC-derived neurons were not able to fully adjust their excitability in response to 4AP-induced hyperactivity.

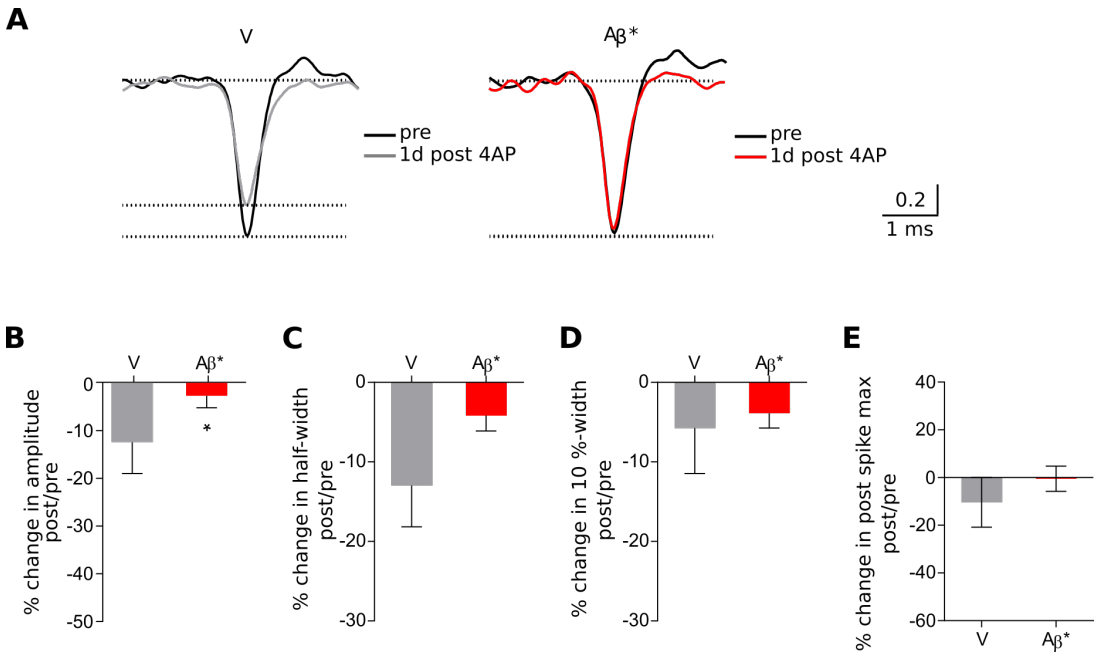

Figure 3.32: **Effects of Aβ* oligomers on 4AP-induced plasticity-dependent changes in spike parameters.** (A) Representative normalized mean extracellular spikes extracted from one electrode of MEA recordings before (pre, black spikes, normalized to 1) and 1 day after removal of 4AP (1 day post, normalized to pre) 4AP in vehicle (gray spike, left) and Aβ* (red spike, right) treated cultures. Effect size, shown as percent change in (B) amplitude, (C) half-width, (D) 10 %-width, and (E) post spike max. Mean±SEM, n > 20 electrodes from 2 MEAs. (Two-tailed t test, *p<0.05).

3.4.3 Effects of Aβ* oligomers on 4AP-induced plasticity-dependent changes in synchronous calcium transients

To explore the plasticity-dependent changes in calcium transients of human iPSC-derived networks, pre-treated with vehicle or Aβ* for 6-8 days, Fura 2-based calcium imaging was performed (Figure 3.33A). Calcium transients were imaged before and at acute 4AP treatment from the same coverslip. Activity in 2 day 4AP-treated cultures (2d post) was imaged from sister coverslips.

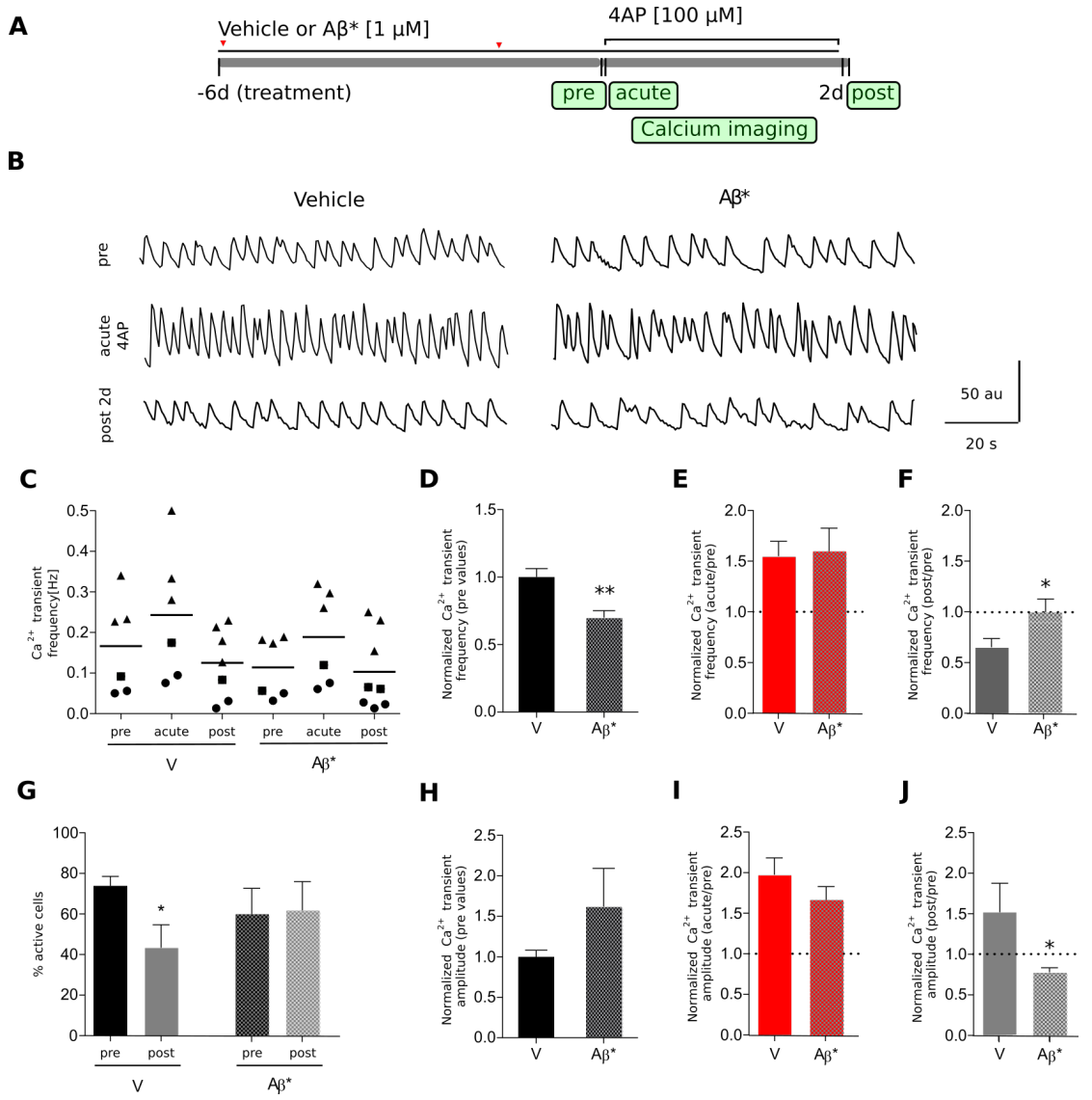

Figure 3.33: **Effects of Aβ* oligomers on 4AP-induced plasticity-dependent changes in synchronous calcium transients.** (A) Schematic treatment and measurement protocol. d: day. Red arrowheads indicate the half medium changes with Aβ* treatments. (B) Representative traces of spontaneous calcium transients before (top), during (middle), and after (bottom) 4AP stimulation of vehicle and Aβ*-treated cultures extracted from one AOI with several neurons. (C) Distribution and mean of calcium transient frequencies at different treatments. Sister coverslips are indicated by symbol shape. Normalized calcium transient (D) frequency and (H) amplitude of vehicle and 6 days Aβ* treated networks. Aβ* values were normalized to the vehicle treated sister coverslips. Data represent mean±SEM, n = 6. (Two-tailed t test, **$p < 0.01$). (E,F) Normalized calcium transient frequency and (I,J) amplitude during (acute) and after (post) 4AP treatment in vehicle and Aβ*-treated cultures. Each value was normalized to the baseline value (pre) of the respective vehicle or Aβ*-treated sister coverslips, data represent mean±SEM, n= 6-8 coverslips. (Two-tailed t test *$p < 0.05$). After removal of 4AP, the spontaneous synchronous calcium transient rate was decreased in vehicle-treated cultures (G) Percentage of synchronously firing cells before and after 4AP treatment in vehicle and Aβ*-treated cultures. Data represent mean±SEM, n > 3 coverslips. (Multiple t test **$p < 0.01$).

The general activity state, that is the presence of synchronous calcium transients, which is a prerequisite for functionality of the 4AP plasticity paradigm was confirmed in 2d post samples by reapplication of 4AP at the end of the measurement. Only cultures, that enhanced transient frequency upon 4AP reapplication, were taken into account. This set of experiments was performed on endogenous neuron-astrocyte cocultures and cocultures of human neurons and rat astroctyes. Both cultures systems yielded variable calcium transient frequencies, which are displayed in Figure 3.33C. For quantitative comparison, each value was normalized to the values received from sister coverslips at baseline activity (pre). Interestingly, calcium transients of Aβ*-treated cultures showed a decreased transient frequency compared to vehicle-treated sister networks (Figure 3.33B, pre, and Figure 3.33D). Upon 4AP treatment (Figure 3.33B, acute and Figure 3.33E and F, red bars) both conditions showed a similar increase in their calcium transient frequency. However, after 2 days of 4AP, a decreased calcium transient rate was only observed in vehicle treated cultures (Figure 3.33E and F, grey bars). Upon 4AP-induced hyperactivity, the number of active cells was only decreased in vehicle treated cultures (Figure 3.33G). The transient amplitude which was extracted from active cells showed a tendency to be increased in Aβ* as compared to vehicle treated cultures (Figure 3.33B, pre, and Figure 3.33H). After removal of 4AP, in Aβ*-treated cultures the amplitude was slightly reduced compared to vehicle treated cultures (Figure 3.33J). In conclusion, these data confirm the preliminary results from MEA recordings, showing that in presence of Aβ*, the homeostatic response was impaired and cells were not able to change their properties to adjust overall network activity.

3.4.4 Changes in REST expression upon synthetic Aβ* treatment in mature cultures

REST was previously reported to be upregulated in the aging brain. However, this upregulation was found to be impaired in the brain of AD patients (Lu et al. 2014), suggesting that dysregulation of REST may play a role in the pathogenesis of AD. Here, I wanted to address, whether Aβ*, a well-established causative factor in AD etiology, exerts its effect on homeostatic plasticity by impairing REST upregulation during periods of hyperactivity. Therefore, mature human iPSC-derived neurons were treated with vehicle or synthetic Aβ* oligomers and REST expression was compared to untreated controls (Figure 3.34A) by immunocytochemistry.

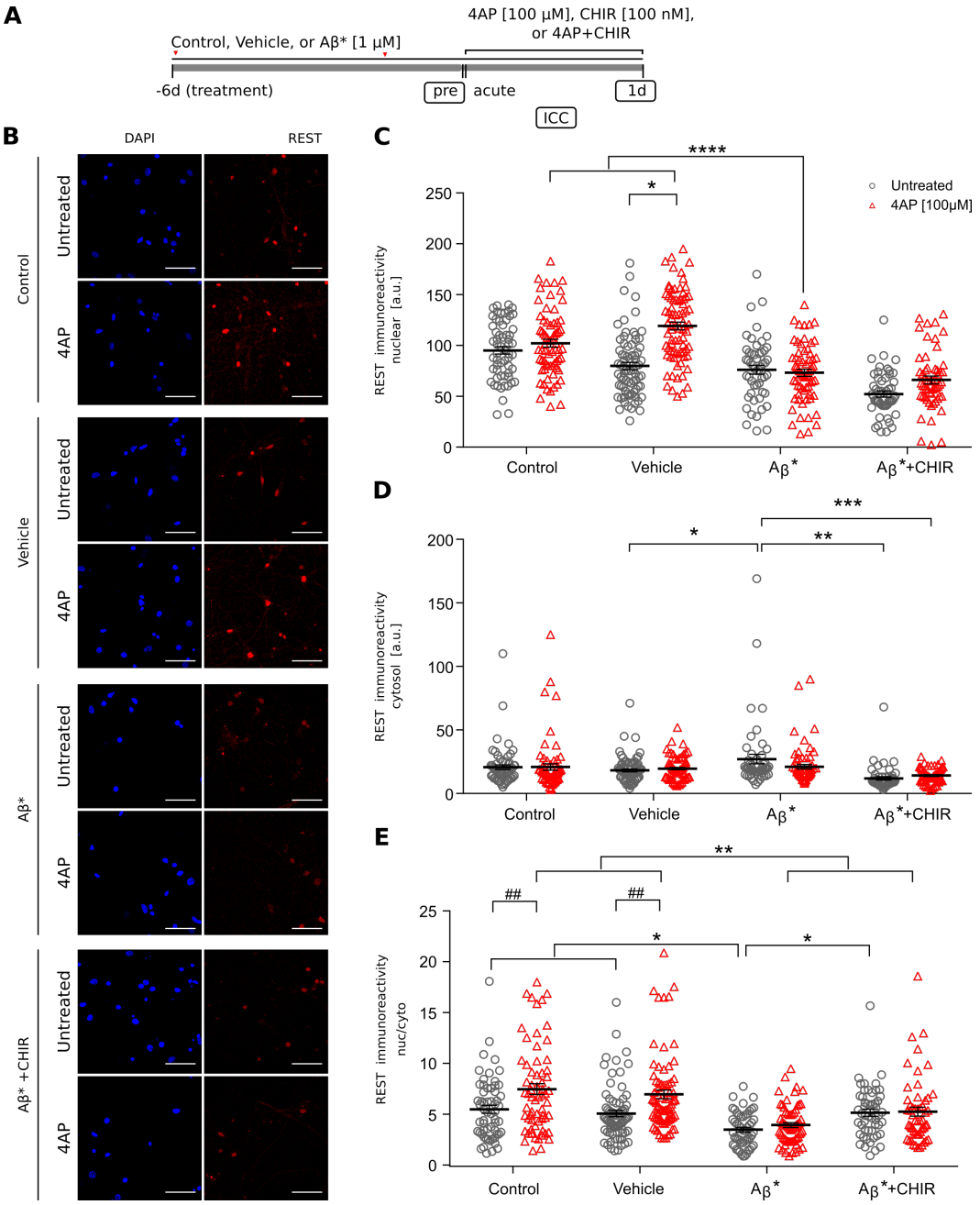

Figure 3.34: **Effects of synthetic Aβ* on 4AP-induced changes in REST expression.** Mature human neurons were treated with control medium, HFIP-vehicle and Aβ* for 8 days. Subsequently, these cultures were further cultured for 24 h in the absence (untreated) or presence of 100 µM 4AP. Three of the Aβ* treated cultures were additionally treated with 100 nM CHIR in parallel to the 4AP treatment (Aβ* + CHIR). (A) Schematic treatment and analysis protocol. (B) Example confocal micrographs of control, vehicle, Aβ*, and Aβ* + CHIR treated human neurons after 24 h with or w/o 4AP. Neurons were immunocytochemically stained for REST (red). Nuclei were stained with DAPI (blue). Quantification of the mean fluorescent intensity of (C) nuclear and (D) cytosolic REST under different conditions. (E) Nuclear vs cytosolic REST ratio. Data are represented as single data points, representing values from one neuron and mean, n > 20 neurons from 3 coverslips. (Two-way ANOVA Tukey's multiple comparisons test *p < 0.05, **p < 0.01, ***p < 0.001, ##p < 0.01). Scale bar, 50 µm.

Representative merged confocal images (REST, red; Nuclei, blue) of each treatment was displayed (Figure 3.34B) before (untreated, upper panel) and after 24 h 4AP treatment (4AP, lower panel). The nuclear/cytosolic ratio of REST expression showed a reduction in Aβ*-treated cultures (Figure 3.34E). Furthermore, 4AP did not lead to an increase of nuclear/cytosolic REST in Aβ*-treated cultures, whereas control and vehicle cells responded to the 4AP stimulation with a comparable increase in nuclear/cytosolic REST (Figure 3.34E). CHIR is known to increase REST expression within 24 h (Figure 3.18). Therefore, to rescue the Aβ*-related REST alterations and impaired increase of nuclear/cytosolic REST, Aβ* pre-treated neurons were subjected to CHIR treatment for 24 h, in parallel to 4AP or control treatment. CHIR treatment increased nuclear/cytoplasmic REST ratios in Aβ* treated cells (Figure 3.34E). However, CHIR and 4AP co-treatment did not lead to a further increase of nuclear/cytosolic REST.

3.4.5 Effect of CHIR on 4AP-induced changes in the calcium transient frequency in human mature neurons

In parallel to studying the effect of CHIR on 4AP-induced upregulation in Aβ*-treated cultures, I also wanted to address how CHIR affects homeostatic plasticity at the activity level. Therefore, vehicle or Aβ* (6 days) pre-treated human iPSC-derived networks were subjected to a 48 h CHIR and 4AP co-stimulation. In vehicle treated cultures, CHIR treatment (post +CHIR, 3.35B) did not lead to a further decrease in network activity upon 4AP removal (post, 3.35B). However, compared to the activity after removal of 4AP (post, 3.35D) in Aβ* pre-treated cultures, CHIR lead to a non-significant increase in activity (post + CHIR, 3.35D). To conclude, the pharmacological intervention to rescue REST levels and thereby impaired homeostatic plasticity by CHIR treatment was not successful at the level of REST induction and thus, did not improve homeostatic plasticity in Aβ*-treated cultures.

Taken together, Aβ* treatment showed no effect on cell viability and spontaneous activity. However, when the network was shifted towards hyperactivity by 4AP treatment, Aβ*-treated cultures were incapable of changing the excitability of single neurons for re-setting the firing rates to basal levels. Additionally, general REST expression and plasticity-dependent regulation of REST expression were impaired by Aβ*, which indicated an important role of REST in AD-related plasticity dysfunction. As a consequence, REST dysregulation may lead to prolonged periods of hyperactivity, which may explain the frequent occurrence of epileptic activity in the brain of Alzheimer

patients.

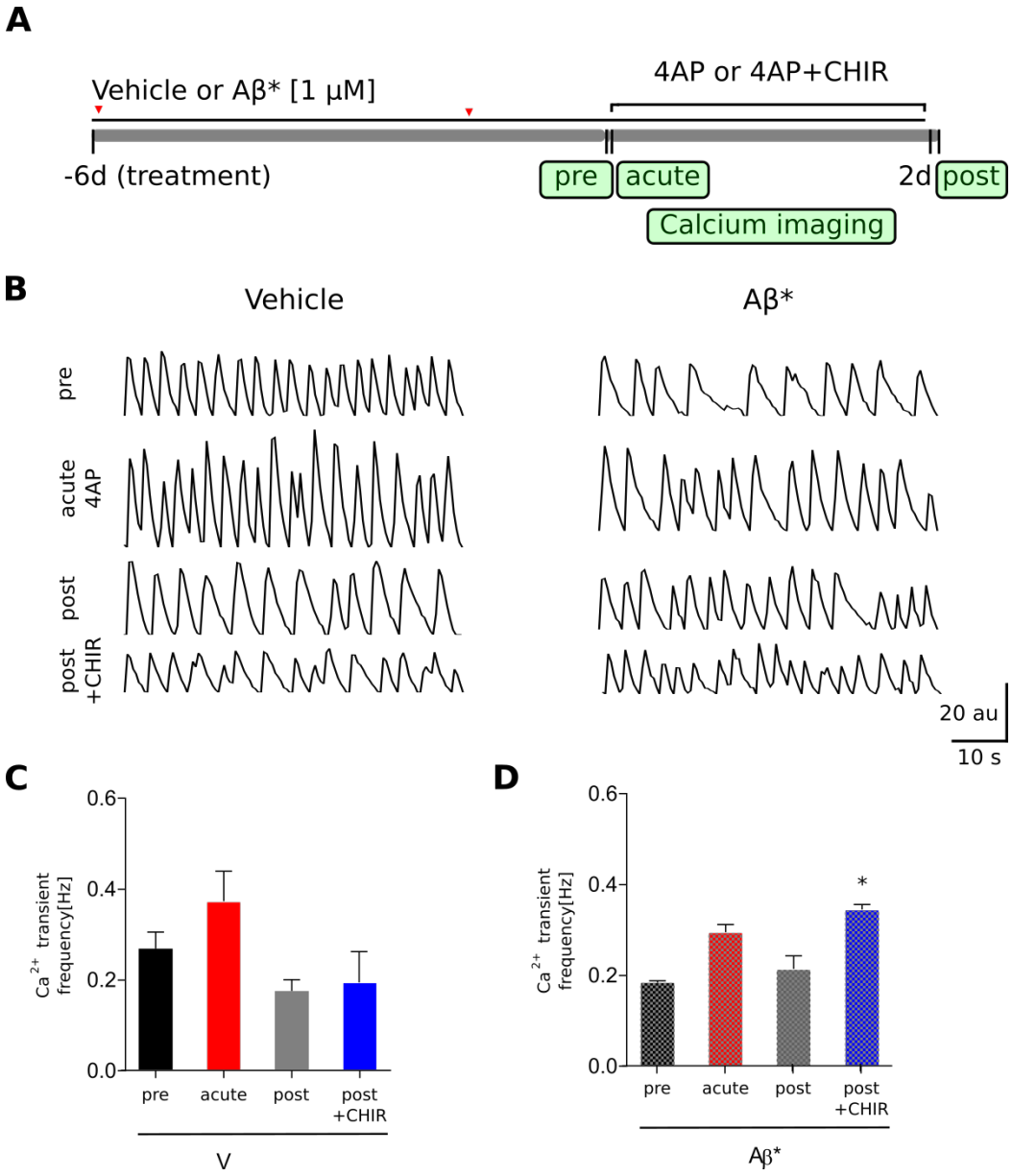

Figure 3.35: **Effect of CHIR on 4AP-induced changes in the calcium transient frequency in human mature neurons.** (A) Schematic treatment and measurement protocol. (B) Representative traces of spontaneous calcium transients. Quantification of calcium transient frequencies in (C) vehicle and 6 days (D) Aβ* treated networks before, during and after 48 h of 4AP treatment and after 48 h of CHIR + 4AP treatment. Data represent mean±SEM, n = 3 coverslips. Aβ*+CHIR treated cultures showed increased frequency after the removal of 4AP (post +CHIR) compared to before 4AP treatment (pre) only in Aβ*-treated cultures. (One-way ANOVA Dunn's multiple comparisons test, *p < 0.05).

4. Discussion

4.1 Human iPSC-derived neuronal networks: cell types, network activity, and assay development

Neurological disease modeling until this decade mainly relied on animal models and non-neuronal human cell lines because of the lack of human material. However, although the contribution of those models to our understanding disease mechanisms cannot be denied, developed drugs by using the models failed in clinical trials. Fortunately, ten years ago, the first successful reprogramming attempt was made by using human cells to create stem cell-like cells (Takahashi et al. 2007) which could be further differentiated into neurons for disease modeling (Yagi et al. 2011). However, the maturity of differentiated human neurons from iPSCs is still debated and establishing networks with spontaneous activity is challenging and requires long-term culturing. Moreover, it has been shown that murine astrocytes help human iPSC-derived neurons to develop spontaneous network activity (Odawara et al. 2014).

In this study, human iPSC-derived neurons were differentiated and the cell type composition was characterized by immunocytochemistry. Functional maturation was evaluated by MEA recordings and by calcium imaging and correlated with synchronous network activity. Finally, the eligibility of human networks for toxicity assays was investigated by western blot and calcium imaging upon BoNT/A treatment.

4.1.1 Differentiation and characterization of human iPSC-derived neuronal networks

Establishing mature human neuronal networks from iPSCs is a critical step for disease modeling. In this study, to obtain networks with cortical identity, iPSCs were directed towards the neural lineage by dual SMAD inhibition to induce neuroectoderm formation (Chambers et al. 2009) alone or in combination with the tankyrase-inhibitor XAV939 (Huang et al. 2009) which was replaced recombinant DKK1 for forebrain fate determination by inhibiting WNT. After differentiation, immature postmitotic neurons were enriched by NCAM immunopanning (Nieweg et al. 2015). Immature post mitotic neurons showed the expression of mainly deep-layer cortical markers which overlaps with the finding of other studies, showing dorsal forebrain characteristic (Chen et al. 2008). and, to a lesser extent, upper layer cortical markers (Figure 3.1) which overlaps

with the findings of the studies of dorsal forebrain characteristics (Chen et al. 2008, Alcamo et al. 2008). This result may be explained by the fact that these are early born neurons and longer culturing of the networks might give rise to more upper layer neurons. Interestingly, although cortical induction would not allow the generation of GABAergic interneurons, a few GAD67-positive GABAergic interneurons were observed in the immature cultures. The reason for this is not clear but it may have something to do with the fact that GABA acts as excitatory transmitter to depolarize the young neurons via chloride permeable channels (Cherubini et al. 1991).

After neuronal enrichment by NCAM immunopanning of hiPSC-derived neurons were either treated with DM and PD for internal glial development, or cocultured with rat cortical astrocytes for maturation. Cocultures were treated with AraC to kill all proliferating cells. Cultures were incubated for at least eight weeks post immunopanning to ensure morphological and functional maturation. During the normal development of the nervous system, electrophysiological development of the neurons is the critical step for maturation (Spitzer 2006). Since the cultures were mainly consisted of excitatory neurons and, to a lesser extent, GABAergic interneurons, the network activity was monitored by MEA recordings with gabazine treatment (Figure 3.2). Gabazine inhibits chloride flux across the cell membrane and thus inhibiting neuronal hyperpolarization. Surprisingly, although GAD67 expression in the cultures was observed, gabazine treatment did not cause any alterations in the network activity. There are several possible explanations for this result. Since the cortical forebrain GABAergic cells mainly develop from medial and caudal ganglionic eminences, the forebrain fate direction eliminated the GABAergic development. However, this does not explain the presence of GAD67 expressing neurons in the cultures to begin with. Another explanation would be that the inhibitory input caused changes in the network activity which was under the detection limits of MEA recordings. A further possible explanation for this result may be the lack of adequate glial support for functional inhibitory interneuron development. It is possible to overcome the problem of lacking inhibitory interneurons by differentiating them from iPSCs separately (Liu et al. 2013) and coculture them with the excitatory pyramidal neurons. However, this issue was not addressed in this study and a future study investigating the inhibitory interneuronal input to the network activity would be very interesting.

4.1.2 Network activity

The major aim of generating human iPSC-derived neurons is to better model neurological diseases. Since neurons do not function as a single entity, it is necessary to have functional synapses and networks to be able to study neuronal function. The synchronous burst firing is a sign of the maturity in dissociated neuronal networks in vitro (Chiappalone et al. 2006). For networks to function, synapses have to be maintained via synaptic transmission which occurs via the calcium influx dependent-vesicular release upon the arrival of an AP to the presynaptic terminal (Llinás 1991). Therefore, extracellular calcium ion dependent-network activity changes were monitored by MEA recordings (Figure 3.4). Contrary to expectation, increasing extracellular Ca^{2+} reduced the frequency of synchronous network bursts to almost zero. A possible explanation for these results may be the surface charge effect which is a negative charge masking effect by divalent ions, mainly Ca^{2+} on the outside of the cell membrane (Hille 1978). Lowering extracellular Ca^{2+} concentration showed first increased than reduced spikes and synchronous network bursts probably first removing the surface charge effect but then inhibiting the vesicle release. Overall, calcium is an important player in network activity and the stable extracellular calcium ion levels have to be maintained for stable firing rate acquisition during MEA recordings.

The functional maturation of human iPSC-derived neurons was closely correlated with the presence of fully functional AMPA and NMDA receptors. AMPA and NMDA receptors mediate learning-related neuroplasticity and AMPA receptors are important because of their involvement in synaptic scaling, a form of homeostatic plasticity (Pozo & Goda 2010). Moreover, overactivity of NMDA receptors was implicated in neurodegenerative diseases. Therefore, to ensure that the recorded neuronal activity was a result of the synaptic connectivity, extracellular network activity changes were monitored by MEA recordings upon introducing APV and DNQX (Figure 3.3). As expected, inhibition of NMDA and AMPA type glutamate receptors by APV and DNQX resulted in strong reduction of synchronous bursts suggesting that the occurrence of bursts are exclusively mediated by excitatory synaptic transmission. Thus, NMDA and AMPA receptors were pharmacologically functional in these cells. On the other hand, individual action potentials also appear to be caused by spontaneous (non-synaptic) depolarization of individual neurons since they were only partially reduced. These findings are in line with the findings of synchronously burst firing long-term human iPSC-derived cultures from

another group (Odawara et al. 2016).

Network activity can be monitored by calcium imaging since synchronous calcium transients are associated with neuronal bursting (Opitz et al. 2002). As an alternative to MEA recordings, calcium imaging with Fura-2-AM was used to visualize spontaneous network activity of human iPSC-derived neuronal cultures. It was ensured that during measurements, environmental temperature was set to 37°C since the synaptic transmission is temperature dependent (Hardingham & Larkman 1998). To distinguish the neurons from astrocytes, KCl was applied at the end of each recording because astrocytes give a delayed response. Application of APV, DNQX, and gabazine blocked the occurrence of spontaneous synchronous calcium transients indicating that they are exclusively outcome of the synaptic activity.

In conclusion, the MEA and calcium imaging assays using pharmacologically manipulated hiPSC-derived cortical neuronal networks showed that synchronous burst firing is the main outcome of synaptic activity. Nonetheless, the spike frequency is also affected by synaptic blockage and allows an insight into the network activity. Finally, synchronously burst firing human iPSC-derived neuronal networks provide a powerful tool to study pharmacological and toxicological characteristics of a compound of interests.

4.1.3 BoNT/A toxicity assays

The botulinum neurotoxin type A (BoNT/A) is a lethal substance produced by the bacteria *Clostridium botulinum* which is used to treat neuromuscular disorders, chronic pain, and in cosmetics (Jankovic 2004). BoNT/A is a useful compound in the pharmaceutical industry however it needs to be carefully titrated. The main method for testing BoNT/A activity is an in vivo mouse bioassay (MBA), in which intraperitoneally or intravenously injected BoNT/A leads to the death of a mouse due to respiratory arrest with the sensitivity limit at 20 pg/ml (0.13 pM BoNT/A) (Schantz & Johnson 1990). BoNT/A is known to act on the SNAP25 and its cleavage leads to the inhibition of neurotransmitter release (Rossetto et al. 2014). Therefore, to investigate the synaptic impairments of the in vitro cultures, the SNAP25 cleavage assay is the most frequently used in vitro test for BoNT/A activity (Cai, Reinisch & Ferro-Novick 2007).

In this part of the study, human iPSC-derived neuronal networks were subjected to BoNT/A for toxicity testing using calcium imaging to monitor synchronous calcium transients as functional synaptic output and western blot for SNAP25 cleavage. It was

observed in calcium imaging experiments that 200 pg/ml BoNT/A after 48 h (also 100 pg/ml BoNT/A after 96 h and 10 pg/ml BoNT/A after 120 h) resulted in complete network silencing. However, western blot results suggested that indicated concentrations only caused less than 50% of the SNAP25 cleavage. Interestingly, the SNAP25 cleavage assay indicated different sensitivity levels for 48 and 72 h BoNT/A but not 120 h treatments in human networks in comparison with the rat primary cortical cultures. Overall, such a synapse-specific effect of BoNT/A might also cause the altered cleavage of human SNAP25.

In summary, the results have shown that detection of synchronous network activity and SNAP25 cleavage assay using iPSC-derived human neuronal networks provide an alternative to animal-related BoNT/A toxicity screening. However, further optimization of the human iPSC-derived neuronal cultures would be beneficial to obtain more accurate and reproducible results.

4.2 Homeostatic plasticity models with human iPSC-derived neuronal networks

This study is the first one to address the homeostatic network plasticity in human iPSC-derived cultures. Homeostatic plasticity is a fundamental mechanism through which the neuronal networks regulate their activity pattern. The underlying processes include presynaptic and postsynaptic alterations as well as modulations of intrinsic excitability (Turrigiano 2012). The existing body of research on homeostatic plasticity was done primarily in vivo and in vitro murine models and it is still not known whether human iPSC-derived neuronal networks share similar properties. In this part of the study, responses to chronic manipulations of human neuronal network activity over several hours to days were monitored by MEA recordings and calcium imaging.

4.2.1 Silencing model with TTX

One of the main homeostatic plasticity mechanisms is the modulation of intrinsic excitability (Turrigiano 2011). Network silencing-driven homeostatic changes upon long-term TTX treatment, a voltage-gated Na^+ channel blocker, were previously investigated in rat cortical neurons and the findings include an increase in voltage-gated Na^+ current and a downregulation of the persistent K^+ current (Desai et al. 1999). It has been reported that chronic TTX treatment of OHSCs induces plasticity and upon removal of TTX, the impact of synaptic plasticity results in spontaneous seizures

(Bausch et al, 2006). In human iPSC-derived neurons, voltage-gated Na^+ currents were fully blocked by 1 μM TTX (Haythornthwaite et al. 2012). Our findings from the blockage of voltage-gated Na^+ current and overall network activity using 1 μM 72 h TTX treatment in human iPSC-derived neuronal networks showed an increase in spontaneous spike and burst activity in MEA recordings (Figure 3.8). These findings suggest that the network activity of human iPSC-derived cultures can be manipulated by TTX. As a result of homeostatic plasticity response to TTX-induced network silencing, human networks have the capability to increase their firing rates.

Extracellular recordings with MEA allow us to monitor changes non-invasively during the course of long-term experiments. Recorded traces contain information of single extracellular spike properties. It has been reported that intracellular spike parameters can be extracted from extracellular spike properties and the negative phase of the extracellular spike coincides with the depolarization of the intracellular spike (Henze et al. 2000). In this study, to eliminate the differences which might occur because of the distance between the electrode and the cell, each electrode was analyzed and compared separately. Single extracellular spike analysis showed an increase in the spike amplitude, in widths, and a decrease in the second maximum (Figure 3.9). The amplitude of the spike depends on the abundance of voltage-gated Na^+ channels whereas, the width of the spike represented the changes in K^+ channels. Hence, it could be hypothesized that the homeostatic response of human iPSC-derived neurons to TTX blockage was an increase in voltage-gated Na^+ channels and a decrease in voltage-gated K^+ channels to increase neuronal excitability. However, this model was to prove the concept of homeostatic plasticity in human iPSC-derived neuronal networks. More detailed analysis at the single cell level by patch clamp recordings should be further performed to support the findings of extracellular spike analysis. Furthermore, to see the opposite effects, hyperactivity-induced homeostatic plasticity was investigated in human neuronal networks.

4.2.2 Hyperactivity model with 4AP

Increasing neuronal activity is followed by a reduction in intrinsic excitability due to an increase in K^+ leak currents (O'Leary et al. 2010) and a decrease in Na^+ currents, Na^+ channel expression and overall network activity (O'brien et al. 2010, Pozzi et al. 2013). In this study, network hyperactivity-driven homeostatic changes with long-term 4-Aminoprydine (4AP) treatment, a voltage-gated A-type K^+ channel blocker, were investigated in human iPSC-derived immature (spike firing) and mature (burst firing)

networks (Figure 3.10 and 3.12). 4AP acts by blocking the delayed rectifier type K^+ channels, allowing for excessive neuronal depolarization. Network activity analysis revealed that only mature human networks responded to the acute 4AP treatment and that the overall network activity was downregulated within 24 h. These results are consistent with an earlier study that 4AP-treatment acutely caused epileptiform activity in rat organotypic hippocampal slice cultures (Albus et al. 2008). The different responses observed in mature and immature human neuronal networks to 4AP stimulation might be attributed to the lack of A-type K^+ channel expression in immature neurons. Another possible explanation for this result is that although the A-type K^+ channels were present in the immature neurons, the synaptic connectivity of immature human networks was not fully developed. Therefore, extracellular spike analysis was the next step to examine the effects of acute 4AP in detail.

Extracellular spike amplitude was not altered by acute 4AP treatment in both immature and mature neurons (Figure 3.11 and 3.13), indicating that Na^+ channels were not affected. It is known that 4AP increases the width of action potential by blocking voltage-gated K^+ channels (Lien & Jonas 2003). In this study, the increase in spike width and the decrease in second maximum values were only present in the mature human neurons. These results are likely to be related to the presence of A-type K^+ channels in the mature neuronal membranes. In a recent study, 10 mM 4AP inhibited the initial, transient phase of outward K^+ currents in human neurons (Haythornthwaite et al. 2012). Furthermore, immature and mature neuronal differences were observed in extracellular spike properties (Figure 3.14) where the spike widths of immature neurons were larger compared to mature neurons. This result is in agreement with a decrease in the extracellular spike half-width that is observed during the maturation of primary mouse cortical neurons (Weir et al. 2015). Moreover, long-term effects of 4AP treatment with a decrease of the amplitude and an increase of the spike-width were obtained after the removal of 4AP (Figure 3.15). These results indicated the decrease of Na^+ channels and the increase of K^+ channels and support previous research in hyperactivity related homeostatic plasticity which links the decreased intrinsic excitability and increase in K^+ leak currents (O'Leary et al. 2010).

Long-term changes in networks were investigated by calcium imaging (Figure 3.16). In fact, 4AP treatment resulted in an acute increase in the synchronous calcium transient frequency followed by a reduction after removal of 4AP after 2 d supporting the findings of MEA recordings. This combination of findings provides some support for the conceptual premise that mature human iPSC-derived neuronal cultures are useful tools

for homeostatic plasticity-related research.

4.3 Effects of Aβ on human iPSC-derived neuronal networks

Alzheimer's disease is the most common neurodegenerative disease and the main culprit of the disease is the senile plaque forming amyloid-beta (Aβ). Even though Aβ has been the main focus of AD research, important questions regarding the physiological and neurotoxicological role of it still remain. Recently, small soluble oligomeric Aβ species are considered to be the toxic mediators of the disease (Sengupta et al. 2016). The present study characterized the cell-derived and synthetic Aβ species and investigated the effects of them in the human iPSC-derived neuronal cultures at cellular and network levels.

4.3.1 Characterization of cell-derived Aβ

Cell-derived Aβ was collected from the conditioned medium of stably APP overexpressing 7PA2 cells. Cell-derived Aβ did not cause changes in cell viability measured with an MTT assay in primary rat cortical neurons. However, the network activity of mature human cultures showed instability in immunodepleted control conditioned medium making impossible to use it as an experimental control.

4.3.2 Dissolving and oligomerizing synthetic Aβ

In this study, to establish better defined oligomer preparations and eliminate the batch-to-batch differences of cell-derived Aβ, synthetic Aβ was used. The Aβ peptide is hydrophobic and tends to aggregate; therefore, dissolving the synthetic Aβ peptide is complicated. Purchased Aβ arrives as lyophilized powder and monomerization is necessary to dissolve pre-existing aggregates for further use in the experiments. These aggregates could work as seeds and accelerate the aggregation which then might cause experimental inconsistencies. Furthermore, visualizing the Aβ oligomer profile is another difficulty since the mainly used method is SDS-PAGE and SDS-PAGE is not a reliable method for characterization of Aβ oligomers. SDS alters the oligomer profile of Aβ preparations by breaking down higher oligomers or even inducing artificial oligomerization (Bitan et al. 2005). This study addressed both of those issues. First of all, another type of Aβ was used since it has been described that N-terminal truncated and pGlu-modified Aβ species (Pyroglutamylated $A\beta_{3-42}$ ([Pyr3]$A\beta_{3-42}$,) in particular are present in large quantities in the AD brains (Saido et al. 1995). The preparation of [Pyr3]$A\beta_{3-42}$ was performed according to the published protocol (Nussbaum et al.

2012). For the monomerization of all synthetic Aβ species, HFIP was used which is the main solvent for dissolving Aβ (Fa et al. 2010). Native and semi-native methods were used to investigate the oligomeric state of preparations and semi-native was preferred since it includes small amount of SDS to help peptides to run but not dissolve them. Semi-native WBs with $A\beta_{1-42}$ and the Aβ* were compared and the results of these two preparations were similar. It was not possible to separate single bands by native WB. Moreover, different solvents were used such as DMSO and NB phenol free. Phenol plus NB medium was avoided because phenol seems to interfere with oligomerization (Ono et al. 2012). Furthermore, using DMSO to dissolve Aβ creates problems because DMSO is toxic to cells. Studies have shown that DMSO caused cell loss in an in vitro rat hippocampal culture preparation at 0.5 % concentration and 0.06 % DMSO had a negative effect on the neurite network (Hanslick et al. 2009, Götte et al. 2010). A temperature effect was also observed since all chemical reactions depend on the temperature. 37 °C preparations showed fibrillar forms in semi-native WB. The lanes were more like a smear in the WB and it was not possible to distinguish sizes. Therefore, the 4 °C preparation of Aβ was selected. Finally, the duration of oligomerization was optimal at 2 d where monomer and also some tetramer was detectable in phenol-free NB. It was surprising that after treating the human iPSC-derived neurons with Aβ* oligomers, there was no further oligomerization. This inconsistency may be due to the phenol plus media and retinoic acid in the B27 supplement which might block further oligomerization even at 37 °C. The final concentration of Aβ or Aβ* used for cellular incubation was 1 μM. This concentration is much higher compared to ELISA (enzyme-linked immunosorbent assay) reports of human brain extracts which shows 1 ng/ml Aβ in CSF (Hulstaert et al. 1999). Even though the used concentration was much higher, it was necessary to use Aβ for modeling AD-related changes in a shorter time window and it is also widely used concentration.

4.3.3 Effects of Aβ on neurons

Characterized Aβ and Aβ* oligomers were used in cell viability assays using primary rat cortical neurons. In this study, the oligomer preparations did not cause any alterations in cell viability. This outcome is contrary to that of Nussbaum et al. (2012) who found cytotoxicity of Aβ* using the same concentration. This might be explained by differences of Aβ* resistance of mouse and rat neurons. Moreover, Aβ was used to see the differences in excitability of human iPSC-derived neurons. Patch-clamp input-output curve showed delayed response in early current injection steps. A possible explanation

for this result may be the masking effect of Aβ oligomers on the neuronal membrane which interferes with channel function for AP firing. However, it seems to be overcome by more current injection. Single AP analysis showed no differences in any parameters which suggest that the properties of the channels did not change upon Aβ treatment.

4.3.4 Effects of Aβ on spontaneous activity

A strong relationship between early phases AD and network hyperactivity has been reported in the literature (Busche et al. 2012) suggesting that primary neuronal dysfunction is mediated by amyloid pathology related hyperactivity. In this study, spontaneously active human iPSC-derived neuronal networks were subjected to Aβ* treatment (Figure 3.28). Long-term Aβ* treatment did not affect spontaneous firing rates of human networks. The result seems to be consistent with other research which found no alteration in the spike rate of 1 μM Aβ-treated mouse cortical cultures (Charkhkar et al. 2015). Another study showed that the application of CSF obtained from individuals with MCI did not change the global network activity of rat cortical neurons compared to healthy controls (Görtz et al. 2013). Furthermore, control and FAD iPSC-derived neuronal networks with the London (V717I) APP mutation did not differ in their spontaneous activity (Muratore et al. 2014). Spike analysis of Aβ oligomer-treated neurons showed no significant differences in spike parameters (Figure 3.29). These findings are in line with the findings of Muratore et al. (2014) in FAD vs control neurons.

In the present study, long-term Aβ* oligomer treatment resulted in the decreased synchronous calcium transient frequency and a trend to increased calcium transient amplitude. To note, calcium imaging in this study was used to optically detect AP evoked calcium increase (so called 'calcium transients') which is occurring via the calcium influx through the voltage-gated calcium channels as a result of action potential generation (Grienberger & Konnerth 2012). Otherwise, calcium alterations are linked to AD (LaFerla 2002) and oligomeric Aβ is known to increase calcium load in neuronal cell bodies and dendritic spines (Arbel-Ornath et al. 2017).

4.3.5 Effects of Aβ on homeostatic plasticity

Previous results of this work demonstrated that Aβ* oligomers showed no significant changes in the spontaneous network activity. Therefore, this study focused on the homeostatic response of Aβ* oligomer-treated networks when there was a hyperactivity situation (Figure 3.30). Vehicle and Aβ* oligomer-treated networks reacted similarly to 4AP stimulation by increasing network activity. However, the increase in the 10 %-width

showed reduction in Aβ* oligomer-treated neurons compared to spike waveform of vehicle-treated neurons. The most interesting finding was that the decrease in firing rates of Aβ* oligomer-treated cultures did not reach the levels of vehicle-treated ones. This outcome was supported by calcium imaging since the decrease in spontaneous synchronous calcium transient frequency was not observed Aβ* oligomer-treated cultures. Furthermore, the percentage of active cells contributing to neuronal networks were not reduced in the Aβ* oligomer-treated cultures (Figure 3.33). The outcome suggests that the decrease in neuronal excitability as a result of the homeostatic network plasticity did not occur in Aβ* oligomer-treated cultures. The elevated voltage-gated Na^+ expressions, especially voltage-gated Na^+ 1.6 subtype, was observed in cultured mouse neurons treated with Aβ or the brains of APP/PS1 mice compared to control groups which might suggest an intrinsic neuronal hyperexcitability as the underlying mechanism of epileptiform activity in AD (Wang et al. 2016). This is the first study to show the relationship between homeostatic plasticity and AD-related Aβ* oligomers using iPSC-derived human neuronal networks. This finding, while preliminary, suggests that homeostatic plasticity was impaired in Aβ* oligomer-treated human neuronal cultures.

4.4 REST as a key role player in Aβ-induced homeostatic plasticity impairment

REST (Repressor Element-1 Silencing Transcription Factor, also known as NRSF, Neuron-Restrictive Silencer Factor) is a transcription inhibitor which orchestrates many neuron specific genes (Zhao et al. 2017). REST is important regarding this study for two main reasons. Firstly, its role in homeostatic plasticity was shown in a 4AP model of increased activity (Pozzi et al. 2013). Involvement of REST in homeostatic response mechanism has been reported in another study which shows that REST deletion caused epileptogenesis (Hu et al. 2011). The study of Pozzi et al. (2013) showed that REST expression increases after 96 h of 4AP treatment in mouse hippocampal cultures, in contrast, REST upregulation reached its peak within 24 h in human iPSC-derived neuronal cultures. Furthermore, kainaic acid treatment leads to an increase in REST mRNA in hippocampus suggesting the important role in neuronal activity dependent processes (Baldelli & Meldolesi 2015). The splice isoforms of REST are indicated in epilepsy related gene expression which may therefore relevant to the progression of epileptogenesis (Spencer et al. 2006). Secondly, aging related-REST increase in human

neurons were not observed in AD brains (Lu et al. 2014). The reduced nuclear REST expression in neurons of the prefrontal cortex has been correlated with Alzheimer's disease progression in both humans with AD (Lu et al. 2014) and mouse model of AD (12 month-old APP23 mice) (Van Acker et al. 2017). It is also known that REST regulates Na^+ channel expression (Chong et al. 1995). With respect to those studies, the role of REST in homeostatic plasticity impairment was investigated by using Aβ* oligomer-treated human neuronal cultures. In this study, the increase in nuclear/cyto REST levels upon 4AP treatment was not observed in Aβ* oligomer-treated whereas this was the case in both untreated control or vehicle-treated human iPSC-derived neurons. Findings in this study are in line with the previously shown REST impairment in AD and indicate that Aβ oligomers are directly responsible for REST expression alterations. To note, in this study, the alterations in REST levels were not investigated at mRNA level by RT-q-PCR or at protein level by western blot since cultures include astrocytes and REST is expressed in GFAP-positive astrocytes (Kohyama et al. 2010) which would interfere the outcome of those experiments. Furthermore, REST is controlled by the canonical Wnt pathway (Nishihara et al. 2003). It was shown that Wnt-beta-catenin/REST signaling plays critical and collaborative roles in neuroprotection in prion diseases and associated neurodegenerative diseases, as transient REST elevation maintained homeostasis and plasticity in neurons (Song et al. 2016). CHIR treatment showed increased REST levels possibly by blocking GSK-3β which is upstream of REST. However, REST expression upon CHIR and 4AP treatment was not fully recovered in Aβ* treated cultures. It was shown that the activity of GSK-3β is increased in AD and that somatodendritic accumulation and activation of GSK-3β is an early event preceding and accompanying the formation of NFT and of other tau-positive inclusions (Leroy et al. 2007). Furthermore, PSEN1 mutation destabilizes β-catenin (Zhang et al. 1998). REST is also implicated in epigenetic regulations with the interaction of long-non coding RNA (Wu et al. 2013). Thus, a cascade, where Aβ leads to the activation of GSK-3β which further leads to a reduced REST expression may eventually explain the link between increased levels of Aβ and impaired homeostatic network plasticity. REST deficiency would then cause prolonged periods of hyperactive states, which may be detectable as epileptiform activity in AD patients. In conclusion, although both the involvement of REST in homeostatic plasticity and the loss of REST in AD neurons has been shown before, the outcome of this thesis combines both phenomena for the first time and concludes that REST might be a key player in AD-related network dysfunction. A deeper understanding of REST activation and the

upstream and downstream molecular mechanisms in neurodegeneration are crucial for developing a therapeutic strategy.

4.5 Conclusion and outlook

AD research has focused on the Aβ peptide for many years; nonetheless, important questions regarding this peptide still remain. Recent studies confirmed Aβ-related epileptiform activity in patients with memory decline (O'brien et al. 2010) and mild cognitive impairment (Dickerson et al. 2005). Aβ-related hyperactivity has also been described in cognitively normal elderly (Oh et al. 2015). Human iPSC-derived neurons have been emerging as valuable research tools in the field of neurodegenerative diseases. Several studies, reviewed in Arber et al. (2017), thoroughly demonstrated successful neuronal differentiation from SAD and FAD patient-derived iPSCs and reported differential Aβ production upon pharmacological interventions. However, so far, the AD-related electrophysiological changes in the cellular and synaptic levels were only addressed using iPSC-derived neurons by Nieweg et al. (2015). Therefore, this is the first study which has reported the AD-related network alterations using human iPSC-derived neurons.

The major limitation of this study is the number of cultures developing spontaneous synchronous network activity. Therefore, further optimizations of culture conditions are required. Since astrocytes are important for neuronal maturation, they would accelerate the generation of active cultures. However, the presence of astrocytes in direct coculture systems prevents to study neuron specific changes in bulk-molecular approaches. Recently, indirect-contact co-cultures of neurons and astrocytes were developed (Clarke & Barres 2013) and would be useful to overcome this issue. Another step towards a more physiological AD model would be the generation of 3D cultures allowing plaque formation in the dish, as described by Choi et al. (2014). This study aimed at generating a valuable model that allows a mechanistic insight at the phenomenon of hyperactivity in the early phase of AD. The study presented in this dissertation provides a powerful new model of homeostatic plasticity utilizing human iPSC-derived neuronal networks. This study also demonstrates the usage of this model to mimic AD-related hyperactivity. It shows that increased levels of Aβ lead to impaired homeostatic plasticity, resulting in prolonged periods of neuronal hyperactivity. Moreover, it describes REST as a potential molecular player in the Aβ-induced process, hinting at a novel therapeutic target.

REST is controlled by the canonical Wnt pathway (Nishihara et al. 2003), where

activation of Wnt signaling leads to increased REST expression. Wnt activation also exerts homeostatic effects by stabilizing the aberrant network activity (Oliva & Inestrosa 2015). Moreover, activation of GSK-3β was shown to be AD-related (Leroy et al. 2007) and GSK-3β interferes with the Wnt signaling pathway through β-catenin degradation. Thus, the observed downregulation of nuclear REST expression by Aβ could be explained by the Aβ-induced activation of GSK-3β. Further studies need to be carried out in order to understand the effects of those proteins in Aβ-related homeostatic plasticity impairments.

Finally, while other studies using human iPSC-derived neurons have attempted to analyze the Aβ-related molecular and cellular changes, this study looked at AD from an electrophysiological perspective and has thrown up many questions in need of further investigations which would collectively improve our understanding of AD pathogenesis and help to find new targets to develop effective therapeutics.

5. References

Abbott, L. F. & Nelson, S. B. (2000), 'Synaptic plasticity: taming the beast', *Nature neuroscience* **3**(11s), 1178.

Albus, K., Wahab, A. & Heinemann, U. (2008), 'Standard antiepileptic drugs fail to block epileptiform activity in rat organotypic hippocampal slice cultures', *British journal of pharmacology* **154**(3), 709–724.

Alcamo, E. A., Chirivella, L., Dautzenberg, M., Dobreva, G., Fariñas, I., Grosschedl, R. & McConnell, S. K. (2008), 'Satb2 regulates callosal projection neuron identity in the developing cerebral cortex', *Neuron* **57**(3), 364–377.

Allsop, D., Wong, C. W., Ikeda, S., Landon, M., Kidd, M. & Glenner, G. G. (1988), 'Immunohistochemical evidence for the derivation of a peptide ligand from the amyloid beta-protein precursor of alzheimer disease', *Proceedings of the National Academy of Sciences* **85**(8), 2790–2794.

Alzheimer, A. (1907), 'Uber eine eigenartige erkrankung der hirnrinde', *Allgemeine Zeitschrife Psychiatrie* **64**, 146–148.

Arancio, O., Zhang, H. P., Chen, X., Lin, C., Trinchese, F., Puzzo, D., Liu, S., Hegde, A., Yan, S. F., Stern, A. et al. (2004), 'Rage potentiates aβ-induced perturbation of neuronal function in transgenic mice', *The EMBO journal* **23**(20), 4096–4105.

Arbel-Ornath, M., Hudry, E., Boivin, J. R., Hashimoto, T., Takeda, S., Kuchibhotla, K. V., Hou, S., Lattarulo, C. R., Belcher, A. M., Shakerdge, N. et al. (2017), 'Soluble oligomeric amyloid-β induces calcium dyshomeostasis that precedes synapse loss in the living mouse brain', *Molecular neurodegeneration* **12**(1), 27.

Arber, C., Lovejoy, C. & Wray, S. (2017), 'Stem cell models of alzheimer's disease: progress and challenges', *Alzheimer's Research & Therapy* **9**(1), 42.

Ashe, K. H. & Zahs, K. R. (2010), 'Probing the biology of alzheimer's disease in mice', *Neuron* **66**(5), 631–645.

Ashton, N., Hye, A., Leckey, C., Jones, A., Gardner, A., Elliott, C., Wetherell, J., Lenze, E., Killick, R. & Marchant, N. (2017), 'Plasma rest: a novel candidate biomarker of alzheimer's disease is modified by psychological intervention in an at-risk population', *Translational Psychiatry* **7**(6).

AxolBio, E. S. A. P. (2016), 'Whole cell patch clamp recordings for characterizing neuronal electrical properties of ipsc-derive neurons', *https://www.axolbio.com/page/whole-cell-patch-clamp-protocol* .

Baldelli, P. & Meldolesi, J. (2015), 'The transcription repressor rest in adult neurons: physiology, pathology, and diseases', *eNeuro* **2**(4), ENEURO–0010.

Bean, B. P. (2007), 'The action potential in mammalian central neurons', *Nature reviews. Neuroscience* **8**(6), 451.

Ben-Ari, Y. (2002), 'Excitatory actions of gaba during development: the nature of the nurture', *Nature Reviews Neuroscience* **3**(9), 728–739.

Beske, P. H., Scheeler, S. M., Adler, M. & McNutt, P. M. (2015), 'Accelerated intoxication of gabaergic synapses by botulinum neurotoxin a disinhibits stem cell-derived neuron networks prior to network silencing', *Frontiers in cellular neuroscience* **9**.

Bierer, L. M., Hof, P. R., Purohit, D. P., Carlin, L., Schmeidler, J., Davis, K. L. & Perl, D. P. (1995), 'Neocortical neurofibrillary tangles correlate with dementia severity in alzheimer's disease', *Archives of neurology* **52**(1), 81–88.

Bitan, G., Fradinger, E. A., Spring, S. M. & Teplow, D. B. (2005), 'Neurotoxic protein oligomers—what you see is not always what you get', *Amyloid* **12**(2), 88–95.

Blennow, K., Hampel, H., Weiner, M. & Zetterberg, H. (2010), 'Cerebrospinal fluid and plasma biomarkers in alzheimer disease', *Nature Reviews Neurology* **6**(3), 131–144.

Braak, H. & Braak, E. (1991), 'Neuropathological stageing of alzheimer-related changes', *Acta neuropathologica* **82**(4), 239–259.

Brown, T. H., Chapman, P. F., Kairiss, E. W. & Keenan, C. L. (1988), 'Long-term synaptic potentiation', *Science* **242**(4879), 724–728.

Buée, L., Bussière, T., Buée-Scherrer, V., Delacourte, A. & Hof, P. R. (2000), 'Tau protein isoforms, phosphorylation and role in neurodegenerative disorders', *Brain Research Reviews* **33**(1), 95–130.

Bugaysen, J., Bronfeld, M., Tischler, H., Bar-Gad, I. & Korngreen, A. (2010), 'Electrophysiological characteristics of globus pallidus neurons', *PloS one* **5**(8), e12001.

Busche, M. A., Chen, X., Henning, H. A., Reichwald, J., Staufenbiel, M., Sakmann, B. & Konnerth, A. (2012), 'Critical role of soluble amyloid-β for early hippocampal hyperactivity in a mouse model of alzheimer's disease', *Proceedings of the National Academy of Sciences* **109**(22), 8740–8745.

Busche, M. A., Eichhoff, G., Adelsberger, H., Abramowski, D., Wiederhold, K.-H., Haass, C., Staufenbiel, M., Konnerth, A. & Garaschuk, O. (2008), 'Clusters of hyperactive neurons near amyloid plaques in a mouse model of alzheimer's disease', *Science* **321**(5896), 1686–1689.

Caceres, A., Banker, G., Steward, O., Binder, L. & Payne, M. (1984), 'Map2 is localized to the dendrites of hippocampal neurons which develop in culture', *Developmental Brain Research* **13**(2), 314–318.

Cai, H., Reinisch, K. & Ferro-Novick, S. (2007), 'Coats, tethers, rabs, and snares work together to mediate the intracellular destination of a transport vesicle', *Developmental cell* **12**(5), 671–682.

Cai, S., Singh, B. R. & Sharma, S. (2007), 'Botulism diagnostics: from clinical symptoms to in vitro assays', *Critical reviews in microbiology* **33**(2), 109–125.

Chambers, S. M., Fasano, C. A., Papapetrou, E. P., Tomishima, M., Sadelain, M. & Studer, L. (2009), 'Highly efficient neural conversion of human es and ips cells by dual inhibition of smad signaling', *Nature biotechnology* **27**(3), 275–280.

Charbord, J., Poydenot, P., Bonnefond, C., Feyeux, M., Casagrande, F., Brinon, B., Francelle, L., Aurégan, G., Guillermier, M., Cailleret, M. et al. (2013), 'High throughput screening for inhibitors of rest in neural derivatives of human embryonic stem cells reveals a chemical compound that promotes expression of neuronal genes', *Stem Cells* **31**(9), 1816–1828.

Charkhkar, H., Meyyappan, S., Matveeva, E., Moll, J. R., McHail, D. G., Peixoto, N., Cliff, R. O. & Pancrazio, J. J. (2015), 'Amyloid beta modulation of neuronal network activity in vitro', *Brain research* **1629**, 1–9.

Chen, B., Wang, S. S., Hattox, A. M., Rayburn, H., Nelson, S. B. & McConnell, S. K. (2008), 'The fezf2–ctip2 genetic pathway regulates the fate choice of subcortical projection neurons in the developing cerebral cortex', *Proceedings of the National Academy of Sciences* **105**(32), 11382–11387.

Cherubini, E., Gaiarsa, J. L. & Ben-Ari, Y. (1991), 'Gaba: an excitatory transmitter in early postnatal life', *Trends in neurosciences* **14**(12), 515–519.

Chiappalone, M., Bove, M., Vato, A., Tedesco, M. & Martinoia, S. (2006), 'Dissociated cortical networks show spontaneously correlated activity patterns during in vitro development', *Brain research* **1093**(1), 41–53.

Choi, S. H., Kim, Y. H., Hebisch, M., Sliwinski, C., Lee, S., D'Avanzo, C., Chen, J., Hooli, B., Asselin, C., Muffat, J. et al. (2014), 'A three-dimensional human neural cell culture model of alzheimer's disease', *Nature* **515**(7526), 274.

Chong, J. A., Tapia-Ramirez, J., Kim, S., Toledo-Aral, J. J., Zheng, Y., Boutros, M. C., Altshuller, Y. M., Frohman, M. A., Kraner, S. D. & Mandel, G. (1995), 'Rest: a mammalian silencer protein that restricts sodium channel gene expression to neurons', *Cell* **80**(6), 949–957.

Chong, S.-A., Benilova, I., Shaban, H., De Strooper, B., Devijver, H., Moechars, D., Eberle, W., Bartic, C., Van Leuven, F. & Callewaert, G. (2011), 'Synaptic dysfunction in hippocampus of transgenic mouse models of alzheimer's disease: A multi-electrode array study', *Neurobiology of disease* **44**(3), 284–291.

Clarke, L. E. & Barres, B. A. (2013), 'Emerging roles of astrocytes in neural circuit development', *Nature Reviews. Neuroscience* **14**(5), 311.

Cohen, L. (1973), 'Changes in neuron structure during action potential propagation and synaptic transmission.', *Physiological reviews* **53**(2), 373–418.

Danjo, T., Eiraku, M., Muguruma, K., Watanabe, K., Kawada, M., Yanagawa, Y., Rubenstein, J. L. & Sasai, Y. (2011), 'Subregional specification of embryonic stem cell-derived ventral telencephalic tissues by timed and combinatory treatment with extrinsic signals', *Journal of Neuroscience* **31**(5), 1919–1933.

Davis, K. E., Fox, S. & Gigg, J. (2014), 'Increased hippocampal excitability in the 3xtgad mouse model for alzheimer's disease in vivo', *PLoS One* **9**(3), e91203.

De Gois, S., Schäfer, M. K.-H., Defamie, N., Chen, C., Ricci, A., Weihe, E., Varoqui, H. & Erickson, J. D. (2005), 'Homeostatic scaling of vesicular glutamate and gaba transporter expression in rat neocortical circuits', *Journal of Neuroscience* **25**(31), 7121–7133.

De Strooper, B. & Karran, E. (2016), 'The cellular phase of alzheimer's disease', *Cell* **164**(4), 603–615.

Desai, N. S. (2003), 'Homeostatic plasticity in the cns: synaptic and intrinsic forms', *Journal of Physiology-Paris* **97**(4), 391–402.

Desai, N. S., Rutherford, L. C. & Turrigiano, G. G. (1999), 'Plasticity in the intrinsic excitability of cortical pyramidal neurons.', *Nature neuroscience* **2**(6).

Deshpande, A., Mina, E., Glabe, C. & Busciglio, J. (2006), 'Different conformations of amyloid β induce neurotoxicity by distinct mechanisms in human cortical neurons', *Journal of Neuroscience* **26**(22), 6011–6018.

Dickerson, B., Salat, D., Greve, D., Chua, E., Rand-Giovannetti, E., Rentz, D., Bertram, L., Mullin, K., Tanzi, R., Blacker, D. et al. (2005), 'Increased hippocampal activation in mild cognitive impairment compared to normal aging and ad', *Neurology* **65**(3), 404–411.

Egelman, D. M. & Montague, P. R. (1999), 'Calcium dynamics in the extracellular space of mammalian neural tissue', *Biophysical Journal* **76**(4), 1856–1867.

Fa, M., Orozco, I. J., Francis, Y. I., Saeed, F., Gong, Y. & Arancio, O. (2010), 'Preparation of oligomeric β-amyloid1-42 and induction of synaptic plasticity impairment on hippocampal slices', *Journal of visualized experiments: JoVE* (41).

Fontana, R., Agostini, M., Murana, E., Mahmud, M., Scremin, E., Rubega, M., Sparacino, G., Vassanelli, S. & Fasolato, C. (2017), 'Early hippocampal hyperexcitability in ps2app mice: role of mutant ps2 and app', *Neurobiology of aging* **50**, 64–76.

Francis, P. T., Palmer, A. M., Snape, M. & Wilcock, G. K. (1999), 'The cholinergic hypothesis of alzheimer's disease: a review of progress', *Journal of Neurology, Neurosurgery & Psychiatry* **66**(2), 137–147.

Friedman, D., Honig, L. S. & Scarmeas, N. (2012), 'Seizures and epilepsy in alzheimer's disease', *CNS neuroscience & therapeutics* **18**(4), 285–294.

Fu, A. K., Hung, K.-W., Fu, W.-Y., Shen, C., Chen, Y., Xia, J., Lai, K.-O. & Ip, N. Y. (2011), 'Apccdh1 mediates epha4-dependent downregulation of ampa receptors in homeostatic plasticity', *Nature neuroscience* **14**(2), 181–189.

Gendron, T. F. & Petrucelli, L. (2009), 'The role of tau in neurodegeneration', *Molecular neurodegeneration* **4**(1), 13.

Glenner, G. G. & Wong, C. W. (1984), 'Alzheimer's disease and down's syndrome: sharing of a unique cerebrovascular amyloid fibril protein', *Biochemical and biophysical research communications* **122**(3), 1131–1135.

Goate, A., Chartier-Harlin, M.-C. et al. (1991), 'Segregation of a missense mutation in the amyloid precursor protein gene with familial alzheimer's disease', *Nature* **349**(6311), 704.

Goold, C. P. & Nicoll, R. A. (2010), 'Single-cell optogenetic excitation drives homeostatic synaptic depression', *Neuron* **68**(3), 512–528.

Görtz, P., Siebler, M., Ihl, R., Henning, U., Luckhaus, C., Supprian, T. & Lange-Asschenfeldt, C. (2013), 'Multielectrode array analysis of cerebrospinal fluid in alzheimer's disease versus mild cognitive impairment: a potential diagnostic and treatment biomarker', *Biochemical and biophysical research communications* **434**(2), 293–297.

Götte, M., Hofmann, G., Michou-Gallani, A.-I., Glickman, J. F., Wishart, W. & Gabriel, D. (2010), 'An imaging assay to analyze primary neurons for cellular neurotoxicity', *Journal of neuroscience methods* **192**(1), 7–16.

Grienberger, C. & Konnerth, A. (2012), 'Imaging calcium in neurons', *Neuron* **73**(5), 862–885.

Grundke-Iqbal, I., Iqbal, K., Tung, Y.-C., Quinlan, M., Wisniewski, H. M. & Binder, L. I. (1986), 'Abnormal phosphorylation of the microtubule-associated protein tau (tau) in alzheimer cytoskeletal pathology', *Proceedings of the National Academy of Sciences* **83**(13), 4913–4917.

Güntert, A., Döbeli, H. & Bohrmann, B. (2006), 'High sensitivity analysis of amyloid-beta peptide composition in amyloid deposits from human and ps2app mouse brain', *Neuroscience* **143**(2), 461–475.

Hanslick, J. L., Lau, K., Noguchi, K. K., Olney, J. W., Zorumski, C. F., Mennerick, S. & Farber, N. B. (2009), 'Dimethyl sulfoxide (dmso) produces widespread apoptosis in the developing central nervous system', *Neurobiology of disease* **34**(1), 1–10.

Hardingham, N. R. & Larkman, A. U. (1998), 'The reliability of excitatory synaptic transmission in slices of rat visual cortex in vitro is temperature dependent', *The Journal of Physiology* **507**(1), 249–256.

Hardy, J. & Allsop, D. (1991), 'Amyloid deposition as the central event in the aetiology of alzheimer's disease', *Trends in pharmacological sciences* **12**, 383–388.

Hardy, J. & Selkoe, D. J. (2002), 'The amyloid hypothesis of alzheimer's disease: progress and problems on the road to therapeutics', *science* **297**(5580), 353–356.

Haythornthwaite, A., Stoelzle, S., Hasler, A., Kiss, A., Mosbacher, J., George, M., Brüggemann, A. & Fertig, N. (2012), 'Characterizing human ion channels in induced pluripotent stem cell–derived neurons', *Journal of biomolecular screening* **17**(9), 1264–1272.

Heinricher, M. M. (2004), 'Principles of extracellular single-unit recording', *Microelectrode Recording in Movement Disorder Surgery* **8**.

Henze, D. A., Borhegyi, Z., Csicsvari, J., Mamiya, A., Harris, K. D. & Buzsáki, G. (2000), 'Intracellular features predicted by extracellular recordings in the hippocampus in vivo', *Journal of neurophysiology* **84**(1), 390–400.

Hille, B. (1978), 'Ionic channels in excitable membranes. current problems and biophysical approaches', *Biophysical Journal* **22**(2), 283–294.

Holtzman, D. M., Morris, J. C. & Goate, A. M. (2011), 'Alzheimer's disease: the challenge of the second century', *Science translational medicine* **3**(77), 77sr1–77sr1.

Honda, M., Minami, I., Tooi, N., Morone, N., Nishioka, H., Uemura, K., Kinoshita, A., Heuser, J. E., Nakatsuji, N. & Aiba, K. (2016), 'The modeling of alzheimer's disease by the overexpression of mutant presenilin 1 in human embryonic stem cells', *Biochemical and biophysical research communications* **469**(3), 587–592.

Hossini, A. M., Megges, M., Prigione, A., Lichtner, B., Toliat, M. R., Wruck, W., Schröter, F., Nuernberg, P., Kroll, H., Makrantonaki, E. et al. (2015), 'Induced pluripotent stem cell-derived neuronal cells from a sporadic alzheimer's disease donor as a model for investigating ad-associated gene regulatory networks', *BMC genomics* **16**(1), 84.

Hsia, A. Y., Masliah, E., McConlogue, L., Yu, G.-Q., Tatsuno, G., Hu, K., Kholodenko, D., Malenka, R. C., Nicoll, R. A. & Mucke, L. (1999), 'Plaque-independent disruption of neural circuits in alzheimer's disease mouse models', *Proceedings of the National Academy of Sciences* **96**(6), 3228–3233.

Hsieh, H., Boehm, J., Sato, C., Iwatsubo, T., Tomita, T., Sisodia, S. & Malinow, R. (2006), 'Ampar removal underlies aβ-induced synaptic depression and dendritic spine loss', *Neuron* **52**(5), 831–843.

Hu, J.-H., Park, J. M., Park, S., Xiao, B., Dehoff, M. H., Kim, S., Hayashi, T., Schwarz, M. K., Huganir, R. L., Seeburg, P. H. et al. (2010), 'Homeostatic scaling requires group i mglur activation mediated by homer1a', *Neuron* **68**(6), 1128–1142.

Hu, X.-L., Cheng, X., Cai, L., Tan, G.-H., Xu, L., Feng, X.-Y., Lu, T.-J., Xiong, H., Fei, J. & Xiong, Z.-Q. (2011), 'Conditional deletion of nrsf in forebrain neurons accelerates epileptogenesis in the kindling model', *Cerebral Cortex* **21**(9), 2158–2165.

Huang, S.-M. A., Mishina, Y. M., Liu, S., Cheung, A., Stegmeier, F., Michaud, G. A., Charlat, O., Wiellette, E., Zhang, Y., Wiessner, S. et al. (2009), 'Tankyrase inhibition stabilizes axin and antagonizes wnt signalling', *Nature* **461**(7264), 614.

Hulstaert, F., Blennow, K., Ivanoiu, A., Schoonderwaldt, H., Riemenschneider, M., De Deyn, P., Bancher, C., Cras, P., Wiltfang, J., Mehta, P. et al. (1999), 'Improved discrimination of ad patients using β-amyloid (1-42) and tau levels in csf', *Neurology* **52**(8), 1555–1555.

Ibata, K., Sun, Q. & Turrigiano, G. G. (2008), 'Rapid synaptic scaling induced by changes in postsynaptic firing', *Neuron* **57**(6), 819–826.

Imayoshi, I., Sakamoto, M., Yamaguchi, M., Mori, K. & Kageyama, R. (2010), 'Essential roles of notch signaling in maintenance of neural stem cells in developing and adult brains', *Journal of Neuroscience* **30**(9), 3489–3498.

Israel, M. A., Yuan, S. H., Bardy, C., Reyna, S. M., Mu, Y., Herrera, C., Hefferan, M. P., Van Gorp, S., Nazor, K. L., Boscolo, F. S. et al. (2012), 'Probing sporadic and familial alzheimer's disease using induced pluripotent stem cells', *Nature* **482**(7384), 216.

Ito, K., Tatebe, T., Suzuki, K., Hirayama, T., Hayakawa, M., Kubo, H., Tomita, T. & Makino, M. (2017), 'Memantine reduces the production of amyloid-β peptides through modulation of amyloid precursor protein trafficking', *European journal of pharmacology* **798**, 16–25.

Jankovic, J. (2004), 'Botulinum toxin in clinical practice', *Journal of Neurology, Neurosurgery & Psychiatry* **75**(7), 951–957.

Johnson, J. W. & Kotermanski, S. E. (2006), 'Mechanism of action of memantine', *Current opinion in pharmacology* **6**(1), 61–67.

Kandel, E. R., Schwartz, J. H., Jessell, T. M., Siegelbaum, S. A., Hudspeth, A. J. et al. (2000), *Principles of neural science*, Vol. 4, McGraw-hill New York.

Kirov, S. A., Sorra, K. E. & Harris, K. M. (1999), 'Slices have more synapses than perfusion-fixed hippocampus from both young and mature rats', *Journal of Neuroscience* **19**(8), 2876–2886.

Klein, W. L. (2013), 'Synaptotoxic amyloid-β oligomers: a molecular basis for the cause, diagnosis, and treatment of alzheimer's disease?', *Journal of Alzheimer's disease* **33**(s1), S49–S65.

Klunk, W. E., Engler, H., Nordberg, A., Wang, Y., Blomqvist, G., Holt, D. P., Bergström, M., Savitcheva, I., Huang, G.-F., Estrada, S. et al. (2004), 'Imaging brain amyloid in alzheimer's disease with pittsburgh compound-b', *Annals of neurology* **55**(3), 306–319.

Knobloch, M., Farinelli, M., Konietzko, U., Nitsch, R. M. & Mansuy, I. M. (2007), 'Aβ oligomer-mediated long-term potentiation impairment involves protein phosphatase 1-dependent mechanisms', *Journal of Neuroscience* **27**(29), 7648–7653.

Koffie, R. M., Meyer-Luehmann, M., Hashimoto, T., Adams, K. W., Mielke, M. L., Garcia-Alloza, M., Micheva, K. D., Smith, S. J., Kim, M. L., Lee, V. M. et al. (2009), 'Oligomeric amyloid β associates with postsynaptic densities and correlates with excitatory synapse loss near senile plaques', *Proceedings of the National Academy of Sciences* **106**(10), 4012–4017.

Kohyama, J., Sanosaka, T., Tokunaga, A., Takatsuka, E., Tsujimura, K., Okano, H. & Nakashima, K. (2010), 'Bmp-induced rest regulates the establishment and maintenance of astrocytic identity', *The Journal of cell biology* pp. jcb–200908048.

Kondo, T., Asai, M., Tsukita, K., Kutoku, Y., Ohsawa, Y., Sunada, Y., Imamura, K., Egawa, N., Yahata, N., Okita, K. et al. (2013), 'Modeling alzheimer's disease with ipscs reveals stress phenotypes associated with intracellular aβ and differential drug responsiveness', *Cell stem cell* **12**(4), 487–496.

Kumar, A., Singh, A. et al. (2015), 'A review on alzheimer's disease pathophysiology and its management: an update', *Pharmacological Reports* **67**(2), 195–203.

Ladiwala, A. R. A., Litt, J., Kane, R. S., Aucoin, D. S., Smith, S. O., Ranjan, S., Davis, J., Van Nostrand, W. E. & Tessier, P. M. (2012), 'Conformational differences between two amyloid β oligomers of similar size and dissimilar toxicity', *Journal of Biological Chemistry* **287**(29), 24765–24773.

LaFerla, F. M. (2002), 'Calcium dyshomeostasis and intracellular signalling in alzheimer's disease', *Nature reviews. Neuroscience* **3**(11), 862.

Lee, H.-K., Sanchez, C. V., Chen, M., Morin, P. J., Wells, J. M., Hanlon, E. B. & Xia, W. (2016), 'Three dimensional human neuro-spheroid model of alzheimer's disease based on differentiated induced pluripotent stem cells', *PloS one* **11**(9), e0163072.

Leroy, K., Yilmaz, Z. & Brion, J.-P. (2007), 'Increased level of active gsk-3β in alzheimer's disease and accumulation in argyrophilic grains and in neurones at different stages of neurofibrillary degeneration', *Neuropathology and applied neurobiology* **33**(1), 43–55.

Levy-Lahad, E., Wasco, W., Poorkaj, P., Romano, D. M., Oshima, J., Pettingell, W. H., Yu, C.-e., Jondro, P. D., Schmidt, S. D., Wang, K. et al. (1995), 'Candidate gene for the chromosome 1 familial alzheimer's disease locus', *Science* pp. 973–977.

Li, S., Hong, S., Shepardson, N. E., Walsh, D. M., Shankar, G. M. & Selkoe, D. (2009), 'Soluble oligomers of amyloid β protein facilitate hippocampal long-term depression by disrupting neuronal glutamate uptake', *Neuron* **62**(6), 788–801.

Lien, C.-C. & Jonas, P. (2003), 'Kv3 potassium conductance is necessary and kinetically optimized for high-frequency action potential generation in hippocampal interneurons', *Journal of Neuroscience* **23**(6), 2058–2068.

Lin, J.-W. (2012), 'Spatial variation in membrane excitability modulated by 4-ap-sensitive k+ channels in the axons of the crayfish neuromuscular junction', *Journal of neurophysiology* **107**(10), 2692–2702.

Liu, Y., Liu, H., Sauvey, C., Yao, L., Zarnowska, E. D. & Zhang, S.-C. (2013), 'Directed differentiation of forebrain gaba interneurons from human pluripotent stem cells', *Nature protocols* **8**(9), 1670.

Llinás, R. R. (1991), 'Depolarization release coupling: an overview', *Annals of the New York Academy of Sciences* **635**(1), 3–17.

Lu, T., Aron, L., Zullo, J., Pan, Y., Kim, H., Chen, Y., Yang, T.-H., Kim, H.-M., Drake, D., Liu, X. S. et al. (2014), 'Rest and stress resistance in aging and alzheimer's disease', *Nature* **507**(7493), 448.

Maffei, A., Nelson, S. B. & Turrigiano, G. G. (2004), 'Selective reconfiguration of layer 4 visual cortical circuitry by visual deprivation', *Nature neuroscience* **7**(12), 1353.

Mahairaki, V., Ryu, J., Peters, A., Chang, Q., Li, T., Park, T. S., Burridge, P. W., Talbot Jr, C. C., Asnaghi, L., Martin, L. J. et al. (2014), 'Induced pluripotent stem cells from familial alzheimer's disease patients differentiate into mature neurons with amyloidogenic properties', *Stem cells and development* **23**(24), 2996–3010.

Mandler, M., Walker, L., Santic, R., Hanson, P., Upadhaya, A. R., Colloby, S. J., Morris, C. M., Thal, D. R., Thomas, A. J., Schneeberger, A. et al. (2014), 'Pyroglutamylated

amyloid-β is associated with hyperphosphorylated tau and severity of alzheimer's disease', *Acta neuropathologica* **128**(1), 67–79.

Marder, E. & Goaillard, J.-M. (2006), 'Variability, compensation and homeostasis in neuron and network function', *Nature reviews. Neuroscience* **7**(7), 563.

Marder, E. & Prinz, A. A. (2003), 'Current compensation in neuronal homeostasis', *Neuron* **37**(1), 2–4.

Maroof, A. M., Keros, S., Tyson, J. A., Ying, S.-W., Ganat, Y. M., Merkle, F. T., Liu, B., Goulburn, A., Stanley, E. G., Elefanty, A. G. et al. (2013), 'Directed differentiation and functional maturation of cortical interneurons from human embryonic stem cells', *Cell stem cell* **12**(5), 559–572.

Martin, S. J., Grimwood, P. D. & Morris, R. G. (2000), 'Synaptic plasticity and memory: an evaluation of the hypothesis', *Annual review of neuroscience* **23**(1), 649–711.

Mertens, J., Marchetto, M. C., Bardy, C. & Gage, F. H. (2016), 'Evaluating cell reprogramming, differentiation and conversion technologies in neuroscience', *Nature Reviews Neuroscience* **17**(7), 424–437.

Mertens, J., Stüber, K., Wunderlich, P., Ladewig, J., Kesavan, J. C., Vandenberghe, R., Vandenbulcke, M., Van Damme, P., Walter, J., Brüstle, O. et al. (2013), 'App processing in human pluripotent stem cell-derived neurons is resistant to nsaid-based γ-secretase modulation', *Stem Cell Reports* **1**(6), 491–498.

Misonou, H., Mohapatra, D. P., Park, E. W., Leung, V., Zhen, D., Misonou, K., Anderson, A. E. & Trimmer, J. S. (2004), 'Regulation of ion channel localization and phosphorylation by neuronal activity', *Nature neuroscience* **7**(7), 711.

Moore, K. L., Persaud, T. V. N. & Torchia, M. G. (2011), *The Developing Human E-Book*, Elsevier Health Sciences.

Moore, S., Evans, L. D., Andersson, T., Portelius, E., Smith, J., Dias, T. B., Saurat, N., McGlade, A., Kirwan, P., Blennow, K. et al. (2015), 'App metabolism regulates tau proteostasis in human cerebral cortex neurons', *Cell reports* **11**(5), 689–696.

Moris, N., Pina, C. & Martinez Arias, A. (2016), 'Transition states and cell fate decisions in epigenetic landscapes'.

Moulder, K. L., Meeks, J. P., Shute, A. A., Hamilton, C. K., de Erausquin, G. & Mennerick, S. (2004), 'Plastic elimination of functional glutamate release sites by depolarization', *Neuron* **42**(3), 423–435.

Müller, U. C. & Zheng, H. (2012), 'Physiological functions of app family proteins', *Cold Spring Harbor perspectives in medicine* **2**(2), a006288.

Muratore, C. R., Rice, H. C., Srikanth, P., Callahan, D. G., Shin, T., Benjamin, L. N., Walsh, D. M., Selkoe, D. J. & Young-Pearse, T. L. (2014), 'The familial alzheimer's disease appv717i mutation alters app processing and tau expression in ipsc-derived neurons', *Human molecular genetics* **23**(13), 3523–3536.

Nägerl, U. V., Eberhorn, N., Cambridge, S. B. & Bonhoeffer, T. (2004), 'Bidirectional activity-dependent morphological plasticity in hippocampal neurons', *Neuron* **44**(5), 759–767.

Nieweg, K., Andreyeva, A., Van Stegen, B., Tanriöver, G. & Gottmann, K. (2015), 'Alzheimer's disease-related amyloid-β induces synaptotoxicity in human ips cell-derived neurons', *Cell death & disease* **6**(4), e1709.

Nishihara, S., Tsuda, L. & Ogura, T. (2003), 'The canonical wnt pathway directly regulates nrsf/rest expression in chick spinal cord', *Biochemical and biophysical research communications* **311**(1), 55–63.

Noble, D. (2015), 'Conrad waddington and the origin of epigenetics', *Journal of Experimental Biology* **218**(6), 816–818.

Noebels, J. (2011), 'A perfect storm: converging paths of epilepsy and alzheimer's dementia intersect in the hippocampal formation', *Epilepsia* **52**(s1), 39–46.

Nussbaum, J. M., Schilling, S., Cynis, H., Silva, A., Swanson, E., Wangsanut, T., Tayler, K., Wiltgen, B., Hatami, A., Rönicke, R. et al. (2012), 'Prion-like behavior and tau-dependent cytotoxicity of pyroglutamylated β-amyloid', *Nature* **485**(7400), 651.

O'brien, J., O'keefe, K., LaViolette, P., DeLuca, A., Blacker, D., Dickerson, B. & Sperling, R. (2010), 'Longitudinal fmri in elderly reveals loss of hippocampal activation with clinical decline', *Neurology* **74**(24), 1969–1976.

Odawara, A., Katoh, H., Matsuda, N. & Suzuki, I. (2016), 'Physiological maturation and drug responses of human induced pluripotent stem cell-derived cortical neuronal networks in long-term culture', *Scientific reports* **6**.

Odawara, A., Saitoh, Y., Alhebshi, A., Gotoh, M. & Suzuki, I. (2014), 'Long-term electrophysiological activity and pharmacological response of a human induced pluripotent stem cell-derived neuron and astrocyte co-culture', *Biochemical and biophysical research communications* **443**(4), 1176–1181.

Oddo, S., Caccamo, A., Shepherd, J. D., Murphy, M. P., Golde, T. E., Kayed, R., Metherate, R., Mattson, M. P., Akbari, Y. & LaFerla, F. M. (2003), 'Triple-transgenic model of alzheimer's disease with plaques and tangles: intracellular aβ and synaptic dysfunction', *Neuron* **39**(3), 409–421.

Oh, H., Steffener, J., Razlighi, Q. R., Habeck, C., Liu, D., Gazes, Y., Janicki, S. & Stern, Y. (2015), 'Aβ-related hyperactivation in frontoparietal control regions in cognitively normal elderly', *Neurobiology of aging* **36**(12), 3247–3254.

O'Leary, T., van Rossum, M. C. & Wyllie, D. J. (2010), 'Homeostasis of intrinsic excitability in hippocampal neurones: dynamics and mechanism of the response to chronic depolarization', *The Journal of physiology* **588**(1), 157–170.

Oliva, C. A. & Inestrosa, N. C. (2015), 'A novel function for wnt signaling modulating neuronal firing activity and the temporal structure of spontaneous oscillation in the entorhinal–hippocampal circuit', *Experimental neurology* **269**, 43–55.

Ono, K., Li, L., Takamura, Y., Yoshiike, Y., Zhu, L., Han, F., Mao, X., Ikeda, T., Takasaki, J.-i., Nishijo, H. et al. (2012), 'Phenolic compounds prevent amyloid β-protein oligomerization and synaptic dysfunction by site-specific binding', *Journal of Biological Chemistry* **287**(18), 14631–14643.

Opitz, T., De Lima, A. D. & Voigt, T. (2002), 'Spontaneous development of synchronous oscillatory activity during maturation of cortical networks in vitro', *Journal of neurophysiology* **88**(5), 2196–2206.

Pakkenberg, B. & Gundersen, H. J. G. (1997), 'Neocortical neuron number in humans: effect of sex and age', *Journal of Comparative Neurology* **384**(2), 312–320.

Palop, J. J., Chin, J. & Mucke, L. (2006), 'A network dysfunction perspective on neurodegenerative diseases', *Nature* **443**(7113), 768.

Palop, J. J., Chin, J., Roberson, E. D., Wang, J., Thwin, M. T., Bien-Ly, N., Yoo, J., Ho, K. O., Yu, G.-Q., Kreitzer, A. et al. (2007), 'Aberrant excitatory neuronal activity and compensatory remodeling of inhibitory hippocampal circuits in mouse models of alzheimer's disease', *Neuron* **55**(5), 697–711.

Palop, J. J. & Mucke, L. (2009), 'Epilepsy and cognitive impairments in alzheimer disease', *Archives of neurology* **66**(4), 435–440.

Palop, J. J. & Mucke, L. (2010), 'Amyloid-[beta]-induced neuronal dysfunction in alzheimer's disease: from synapses toward neural networks', *Nature neuroscience* **13**(7), 812–818.

Pecoraro-Bisogni, F., Lignani, G., Contestabile, A., Castroflorio, E., Pozzi, D., Rocchi, A., Prestigio, C., Orlando, M., Valente, P., Massacesi, M. et al. (2017), 'Rest-dependent presynaptic homeostasis induced by chronic neuronal hyperactivity', *Molecular Neurobiology* pp. 1–14.

Pirazzini, M., Rossetto, O., Eleopra, R. & Montecucco, C. (2017), 'Botulinum neurotoxins: Biology, pharmacology, and toxicology', *Pharmacological Reviews* **69**(2), 200–235.

Portelius, E., Bogdanovic, N., Gustavsson, M. K., Volkmann, I., Brinkmalm, G., Zetterberg, H., Winblad, B. & Blennow, K. (2010), 'Mass spectrometric characterization of brain amyloid beta isoform signatures in familial and sporadic alzheimer's disease', *Acta neuropathologica* **120**(2), 185–193.

Pozo, K. & Goda, Y. (2010), 'Unraveling mechanisms of homeostatic synaptic plasticity', *Neuron* **66**(3), 337–351.

Pozzi, D., Lignani, G., Ferrea, E., Contestabile, A., Paonessa, F., D'alessandro, R., Lippiello, P., Boido, D., Fassio, A., Meldolesi, J. et al. (2013), 'Rest/nrsf-mediated intrinsic homeostasis protects neuronal networks from hyperexcitability', *The EMBO journal* **32**(22), 2994–3007.

Priller, C., Bauer, T., Mitteregger, G., Krebs, B., Kretzschmar, H. A. & Herms, J. (2006), 'Synapse formation and function is modulated by the amyloid precursor protein', *Journal of Neuroscience* **26**(27), 7212–7221.

Purves, D., Augustine, G. & Fitzpatrick, D. (2001), 'et al., editors. neuroscience. sunderland (ma)'.

Qiu, C. & Fratiglioni, L. (2017), 'Epidemiology of alzheimer's', *Alzheimer's Disease* pp. 17–25.

Raja, W. K., Mungenast, A. E., Lin, Y.-T., Ko, T., Abdurrob, F., Seo, J. & Tsai, L.-H. (2016), 'Self-organizing 3d human neural tissue derived from induced pluripotent stem cells recapitulate alzheimer's disease phenotypes', *PloS one* **11**(9), e0161969.

Rossetto, O., Pirazzini, M. & Montecucco, C. (2014), 'Botulinum neurotoxins: genetic, structural and mechanistic insights', *Nature reviews Microbiology* **12**(8), 535–549.

Saido, T. C., Iwatsubo, T., Mann, D. M., Shimada, H., Ihara, Y. & Kawashima, S. (1995), 'Dominant and differential deposition of distinct β-amyloid peptide species, aβ n3 (pe), in senile plaques', *Neuron* **14**(2), 457–466.

Salmon, D. P. & Bondi, M. W. (2009), 'Neuropsychological assessment of dementia', *Annual review of psychology* **60**, 257–282.

Sanchez, P. E., Zhu, L., Verret, L., Vossel, K. A., Orr, A. G., Cirrito, J. R., Devidze, N., Ho, K., Yu, G.-Q., Palop, J. J. et al. (2012), 'Levetiracetam suppresses neuronal network dysfunction and reverses synaptic and cognitive deficits in an alzheimer's disease model', *Proceedings of the National Academy of Sciences* **109**(42), E2895–E2903.

Schantz, E. & Johnson, E. (1990), 'Dose standardisation of botulinum toxin', *The Lancet* **335**(8686), 421.

Scharfman, H. E. (2012), '"untangling" alzheimer's disease and epilepsy', *Epilepsy currents* **12**(5), 178–183.

Scheff, S. W. & Price, D. A. (2003), 'Synaptic pathology in alzheimer's disease: a review of ultrastructural studies', *Neurobiology of aging* **24**(8), 1029–1046.

Selkoe, D. J. (2001), 'Alzheimer's disease: Genes, proteins, and therapy', *Physiological reviews* **81**(2), 741–766.

Selkoe, D. J. & Hardy, J. (2016), 'The amyloid hypothesis of alzheimer9s disease at 25 years', *EMBO molecular medicine* **8**(6), 595–608.

Sengupta, U., Nilson, A. N. & Kayed, R. (2016), 'The role of amyloid-β oligomers in toxicity, propagation, and immunotherapy', *EBioMedicine* **6**, 42–49.

Shankar, G. M., Li, S., Mehta, T. H., Garcia-Munoz, A., Shepardson, N. E., Smith, I., Brett, F. M., Farrell, M. A., Rowan, M. J., Lemere, C. A. et al. (2008), 'Amyloid β-protein dimers isolated directly from alzheimer brains impair synaptic plasticity and memory', *Nature medicine* **14**(8), 837.

Shen, C.-L. & Murphy, R. M. (1995), 'Solvent effects on self-assembly of beta-amyloid peptide', *Biophysical journal* **69**(2), 640–651.

Sherrington, R., Rogaev, E., Liang, Y. a., Rogaeva, E., Levesque, G., Ikeda, M., Chi, H., Lin, C., Li, G., Holman, K. et al. (1995), 'Cloning of a gene bearing missense mutations in early-onset familial alzheimer's disease', *Nature* **375**(6534), 754–760.

Shew, W. L., Bellay, T. & Plenz, D. (2010), 'Simultaneous multi-electrode array recording and two-photon calcium imaging of neural activity', *Journal of neuroscience methods* **192**(1), 75–82.

Shi, Y., Kirwan, P. & Livesey, F. J. (2012), 'Directed differentiation of human pluripotent stem cells to cerebral cortex neurons and neural networks', *Nature protocols* **7**(10), 1836.

Šišková, Z., Justus, D., Kaneko, H., Friedrichs, D., Henneberg, N., Beutel, T., Pitsch, J., Schoch, S., Becker, A., von der Kammer, H. et al. (2014), 'Dendritic structural degeneration is functionally linked to cellular hyperexcitability in a mouse model of alzheimer's disease', *Neuron* **84**(5), 1023–1033.

Smetters, D., Majewska, A. & Yuste, R. (1999), 'Detecting action potentials in neuronal populations with calcium imaging', *Methods* **18**(2), 215–221.

Song, Z., Zhu, T., Zhou, X., Barrow, P., Yang, W., Cui, Y., Yang, L. & Zhao, D. (2016), 'Rest alleviates neurotoxic prion peptide-induced synaptic abnormalities, neurofibrillary degeneration and neuronal death partially via lrp6-mediated wnt-β-catenin signaling', *Oncotarget* **7**(11), 12035.

Sosa, L. J., Caceres, A., Dupraz, S., Oksdath, M., Quiroga, S. & Lorenzo, A. (2017), 'The physiological role of the amyloid precursor protein (app) as an adhesion molecule in the developing nervous system', *Journal of Neurochemistry* .

Speckmann, E.-J., Hescheler, J., Köhling, R. & Rintelen, H. (2015), *Physiologie*, " Elsevier, Urban&FischerVerlag".

Spencer, E., Chandler, K., Haddley, K., Howard, M., Hughes, D., Belyaev, N., Coulson, J., Stewart, J., Buckley, N., Kipar, A. et al. (2006), 'Regulation and role of rest and rest4 variants in modulation of gene expression in in vivo and in vitro in epilepsy models', *Neurobiology of disease* **24**(1), 41–52.

Spitzer, N. C. (2006), 'Electrical activity in early neuronal development', *Nature* **444**(7120), 707.

Sproul, A. A., Jacob, S., Pre, D., Kim, S. H., Nestor, M. W., Navarro-Sobrino, M., Santa-Maria, I., Zimmer, M., Aubry, S., Steele, J. W. et al. (2014), 'Characterization and molecular profiling of psen1 familial alzheimer's disease ipsc-derived neural progenitors', *PloS one* **9**(1), e84547.

Stargardt, A., Swaab, D. F. & Bossers, K. (2015), 'The storm before the quiet: neuronal hyperactivity and aβ in the presymptomatic stages of alzheimer's disease', *Neurobiology of aging* **36**(1), 1–11.

Sterneckert, J. L., Reinhardt, P. & Schöler, H. R. (2014), 'Investigating human disease using stem cell models', *Nature Reviews Genetics* **15**(9), 625–639.

Stiles, J. & Jernigan, T. L. (2010), 'The basics of brain development', *Neuropsychology review* **20**(4), 327–348.

Surmeier, D. J. & Foehring, R. (2004), 'A mechanism for homeostatic plasticity', *Nature neuroscience* **7**(7), 691–692.

Takahashi, K., Tanabe, K., Ohnuki, M., Narita, M., Ichisaka, T., Tomoda, K. & Yamanaka, S. (2007), 'Induction of pluripotent stem cells from adult human fibroblasts by defined factors', *cell* **131**(5), 861–872.

Takahashi, K. & Yamanaka, S. (2006), 'Induction of pluripotent stem cells from mouse embryonic and adult fibroblast cultures by defined factors', *cell* **126**(4), 663–676.

Takashima, A., Noguchi, K., Michel, G., Mercken, M., Hoshi, M., Ishiguro, K. & Imahori, K. (1996), 'Exposure of rat hippocampal neurons to amyloid β peptide (25–35) induces the inactivation of phosphatidyl inositol-3 kinase and the activation of tau protein kinase i/glycogen synthase kinase-3β', *Neuroscience letters* **203**(1), 33–36.

Terry, R. D., Masliah, E., Salmon, D. P., Butters, N., DeTeresa, R., Hill, R., Hansen, L. A. & Katzman, R. (1991), 'Physical basis of cognitive alterations in alzheimer's disease: synapse loss is the major correlate of cognitive impairment', *Annals of neurology* **30**(4), 572–580.

Tombaugh, T. N. & McIntyre, N. J. (1992), 'The mini-mental state examination: a comprehensive review', *Journal of the American Geriatrics Society* **40**(9), 922–935.

Townsend, M., Mehta, T. & Selkoe, D. J. (2007), 'Soluble aβ inhibits specific signal transduction cascades common to the insulin receptor pathway', *Journal of Biological Chemistry* **282**(46), 33305–33312.

Turrigiano, G. (2011), 'Too many cooks? intrinsic and synaptic homeostatic mechanisms in cortical circuit refinement', *Annual review of neuroscience* **34**, 89–103.

Turrigiano, G. (2012), 'Homeostatic synaptic plasticity: local and global mechanisms for stabilizing neuronal function', *Cold Spring Harbor perspectives in biology* **4**(1), a005736.

Turrigiano, G. G. (1999), 'Homeostatic plasticity in neuronal networks: the more things change, the more they stay the same', *Trends in neurosciences* **22**(5), 221–227.

Turrigiano, G. G. (2008), 'The self-tuning neuron: synaptic scaling of excitatory synapses', *Cell* **135**(3), 422–435.

Turrigiano, G. G. & Nelson, S. B. (2004), 'Homeostatic plasticity in the developing nervous system', *Nature reviews. Neuroscience* **5**(2), 97.

Van Acker, Z. P., Luyckx, E., Van Leuven, W., Geuens, E., De Deyn, P. P., Dam, D. V. & Dewilde, S. (2017), 'Impaired hypoxic tolerance in app23 mice: A dysregulation of neuroprotective globin levels', *FEBS letters* .

Verret, L., Mann, E. O., Hang, G. B., Barth, A. M., Cobos, I., Ho, K., Devidze, N., Masliah, E., Kreitzer, A. C., Mody, I. et al. (2012), 'Inhibitory interneuron deficit links altered network activity and cognitive dysfunction in alzheimer model', *Cell* **149**(3), 708–721.

Vossel, K. A., Beagle, A. J., Rabinovici, G. D., Shu, H., Lee, S. E., Naasan, G., Hegde, M., Cornes, S. B., Henry, M. L., Nelson, A. B. et al. (2013), 'Seizures and epileptiform activity in the early stages of alzheimer disease', *JAMA neurology* **70**(9), 1158–1166.

Vossel, K. A., Tartaglia, M. C., Nygaard, H. B., Zeman, A. Z. & Miller, B. L. (2017), 'Epileptic activity in alzheimer's disease: causes and clinical relevance', *The Lancet Neurology* **16**(4), 311–322.

Walsh, D. M., Klyubin, I., Fadeeva, J. V., Cullen, W. K., Anwyl, R., Wolfe, M. S., Rowan, M. J. & Selkoe, D. J. (2002), 'Naturally secreted oligomers of amyloid β protein potently inhibit hippocampal long-term potentiation in vivo', *Nature* **416**(6880), 535–539.

Wang, Q., Walsh, D. M., Rowan, M. J., Selkoe, D. J. & Anwyl, R. (2004), 'Block of long-term potentiation by naturally secreted and synthetic amyloid β-peptide in hippocampal slices is mediated via activation of the kinases c-jun n-terminal kinase, cyclin-dependent kinase 5, and p38 mitogen-activated protein kinase as well as metabotropic glutamate receptor type 5', *Journal of Neuroscience* **24**(13), 3370–3378.

Wang, X., Zhang, X.-G., Zhou, T.-T., Li, N., Jang, C.-Y., Xiao, Z.-C., Ma, Q.-H. & Li, S. (2016), 'Elevated neuronal excitability due to modulation of the voltage-gated sodium channel nav1. 6 by aβ1- 42', *Frontiers in neuroscience* **10**.

Weir, K., Blanquie, O., Kilb, W., Luhmann, H. J. & Sinning, A. (2015), 'Comparison of spike parameters from optically identified gabaergic and glutamatergic neurons in sparse cortical cultures', *Frontiers in cellular neuroscience* **8**, 460.

Weisemann, J., Krez, N., Fiebig, U., Worbs, S., Skiba, M., Endermann, T., Dorner, M. B., Bergström, T., Muñoz, A., Zegers, I. et al. (2015), 'Generation and characterization of six recombinant botulinum neurotoxins as reference material to serve in an international proficiency test', *Toxins* **7**(12), 5035–5054.

Woodruff, G., Young, J. E., Martinez, F. J., Buen, F., Gore, A., Kinaga, J., Li, Z., Yuan, S. H., Zhang, K. & Goldstein, L. S. (2013), 'The presenilin-1 δe9 mutation results in reduced γ-secretase activity, but not total loss of ps1 function, in isogenic human stem cells', *Cell reports* **5**(4), 974–985.

Wu, P., Zuo, X., Deng, H., Liu, X., Liu, L. & Ji, A. (2013), 'Roles of long noncoding rnas in brain development, functional diversification and neurodegenerative diseases', *Brain research bulletin* **97**, 69–80.

Yagi, T., Ito, D., Okada, Y., Akamatsu, W., Nihei, Y., Yoshizaki, T., Yamanaka, S., Okano, H. & Suzuki, N. (2011), 'Modeling familial alzheimer's disease with induced pluripotent stem cells', *Human molecular genetics* **20**(23), 4530–4539.

Yahata, N., Asai, M., Kitaoka, S., Takahashi, K., Asaka, I., Hioki, H., Kaneko, T., Maruyama, K., Saido, T. C., Nakahata, T. et al. (2011), 'Anti-aβ drug screening platform using human ips cell-derived neurons for the treatment of alzheimer's disease', *PloS one* **6**(9), e25788.

Zhang, D., Pekkanen-Mattila, M., Shahsavani, M., Falk, A., Teixeira, A. I. & Herland, A. (2014), 'A 3d alzheimer's disease culture model and the induction of p21-activated kinase mediated sensing in ipsc derived neurons', *Biomaterials* **35**(5), 1420–1428.

Zhang, S., Smailagic, N., Hyde, C., Han, D., Noel-Storr, A., Takwoingi, Y. & McShane, R. (2013), 'C-pib-pet for the early diagnosis of alzheimer's disease dementia and other dementias in people with mild cognitive impairment (mci)', *Cochrane Database Syst Rev* **7**.

Zhang, Y.-w., Thompson, R., Zhang, H. & Xu, H. (2011), 'App processing in alzheimer's disease', *Molecular brain* **4**(1), 3.

Zhang, Z., Hartmann, H., Do, V. M., Abramowski, D. et al. (1998), 'Destabilization of beta-catenin by mutations in presenilin-1 potentiates neuronal apoptosis', *Nature* **395**(6703), 698.

Zhao, Y., Zhu, M., Yu, Y., Qiu, L., Zhang, Y., He, L. & Zhang, J. (2017), 'Brain rest/nrsf is not only a silent repressor but also an active protector', *Molecular neurobiology* **54**(1), 541–550.

Zuccato, C., Tartari, M., Crotti, A., Goffredo, D., Valenza, M., Conti, L., Cataudella, T., Leavitt, B. R., Hayden, M. R., Timmusk, T. et al. (2003), 'Huntingtin interacts with rest/nrsf to modulate the transcription of nrse-controlled neuronal genes', *Nature genetics* **35**(1), 76.

6. Abbreviations

4AP	4-aminopyridine
Aβ	amyloid beta
AD	Alzheimer's disease
AM	acetoxymethyl
AMPA	α-amino-3-hydroxy-5-methyl-4-isoxazolepropionic acid
AP	action potential
APP	amyloid precursor protein
APV	D,L-2-amino-5-phosphonovaleric acid
AraC	arabinofuranosyl cytidine
BCA	bicinchoninic acid
BDNF	brain derived neurotrophic factor
BMP	bone morphogenic protein
BoNTA	botulinum neurotoxin type A
BSA	bovine serum albumin
CaI	calcium imaging
CaMK	calcium-calmodulin-dependent kinase
CHO	chinese hamster ovary
CNS	central nervous system
CSF	cerebro spinal fluid
CTIP2	chicken ovalbumin upstream promoter transcription factor-interacting protein 2
DAPI	4',6-diamidino-2-phenylindole
DM	dorsomorphin
DMSO	dimethyl sulfoxide
DNQX	6,7-dinitroquinoxaline-2,3-dione
DTT	DL-dithiotreitol
EB	embryoid body
EPSP	excitatory postsynaptic potential
EthD-1	ethidium homodimer

FAD	familial Alzheimer's disease
GABA	γ-aminobutyric acid
GAD67	glutamate decarboxylase 67
GAPDH	glyceraldehyde-3-phosphate-dehydrogenase
HFIP	hexafluoro-2-propanol
IP	immunoprecipitation
iPSC	induced pluripotent stem cell
LTD	long term depression
LTP	long term potentiation
MAP2	microtubule associated protein 2
MEA	multi electrode array
mEPSCs	miniature excitatoty postsynaptic currents
MTT	3-(4,5-dimethylthiazol-2-yl)-2,5-diphenyltetrazolium bromide
NCAM	neuronal cell adhesion molecule
NMDA	N-methyl-D-aspartate
NMM	neuronal maturation medium
NPC	neuronal progenitor cell
PAGE	polyacrylamide gel electrophoresis
PBS-/-	phospate buffer saline without calcium and magnesium
PD	PD0325901
PFA	paraformaldehyde
PI	Propidium iodide
PVDF	Polyvinylidenfluoride
REST	regulatory element 1 silencing transcription factor
RNA	Ribonucleic acid
ROCK	Rho-associated coiled-coil containing protein kinase
ROI	region of interest
RT	room temperature
SAD	sporadic Alzheimer's disease
SDS	sodium dodecyl sulfate
S.E.M.	standard error of the mean
SNAP25	synaptosomal-associated protein 25

TBR1	T-box brain 1
TBS	tris buffer saline
TEMED	tetramethylenethylendiamin
TGFβ	tumor growth factor beta
TTX	tetrodotoxin
VBA	visual basic for applications

7. Scripts and Macros

7.1 Visual basic data extraction

```
Sub resetfile()
    Dim ws As Worksheet
    Application.DisplayAlerts = False
Application.ScreenUpdating = False
    For Each ws In ActiveWorkbook.Worksheets
    If ws.Name <> "options" And ws.Name <> "summary" Then ws.Delete
    Next
With Sheets("summary")
.Range(.Rows(2), .Rows(100)).ClearContents
End With
    Sheets("options").Select
    Application.ScreenUpdating = True
Application.DisplayAlerts = True
End Sub
Sub extractinfo()
    Dim thiswb As Workbook, addRes As String
Dim MyObj As Object, MySource As Object, file As Variant, caseN As Integer, ActN As
Integer, pos As Double, max As Variant, thisfilename, archivo As String
    Dim RepDate As Date, entN, i, j As Integer, sig As Boolean
Dim Nfilas As Single, sname As Name
    Application.ScreenUpdating = False
    thisfilename = ThisWorkbook.Name
Set thiswb = ActiveWorkbook
    folder = Sheets("Options").Range("C4")
beg = Sheets("Options").Range("C5")
lenbeg = Len(beg)
minval = Sheets("Options").Range("C7")
exception = Sheets("Options").Range("C6")
    file = Dir(folder & "\")
n = 2
    While (file <> "")
```

```
    If Left(UCase(file), lenbeg) = UCase(beg) And Right(UCase(file), 4) = ".DAT" And
InStr(file, exception) = 0 Then
    Application.ScreenUpdating = False
newtab = Mid(file, lenbeg + 1, Len(file) - lenbeg - 4)
    Sheets.Add After:=ActiveSheet
ActiveSheet.Name = newtab
    With ActiveSheet.QueryTables.Add(Connection:="TEXT;" & folder & "\" & file,
Destination:=Range("$A$1"))
.Name = Right(file, Len(file) - 4)
.FieldNames = True
.RowNumbers = False
.FillAdjacentFormulas = False
.PreserveFormatting = True
.RefreshOnFileOpen = False
.RefreshStyle = xlInsertDeleteCells
.SavePassword = False
.SaveData = True
.AdjustColumnWidth = True
.RefreshPeriod = 0
.TextFilePromptOnRefresh = False
.TextFilePlatform = 850
.TextFileStartRow = 1
.TextFileParseType = xlDelimited
.TextFileTextQualifier = xlTextQualifierDoubleQuote
.TextFileConsecutiveDelimiter = False
.TextFileTabDelimiter = True
.TextFileSemicolonDelimiter = False
.TextFileCommaDelimiter = False
.TextFileSpaceDelimiter = False
.TextFileColumnDataTypes = Array(1, 1, 1, 1, 1, 1, 1, 1, 1, 1, 1, 1, 1)
.TextFileDecimalSeparator = "."
.TextFileThousandsSeparator = " "
.TextFileTrailingMinusNumbers = True
.Refresh BackgroundQuery:=False
End With
```

```
    Nrows = Sheets(newtab).Cells(Rows.Count, 1).End(xlUp).Row
Ncols = Sheets(newtab).Cells(3, Columns.Count).End(xlToLeft).Column
    With ActiveWorkbook.Worksheets(newtab).Sort
.SortFields.Clear .SortFields.Add Key:=Range("B4", Cells(Nrows, "B")),
SortOn:=xlSortOnValues, Order:=xlAscending, DataOption:=xlSortNormal
.SetRange Range("A3", Cells(Nrows, Ncols))
.Header = xlYes
.MatchCase = False
.Orientation = xlTopToBottom
.SortMethod = xlPinYin
.Apply
End With
    valfound = False
For i = 4 To Nrows
If Cells(i, "B") >= minval And valfound = False Then
valfound = True
first50 = i
End If
    Next i
    Cells(Nrows + 2, "A") = "Average"
Cells(Nrows + 3, "A") = "(Num_Spikes>50)"
Range(Cells(Nrows + 2, "B"), Cells(Nrows + 2, Ncols)).FormulaR1C1 = "=AVERAGE(R"&
first50 & "C:R" & Nrows & "C)"
    Sheets("summary").Cells(n, "A") = newtab
n = n + 1
End If
    file = Dir
    Wend
    With Sheets("summary")
.Range("B2", .Cells(n - 1, "M")).FormulaR1C1 = _
"=INDIRECT(ADDRESS(MATCH(""Average"",INDIRECT(RC1&""!A:A""),FALSE),
MATCH(R1C,INDIRECT(RC1&""!3:3""),FALSE),,,RC1))"
End With
    Application.ScreenUpdating = True
    End Sub
```

7.2 Visual basic spike parameters

```
Sub sumarize_unit(ByVal tab_name As String, ByVal Ncols As Integer, ByVal i As Integer)
    With Sheets("summ_u" & i)
n = .Cells(2, .Columns.Count).End(xlToLeft).Column + 1
.Cells(1, n) = tab_name
    For j = 2 To 9
.Cells(j, n).FormulaR1C1 = _
"=AVERAGEIFS(" & tab_name & "!R" & j & "C2:R" & j & "C" & Ncols & "," & tab_name &
"!R11C2:R11C" & Ncols & ",""Unit=" & i & " "")"
Next j
    End With
    With Sheets(tab_name)
    Nrows = .Cells(.Rows.Count, 1).End(xlUp).Row
chartname = "Unit" & i & " graph"
    If n = 2 Then
Charts.Add.Name = chartname
With Charts(chartname)
.ChartArea.Clear
.ChartType = xlLine
End With
    Charts(chartname).SetSourceData Source:=.Range(.Cells(13, Ncols + 1 + i),
.Cells(Nrows, Ncols + 1 + i))
Charts(chartname).SeriesCollection(1).XValues = .Range(.Cells(13, 1), .Cells(Nrows,
1))
Charts(chartname).SeriesCollection(1).Name = tab_name
Charts(chartname).SetElement (msoElementChartTitleAboveChart)
Charts(chartname).ChartTitle.Text = "Unit" & i & " average spikes"
Sheets(chartname).Move Before:=Sheets("options")
Else
Charts(chartname).SeriesCollection.NewSeries
Charts(chartname).SeriesCollection(n - 1).Name = tab_name
Charts(chartname).SeriesCollection(n - 1).Values = .Range(.Cells(13, Ncols + 1 + i),
.Cells(Nrows, Ncols + 1 + i))
End If
```

```
    End With
    End Sub
    Sub test()
    For i = 0 To 5
Sheets("options").Cells(i + 7, "G") = 0
    Next i
    End Sub
    Sub resetfile()
    Dim ws As Worksheet
Dim chrt As Chart
    Application.DisplayAlerts = False
Application.ScreenUpdating = False
Charts.Add
For Each ws In ActiveWorkbook.Worksheets
    If ws.Name <> "options" And ws.Name <> "summ_u1" And ws.Name <> "summ_u2"
And ws.Name <> "summ_u0" Then ws.Delete
    Next
    For Each chrt In ActiveWorkbook.Charts
chrt.Delete
Next
    With Sheets("summ_u0")
.Range(.Columns(2), .Columns(100)).ClearContents
End With
With Sheets("summ_u1")
.Range(.Columns(2), .Columns(100)).ClearContents
End With
With Sheets("summ_u2")
.Range(.Columns(2), .Columns(100)).ClearContents
End With
    Sheets("options").Select
    Application.ScreenUpdating = True
Application.DisplayAlerts = True
End Sub
    Sub extractinfo()
    Dim thiswb As Workbook, addRes, restfile, newtab As String
```

```
Dim Ncols, z As Integer
Dim MyObj As Object, MySource As Object, file As Variant, caseN, ActN As Integer, pos
As Double, max As Variant, thisfilename, archivo As String
Dim ws As Worksheet, Err As Boolean
Dim curr_chart As ChartObject
Dim RepDate As Date, entN, wchart, hchart, x, y, chartxrow, a, orig_len, umarg, lmarg,
sum_col As Integer, sig As Boolean
Dim Nfilas As Single, sname As Name
Dim ser_range As Range
Dim ex_u0, ex_u1, ex_u2 As Boolean
Dim min_val As Double

    Application.ScreenUpdating = False
    thisfilename = ThisWorkbook.Name
Set thiswb = ActiveWorkbook
    With Sheets("Options")
folder = .Range("C4")
If Right(folder, 1) <> "\" Then folder = folder & "\"
beg = .Range("C5")
lenbeg = Len(beg)
keyword = .Range("C6")
    max2_timeframe = .Range("C8")
End With
    ex_u0 = False
ex_u1 = False
ex_u2 = False

    file = Dir(folder & "\")
n = 2
x = 0
y = 0
sum_col = 2
first = True
    While (file <> "")
    Err = True
```

```
    If Left(UCase(file), lenbeg) = UCase(beg) And Right(UCase(file), 4) = ".DAT" And
InStr(file, keyword) <> 0 Then
    Application.ScreenUpdating = False
restfile = Mid(file, lenbeg + 1, Len(file) - lenbeg - 4)
a = InStr(restfile, "_")
If a < 3 Then a = InStr(3, restfile, "_")
newtab = Left(restfile, a - 1)
orig_len = Len(newtab)
    While Err = True
Err = False
    For Each ws In ActiveWorkbook.Worksheets
    If ws.Name = newtab Then Err = True
    Next
If Err = True Then
If Len(newtab) = orig_len Then
newtab = newtab & "_1"
Else
newtab = Left(newtab, orig_len) & "_" & Val(Right(newtab, 1) + 1)
End If
End If
Wend
    Sheets.Add After:=Sheets("summ_u2")
ActiveSheet.Name = newtab
    With ActiveSheet.QueryTables.Add(Connection:="TEXT;" & folder & file,
Destination:=Range("$A$1"))
.Name = Right(file, Len(file) - 4)
.FieldNames = True
.RowNumbers = False
.FillAdjacentFormulas = False
.PreserveFormatting = True
.RefreshOnFileOpen = False
.RefreshStyle = xlInsertDeleteCells
.SavePassword = False
.SaveData = True
.AdjustColumnWidth = True
```

```
.RefreshPeriod = 0
.TextFilePromptOnRefresh = False
.TextFilePlatform = 850
.TextFileStartRow = 1
.TextFileParseType = xlDelimited
.TextFileTextQualifier = xlTextQualifierDoubleQuote
.TextFileConsecutiveDelimiter = False
.TextFileTabDelimiter = True
.TextFileSemicolonDelimiter = False
.TextFileCommaDelimiter = False
.TextFileSpaceDelimiter = False
.TextFileColumnDataTypes = Array(1, 1, 1, 1, 1, 1, 1, 1, 1, 1, 1, 1, 1)
.TextFileDecimalSeparator = "."
.TextFileThousandsSeparator = " "
.TextFileTrailingMinusNumbers = True
.Refresh BackgroundQuery:=False
End With
    With Sheets(newtab)
    .Rows("1:10").Insert Shift:=xlDown, CopyOrigin:=xlFormatFromLeftOrAbove
    .Range("A8") = "Baseline"
.Range("A9") = "Norm. Minimum"
    .Range("A2") = "max2"
.Range("A3") = "Peak latency"
.Range("A4") = "Amplitude"
.Range("A5") = "Half-width"
.Range("A6") = "70% Width"
.Range("A7") = "90% Width"

    Nrows = .Cells(Rows.Count, 1).End(xlUp).Row
Ncols = .Cells(11, Columns.Count).End(xlToLeft).Column
    time_delta = Abs(.Cells(18, 1) - .Cells(19, 1)) 'increment of time between two random
points
    For k = 2 To Ncols
    Select Case Mid(.Cells(11, k), 6, 1)
    Case "0"
```

```
ex_u0 = True
Case "1"
ex_u1 = True
Case "2"
ex_u2 = True
End Select

    Next k
    pos_1milisec = Application.Match(-0.001, .Columns(1), 0)
    .Cells(11, Ncols + 1).FormulaR1C1 = "Unit=0 "
.Cells(11, Ncols + 2).FormulaR1C1 = "Unit=1 "
.Cells(11, Ncols + 3).FormulaR1C1 = "Unit=2 "

    For n = 0 To 2
If (n = 0 And ex_u0 = True) Or (n = 1 And ex_u1 = True) Or (n = 2 And ex_u2 = True) Then
.Range(.Cells(13, Ncols + 1 + n), .Cells(Nrows, Ncols + 1 + n)).FormulaR1C1 = "=ROUND(SUMIF(R11C2:R11C" & Ncols & ",R11C,RC2:RC" & Ncols & ")/COUNTIF(R11C2:R11C" & Ncols & ",R11C),5)"
End If
Next n
.Range(.Columns(Ncols + 1), .Columns(Ncols + 3)).Font.Bold = True
    For i = 2 To Ncols + 3
    If i <= Ncols Or (i = Ncols + 1 And ex_u0 = True) Or (i = Ncols + 2 And ex_u1 = True) Or (i = Ncols + 3 And ex_u2 = True) Then
    baseline = Application.Average(.Range(.Cells(13, i), .Cells(pos_1milisec, i)))
    .Cells(8, i) = baseline
    Set ser_range = Sheets(newtab).Range(Sheets(newtab).Cells(13, i), Sheets(newtab).Cells(Nrows, i))
Set ser_range2 = Sheets(newtab).Range(Sheets(newtab).Cells(100, i), Sheets(newtab).Cells(150, i))
Set ser_range3 = Sheets(newtab).Range(Sheets(newtab).Cells(120, i), Sheets(newtab).Cells(Nrows, i))
norm_min = Application.Min(ser_range2) - baseline
.Cells(9, i) = norm_min
```

```
    For k = 13 To Nrows 'with this loop we normalize the spike
    .Cells(k, i) = (.Cells(k, i) - baseline) / Abs(norm_min)
    Next k
    min_val = Application.Min(ser_range2)
peak_time_pos = Application.Match(min_val, ser_range2, 0) + 100
max2_timeframe_pos = peak_time_pos + Int(max2_timeframe / time_delta)
peak_tim = .Cells(peak_time_pos, 1)
    max_t = min_val
For j = 100 To Nrows
If .Cells(j, i) >= max_t And j >= peak_time_pos And j <= max2_timeframe_pos Then
max_t = .Cells(j, i)
Next j
    .Cells(2, i) = max_t
.Cells(4, i) = -norm_min
    max2_tim_pos = Application.Match(max_t, ser_range3, 0) + 120
    .Cells(3, i) = .Cells(max2_tim_pos, 1) - peak_tim
    For k = 0 To 2
Select Case k
Case 0
magicpoint = -0.5
Case 1
magicpoint = -0.3
Case 2
magicpoint = -0.1
End Select
    j = peak_time_pos
While Not (.Cells(j, i) <= magicpoint And .Cells(j - 1, i) >= magicpoint)
j = j - 1
Wend
t1 = .Cells(j, 1)
t2 = .Cells(j - 1, 1)
v1 = .Cells(j, i)
v2 = .Cells(j - 1, i)
x1 = (magicpoint - v1) / (v2 - v1) * (t2 - t1) + t1
    j = peak_time_pos
```

```
While Not (.Cells(j, i) <= magicpoint And .Cells(j + 1, i) >= magicpoint)
j = j + 1
Wend
t1 = .Cells(j, 1)
t2 = .Cells(j + 1, 1)
v1 = .Cells(j, i)
v2 = .Cells(j + 1, i)
x2 = (magicpoint - v1) / (v2 - v1) * (t2 - t1) + t1
    .Cells(5 + k, i) = x2 - x1
    Next k
    End If
    Next i
    .Rows("5:7").NumberFormat = "_-* #,##0.000000_-;-* #,##0.000000_-;_-* ""-""??_-;_-
@_-" End With
    For z = 0 To 2
If (z = 0 And ex_u0 = True) Or (z = 1 And ex_u1 = True) Or (z = 2 And ex_u2 = True) Then
Call sumarize_unit(newtab, Ncols, z)
Next z
    End If
    file = Dir
    Wend
    Application.ScreenUpdating = True
    End Sub
```

8. Résumé

8.1 Curriculum vitae

9. Appendix

Experiment	Cell line	Age	Coculture/Treatment	Figure
MEA				
TTX	8/25(PAN9)	11 m	no/DM 3 μM for 7 d	3.8 and 3.9
4AP immature	DF6(PAN22)	4 m	no/DM 3 μM for 7 d	3.10, 3.11, 3.14
4AP immature	DF6(PAN24)	4 m	no/DM 3 μM for 7 d	3.10, 3.11, 3.14
4AP mature	8/25(PAN9)	9-10 m	no/DM 3 μM for 7 d	3.12, 3.13, 3.15
7PA2	8/25(PAN9)	7 m	no/DM 3 μM for 7 d	3.21
7PA2	8/25(PAN9)	8 m	no/DM 3 μM for 7 d	3.21
Control/Vehicle	8/25	8 m	no/AraC 5 μM for 5 d	3.27
Gabazine	8/25(PAN9)	8 m	no/DM 3 μM for 7 d	3.2
AP5/DNQX	8/25	6 m	no/AraC 5 μM for 5 d	3.3
Calcium	8/25	6-7 m	no/AraC 5 μM for 5 d	3.4
Aβ*	8/25(PAN9)	8 m	no/DM 3 μM for 7 d	3.28 and 3.29
Aβ*	8/25(PAN9)	12 m	no/DM 3 μM for 7 d	3.28 and 3.29
Aβ* + 4AP	8/25(PAN9)	12 m	no/DM 3 μM for 7 d	3.30, 3.31, 3.32
CaI				
DNQX + APV	SZ01(PAN1)	2 m	yes/DAPT 1 μM for 7 d	3.5
4AP	DF6(PAN6)	3 m	no/DM 3 μM for 7 d	3.16, square
4AP	DF6(PAN6)	3-4 m	yes/AraC 1 μM for 7 d	3.16 paralelogram
4AP	DF6(PAN6)	3-4 m	no/DAPT 1 μM for 7 d	3.16 tilted square
4AP	SZ02(PAN13)	5 m	yes/AraC 1 μM for 7 d	3.16 hexagon
Aβ + 4AP	DF6(PAN6)	3 m	no/DM 3 μM for 7 d	3.33 circle
Aβ + 4AP	DF6(PAN6)	3-4 m	yes/AraC 1 μM for 7 d	3.33 square
Aβ + 4AP	SZ02(PAN13)	5 m	yes/AraC 1 μM for 7 d	3.33 triangle
ICC				
4AP Timecourse	SZ02(PAN13)	4 m	yes/AraC 1 μM for 7 d	3.18
Aβ + 4AP	SZ02(PAN13)	5 m	yes/AraC 1 μM for 7 d	3.35
PatchC				
Aβ	DF6(PAN2)	4 m	no/AraC 5 μM for 5 d	3.25 and 3.26

10. Acknowledgment

My deep gratitude goes to Jun. Prof. Dr. Katja Nieweg, who expertly guided me through my PhD project. Her unwavering enthusiasm and encouragement kept me constantly engaged with my research. I am also very grateful for the opportunities she provided me to attend several workshops, national and international conferences.

I wish to express my sincere gratitude to my second supervisor Carsten Culmsee for his advises regarding my work, his unequivocal support and welcoming smile.

I would like to thank my dear college Shadan. I am glad that we trusted and supported each other, especially in the dark times of our PhDs. I also would like to mention our postdoc Pretty and students Ani, Nadia, Eva, Senta, and Andrea for their contribution to creating a nice environment.

I am truly thankful to Emma Esser for her incredible personality and for her help in every bureaucratically challenging issue (considering the country we live in which they are not few), without whom this thesis would not ever be existed. I am grateful to Katharina Elsässer and Susen Kutsch for all their support at work and for helping me improve my German.

Great and very special thanks to my friends Yulia Nikonova, Amalia Dolga, Judit Preisenberger, Anna-Lena Krett, and all my colleagues of the Institute of Pharmacology and Clinical Pharmacy.

I would like to thank Robert Grosse, Dominik, and Matthias for the confocal microscopy, Tim Plant for nice conversations and letting me use the calcium imaging microscope and Gerhard Schratt for the primary neurons. I also want to thank Moritz Bünemann, Jens Kockskämper, and Cornelius Krasel for discussions and suggestions.

I would like to thank Reeta, Silvi (#itsmybrain), Robi, Maria, Fede, and Michi for making Marburg so much fun. I cannot and do not want to imagine those times without our extracurricular activities, castle warming parties, christmas markets and Glühwein, weekly massacres, farewells and birthdays.

Although being far away, I would like to thank Mehtap, Baran, and 2010 İTÜ MBG graduates for the never changing feeling whenever we are together.

My best friends Pelin and Mehmet, I would not be me if you were not there.

Special thanks to Moritz Pelz for his incredibly positive personality and keeping me calm

during the last steps of this marathon.

Finally, I am always indebted to my dear family; to my parents, brother, and cousins for their unequivocal love and support at all times from thousands of kilometers away.

List of Figures

List of Tables